FINITE ELEMENT METHODS FOR SECOND ORDER FORMS OF THE TRANSPORT EQUATION

A Dissertation

by

CHRISTOPHER JOHN GESH

Submitted to the Office of Graduate Studies of
Texas A&M University
in partial fulfillment of the requirements for the degree of

DOCTOR OF PHILOSOPHY

December 1999

Major Subject: Nuclear Engineering

FINITE ELEMENT METHODS FOR SECOND ORDER FORMS OF THE TRANSPORT EQUATION

A Dissertation

by

CHRISTOPHER JOHN GESH

Submitted to Texas A&M University
in partial fulfillment of the requirements
for the degree of

DOCTOR OF PHILOSOPHY

Approved as to style and content by:

Marvin Adams (Chair of Committee)	
Raytcho Lazarov (Member)	Paul Nelson (Member)
Dmitriy Anistratov (Member)	Alan Waltar (Head of Department)

December 1999

Major Subject: Nuclear Engineering

ABSTRACT

Finite Element Methods for Second Order
Forms of the Transport Equation. (December 1999)
Christopher John Gesh, B.S., Oregon State University;
M.S.E., University of Michigan
Chair of Advisory Committee: Dr. Marvin Adams

We analyze the behavior of second order forms of the transport equation discretized with finite element methods for problems that contain thick diffusive regions. Our results are quite general in that we make no assumptions regarding the spatial mesh or the specific weight and basis functions.

We find that finite element discretizations of second order forms of the transport equation satisfy the same finite element discretization of the diffusion equation in the thick diffusion limit, albeit with potentially inaccurate boundary conditions. We show that we can construct very accurate scalar flux distributions by averaging the even- and odd-parity solutions to these problems, and discuss the relationship between the parity equations and the self-adjoint angular flux equations.

For multidimensional problems on certain meshes, we find that the most straightforward discretizations of the odd-parity and self-adjoint angular flux equations result in a violation of the discrete *inf-sup* condition. To rectify this problem, we propose to apply certain mixed finite element discretizations, and analyze their behavior for thick diffusive problems.

We then derive and analyze consistent diffusion synthetic acceleration schemes for the discretizations we have considered. We find that it is straightforward to implement these schemes in multidimensional geometry, in contrast to past experience in applying diffusion

synthetic acceleration to discretizations of the first order transport equation. Finally, we provide numerical results that support our predictions and demonstrate that our analysis methods are good predictors of observed performance.

To Michelle, of course

ACKNOWLEDGMENTS

As is invariably the case, this work would have been impossible without the help and support of many others. Dr. Marvin Adams, my friend and mentor, generously contributed both his great knowledge of transport theory and much encouragement during this long and sometimes difficult experience. Sincere gratitude is extended to the members of my committee, Drs. Dmitriy Yu. Anistratov, Raytcho Lazarov, and Paul Nelson. Their experience and patience was invaluable to me. I also wish to thank Drs. David Barrow and Joseph Pasciak for their help in both the technical details of this dissertation and for filling in for absent committee members on very short notice.

Much of this research was performed during my tenure as a DOE Computational Science Fellow. Many thanks are extended to the helpful and generous administrators of that program. Financial support from Texas A&M University and Los Alamos National Laboratory is also gratefully acknowledged.

My comrades in the dank and grim bowels of various graduate student slums deserve the warmest thanks for making what could have been a rather miserable process a lot of fun. These good folks include Halim Alsaed, Chris Castrianni, Amy Caldwell, Jae Chang, Russell Depriest, Troy Guy, Eric Hawkes, Daryl Hawkins, Cable Kurwitz, Amit Majumdar, Mark Nelson, Shawn Pautz, Gilles Ramone, Ivan Tchebeskov, Chris Thompson, Kelly Thompson, Todd Urbatsch, Todd Wareing, Annmarie Wood-Zika and Mike Zika.

Special thanks go out to Todd Palmer, a frequent source of much needed perspective and encouragement, and to Jenny Adams who made us all feel like a part of the Adams family. Chris Thompson, Daryl Hawkins and Mike Zika shared room 60A with me for years (literally). Their friendship and camaraderie will always be remembered. Beth Castrianni, Lori Thompson and Annmarie Wood-Zika, hardened veterans of the graduate student spouses club, deserve a standing ovation for serving in the trenches with Michelle.

I am very thankful for the love and support of my family. Michelle's parents, Noah and Sheryl, not only let me take their daughter to Texas, but stood behind us in prayer every step of the way. My mother and sister, Bonnie and Emily, and my grandparents, Britt and Mary, have lovingly supported my educational pursuits for as long as I can remember.

My boys, Paul and Jake, helped me leave work behind to enjoy the great fun of being a dad. My lovely and radiant wife, Michelle, stood with me through all of this with cheerfulness and unfaltering love. That her life has been disrupted more than anyone else's during the last few years makes her patience and support all the more precious to me.

My deepest gratitude is reserved for my God and Savior, who, in His sovereign power, brings about all good things. *For His merciful kindness is great toward us, and the truth of the Lord endures forever.*

TABLE OF CONTENTS

CHAPTER Page

CHAPTER Page

LIST OF TABLES

LIST OF FIGURES

FIGURE Page

FIGURE Page

FIGURE Page

CHAPTER I

INTRODUCTION

A linear transport process is characterized by the motion and interaction of particles with an underlying medium and is mathematically described by the linear Boltzmann transport equation. As such, a wide variety of physical problems depend on accurate and efficient solutions of this transport equation. These problems include radiative transfer in stellar atmospheres, radiation imaging and oncology, and neutron diffusion in a fission reactor. Unfortunately, analytic solutions of the transport equation exist for only the most idealized problems. Therefore, numerical methods are required for nearly all practical applications.

The transport equation itself is an integro-differential equation that in general must be solved iteratively. Furthermore, solutions of the transport equation can satisfy parabolic, elliptic or hyperbolic equations in certain physical limits, and are functions of up to seven independent variables. There is clearly no single spatial discretization scheme that is appropriate for every transport problem.

Many practical transport problems contain regions that are optically thick and diffusive. Due to practical computational limitations, the spatial grids for such problems contain cells that are many mean free paths thick. Additionally, since the dominant physical process underlying diffusive problems is scattering (or absorption and re-emission), conventional within-group iterative methods are inefficient. Therefore, it is desirable to identify transport discretizations that are both accurate for thick diffusive problems and amenable to iterative acceleration techniques.

Recent work [1, 2, 3, 4] on finite element method (FEM) discretizations of certain second order forms of the transport equation suggests that they may possess both of the above

---

The journal model is *IEEE Transactions on Nuclear Science.*

properties. While much of the deterministic numerical transport research has concentrated on the first order form transport equation, it is well known that second order forms of the equation can offer certain advantages. The most obvious is that second order forms of the transport equation are self-adjoint, and often result in symmetric positive definite (SPD) matrices when spatially discretized. Very efficient and robust methods exist to solve such systems. Additionally, there may be advantages in the form of lower unknown counts, applicability to unstructured grids and ease of parallel implementation.

Our work will focus on: (1) finite element discretizations of second order forms of the transport equation for thick diffusive problems in Cartesian geometry and, (2) iterative acceleration of the resulting linear systems. We will also consider an interesting variation closely related to second order transport formulations. We note that it is physically appealing to locate vector current unknowns on cell surfaces and scalar flux unknowns in cell centers. While the fundamental unknown in the transport equations is, of course, a scalar, we can reformulate traditional second order transport equations as coupled first order equations with scalar and vector unknowns. This reformulation will allow us to apply powerful mixed finite element methods (MFEM) [5] to transport problems and represents a significant departure from conventional FEM transport discretizations.

A. Background

Second order forms of the transport equation were first studied in the early 1960s by researchers in the nuclear engineering and astrophysics communities. It was recognized that self-adjoint forms of the transport equation could be effectively solved by variational methods [6, 7, 8, 9, 10]. Pomraning [7], Vladimirov [6] and Feautrier [11] first identified the even- and odd-parity equations, where the fundamental unknowns are the even and odd components of the angular flux, respectively. The even-parity equation, in particular, be-

came the starting point for a variety of finite element [12, 13, 14, 15, 16], finite difference [11, 17, 18, 19] and variational nodal methods [20, 21]. Finite element [12] or spherical harmonic [22] treatments of the angle variable were often used in conjunction with spatial finite elements for the even-parity equation in an effort to mitigate ray effects associated with discrete ordinates methods. Numerical methods based on the even-parity equation have proved effective for both reactor physics and radiative transfer applications, though sometimes at the expense of greater CPU requirements to achieve accuracy comparable to the best first order methods [23].

Miller [3] analyzed finite difference discretizations of the discrete ordinates even-parity equations in slab geometry with isotropic scattering. He found that is was possible to construct differencing schemes that were strictly positive and second order accurate. Furthermore, he showed that these methods also satisfied diffusion equations in the diffusion limit and could be effectively accelerated with diffusion synthetic acceleration (DSA). Miller [24] also noted that the direct application of linear continuous finite elements to the even-parity equation could admit negative solutions. However, if mass matrix lumping is incorporated, positivity can be guaranteed at the expense of a slight decrease in accuracy (though the spatial truncation error remains second order).

Adams [1] performed a diffusion limit analysis [25, 26, 27, 28, 29, 30] of the continuous finite element method (CFEM) applied to the even-parity equation in three dimensions on an unstructured grid. He found that, to leading order, the even-parity solution satisfied the corresponding continuous finite element approximation of the diffusion equation. However, he also noted that the associated Marshak boundary condition could be very inaccurate for certain problems. A similar result, though with a different boundary condition, was discovered for the slab geometry odd-parity equation [2]. Ackroyd [31] had earlier recognized that for certain reactor physics problems a weighted average of the even- and odd-parity solutions was far more accurate than either the even- or odd-parity solutions

alone. Adams's analysis revealed a similar property for thick diffusive problems. Specifically, while the individual even- and odd-parity diffusion limit boundary conditions can be inaccurate for non-isotropic incident fluxes, their average is an excellent approximation to the exact boundary condition. Additionally, Adams proposed diffusion synthetic acceleration schemes [32, 33, 34, 35, 36] based on the discretized even- and odd-parity diffusion limit equations. Adams confirmed the predicted diffusion limit behavior and the effectiveness of his DSA schemes with discrete ordinates calculations, though only in slab geometry.

Morel and McGhee [23] developed a stable DSA scheme for the discrete ordinates even-parity equation in three dimensions. The performance of their even-parity DSA scheme was comparable to DSA applied to discretizations of the first order form of the transport equation, though they noted a slight degradation when reflective boundary conditions were present. Additionally, Morel and McGhee [37] proposed an effective fission source acceleration scheme for the time dependent even-parity transport equation.

The self adjoint angular flux (SAAF) equation, first identified by Pomraning and Clark [7] in an effort to improve upon standard P_1 theory, has recently been proposed as a basis for numerical methods [4]. Unlike the even- and odd-parity equations, its fundamental unknown is the full range angular flux. Ackroyd [38] has also derived the SAAF through a generalized least squares solution to the first order transport equation. Morel and McGhee [4] have presented a simpler derivation and generated slab geometry numerical results using linear continuous finite elements in space and discrete ordinates in angle.

Of course, there are certain disadvantages common to nearly all second order formulations. The treatment of voids [39, 4] is difficult because of the presence of the total cross section in the denominator of the streaming term. Additionally, the implementation of reflective boundary conditions couples multiple directions in the even- and odd-parity equations, though not in the SAAF [4]. Methods based on second order forms of the transport

equation require the inversion of a symmetric positive definite matrix for each direction, rather than simply sweeping as in first order methods. On the other hand, for unstructured three dimensional grids, this may be an advantage since sweeping can become difficult under those circumstances. Despite these problems, the potential advantages of second order transport formulations, particularly for thick diffusive problems, encourage further study.

B. Organization and Objectives

The organization of the remainder of this work is as follows. In Chapter II we discuss the properties of the analytic transport equation. We begin by reducing the energy and time dependent transport equation to a series of energy and time independent *within-group* problems which are the basis of the numerical methods we develop. We then derive several second-order forms of the transport equation and discuss their characteristics. We discuss the behavior of the transport equation in certain physical limits and briefly describe the iterative methods necessary to solve the within-group scattering problem. We conclude the chapter with a short discussion of angular discretization methods.

In Chapter III, we derive the CFEM approximations to the parity equations and the SAAF equation. We then discuss the formal relationship between the CFEM approximation to the SAAF equation and the average of the even- and odd-parity CFEM systems, which turn out to be identical except on the boundaries. We analyze the behavior of these discretizations in the thick diffusive limit and at the interface between a diffusive and a non-diffusive region. We conclude with a discussion of certain implementational problems we have observed. These problems partially motivate the MFEM approach we propose in Chapter IV.

Chapter IV focuses on the application of mixed finite element methods to transport problems. We apply the Raviart-Thomas [40] method to both the coupled first order parity

equations and to a coupled set of transport equations for the full range angular flux. We then analyze these discretizations in certain physical limits and discuss their behavior and performance.

Chapter V details how we developed and implemented diffusion synthetic acceleration for the spatial discretizations discussed in Chapters III and IV. We present numerical results that support our analyses for both slab and XY geometry problems in Chapter VI. Finally, we summarize our main conclusions and discuss directions for fruitful future research in Chapter VII.

Our main purpose in this dissertation is to develop transport discretizations that are accurate and efficient. We consider important practical issues such as memory requirements and suitability for parallel implementation in terms of both scalability and spatial and angular domain decomposition. At the conclusion of our work, we hope to have achieved the following objectives:

- an improved theoretical understanding of finite element discretizations of second-order forms of the transport equation,
- the development of efficient and stable synthetic acceleration methods for these discretizations,
- a complete understanding of the relationship between the parity equations and the SAAF,
- the application of powerful mixed finite element methods to transport problems,
- the identification of optimal discretization methods for specific problem types, and
- a clear direction for fruitful future research in this area.

CHAPTER II

SPATIALLY CONTINUOUS TRANSPORT PROBLEMS

In this chapter we introduce the linear Boltzmann transport equation and its boundary conditions. We derive several second order forms of the transport equation and discuss their properties. We also present two coupled first order transport formulations that are the basis of the mixed finite element methods we develop in Chapter IV. We then review the behavior of the analytic transport equation for thick diffusive problems. We conclude this chapter with a discussion of the iterative methods used to solve the within group scattering problem.

A. The Transport Equation

The linear transport equation is derived in numerous reactor theory [41, 42] and transport theory [43, 44, 45] textbooks. It is an integro-differential equation with up to seven independent variables. Solutions of transport problems satisfy elliptic, parabolic or hyperbolic equations in various legitimate physical limits. Despite its complexity, it is simply a mathematical expression of particle (e.g. neutrons or photons) balance:

$$\frac{1}{v(E)}\frac{\partial \Psi}{\partial t} + \Omega \cdot \nabla \Psi + \sigma_t(\mathbf{r},E)\Psi(\mathbf{r},\Omega,E,t) = \int_{4\pi}\int_{0}^{\infty} \sigma_s(\mathbf{r},\Omega' \to \Omega, E' \to E)\Psi(\mathbf{r},\Omega',E',t)\, d\Omega' dE' + Q_e(\mathbf{r},\Omega,E,t) \quad \text{for } \mathbf{r} \in \mathbf{D}. \quad (2.1)$$

Here $\mathbf{r}$, Ω, E, and t are the position, direction, energy and temporal variables, respectively, $v(E)$ is the particle speed, σ_t and σ_s are the total and scattering cross sections, and Q_e is the external source. $\mathbf{D}$ is an arbitrary spatial domain with a non-reentrant boundary $\partial\mathbf{D}$ and

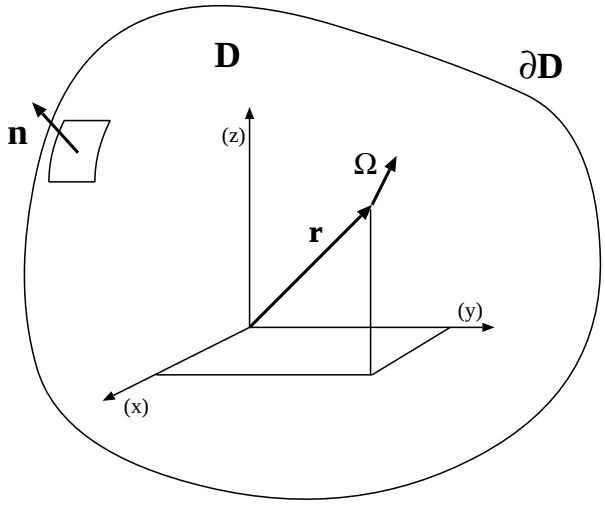

Fig. 1. An arbitrary spatial domain in Cartesian coordinates.

a unit outward normal **n** as shown in Fig. 1.

The *angular flux*, Ψ, is the product of the density of particles at a point in phase space and their speed so that:

$$\underbrace{\sigma_t(\mathbf{r},E)}_{\frac{interactions}{particle-cm}} \times \underbrace{\Psi(\mathbf{r},\Omega,E,t)}_{\frac{particles}{cm^3-sr-eV}\frac{cm}{second}} \times \underbrace{dr}_{cm^3} \times \underbrace{d\Omega}_{sr} \times \underbrace{dE}_{eV} = \underbrace{\text{Reaction Rate}}_{\frac{interactions}{second}}$$

represents the expected rate at which interactions with the background media occur in dr about r, $d\Omega$ about Ω, and dE about E at time t.

We note that all time and energy dependent transport problems can be reduced by implicit time differencing [45] and the multigroup approximation [42, 45] to a series of one-group, steady-state problems that are referred to as *within-group* problems. At this point, we will also make the assumption that sources and scattering are isotropic. While this assumption is valid for many physical problems, we will point out when the presence of anisotropy affects our methods or analyses. Thus, we arrive at the form of the transport

equation that will be the basis for our spatial discretizations:

$$\Omega \cdot \nabla \Psi + \sigma_t(\mathbf{r})\Psi(\mathbf{r},\Omega) = \frac{1}{4\pi}\left[\sigma_s(\mathbf{r}) \int_{4\pi} \Psi(\mathbf{r},\Omega)\, d\Omega + Q(\mathbf{r})\right] \quad \text{for } \mathbf{r} \in \mathbf{D}. \tag{2.2}$$

The source, Q, now consists of both the external source and the known scattering source from other energy groups.

We will often use the following definitions. The *scattering ratio* is defined as the ratio of the scattering and total cross section:

$$c = \frac{\sigma_s}{\sigma_t} \tag{2.3}$$

The *scalar flux* is defined as the angular integral of the angular flux:

$$\Phi(\mathbf{r}) = \int_{4\pi} \Psi(\mathbf{r},\Omega)\, d\Omega. \tag{2.4}$$

The *angular current density* is the product of the angular flux and the direction of particle propagation:

$$\mathbf{G}(\mathbf{r},\Omega) = \Omega\Psi(\mathbf{r},\Omega). \tag{2.5}$$

Finally, the *current* is defined as the angular integral of the angular current density:

$$\mathbf{J}(\mathbf{r}) = \int_{4\pi} \mathbf{G}(\mathbf{r},\Omega)\, d\Omega. \tag{2.6}$$

Physically, $\mathbf{J}(\mathbf{r}) \cdot \mathbf{n} dS$ is the net rate at which particles pass through a surface dS with an outward normal $\mathbf{n}$.

The streaming term, $\Omega \cdot \nabla \Psi$, in equation (2.2) involves only first order spatial derivatives. For that reason we will refer to equation (2.2) as the *first order form* of the transport equation.

1. Boundary Conditions

We must also provide appropriate boundary conditions for the transport equation. Most frequently, the known incident angular flux is specified on all or part of the boundary:

$$\Psi(\mathbf{r},\Omega) = F(\mathbf{r},\Omega) \quad \text{for } \mathbf{r} \in \partial\mathbf{D_i} \text{ and } \mathbf{n}\cdot\Omega < 0. \tag{2.7}$$

Symmetries in the spatial domain can result in reflective boundary conditions:

$$\Psi(\mathbf{r},\Omega) = \Psi(\mathbf{r},\Omega') \quad \text{for } \mathbf{r} \in \partial\mathbf{D_r} \text{ and } \mathbf{n}\cdot\Omega < 0, \tag{2.8}$$

where Ω' is the angle that reflects onto Ω at position $\mathbf{r} \in \partial\mathbf{D_r}$. Albedo boundary conditions set the angular flux entering a region through $\partial\mathbf{D_a}$ as a weighted integral of the angular flux leaving that region through $\partial\mathbf{D_a}$:

$$\Psi(\mathbf{r},\Omega) = \int\limits_{\mathbf{n}\cdot\Omega'>0} \alpha(\mathbf{r},\Omega\cdot\Omega')\Psi(\mathbf{r},\Omega')\,d\Omega \quad \text{for } \mathbf{r} \in \partial\mathbf{D_a} \text{ and } \mathbf{n}\cdot\Omega < 0. \tag{2.9}$$

2. The Balance Equation

The so-called *balance equation* is the angular integral of equation (2.2):

$$\nabla\cdot\mathbf{J}(\mathbf{r}) + \sigma_a(\mathbf{r})\Phi(\mathbf{r}) = Q(\mathbf{r}). \tag{2.10}$$

If we integrate the balance equation over any spatial domain we arrive at a precise mathematical expression for particle conservation within that domain. For example, consider an arbitrary volume $\mathbf{D}$. We integrate equation (2.10) over this domain to obtain:

$$\int_{\mathbf{D}} \nabla\cdot\mathbf{J}(\mathbf{r})\,dV + \int_{\mathbf{D}} \sigma_a(\mathbf{r})\Phi(\mathbf{r})\,dV = \int_{\mathbf{D}} Q(\mathbf{r})\,dV. \tag{2.11}$$

We can apply Green's theorem to obtain:

$$\int_{\partial\mathbf{D}} \mathbf{J}(\mathbf{r})\cdot\mathbf{n}\,dS + \int_{\mathbf{D}} \sigma_a(\mathbf{r})\Phi(\mathbf{r})\,dV = \int_{\mathbf{D}} Q(\mathbf{r})\,dV. \tag{2.12}$$

This is an interesting result. Despite the fact that the current and the scalar flux are both derived from the same scalar variable (the angular flux), the most physically appealing expression for particle balance involves vector and scalar unknowns that are not spatially co-located. This apparent antinomy will partially motivate our development of mixed finite element transport methods.

3. Angular Discretization

We have yet to discuss the discretization of the angle variable. We will continue without invoking an angular discretization for notational simplicity. Thus, the results of our analyses can be thought to apply when the specified angular discretization resolves the angular variations of the solution to the problem being considered.

In practice, we will use the standard discrete ordinates method [46, 45]. In this approximation, angular integrals are replaced with discrete sums:

$$\int_{4\pi} f(\Omega)\, d\Omega \rightarrow \sum_{n=1}^{N} f(\Omega_n) h_n,$$

where Ω_n are the quadrature points (directions) and h_n are the quadrature weights. If the problems of interest are thick and diffusive then the quadrature set should exactly integrate at least linear and quadratic polynomials of the direction cosines Ω_x, Ω_y, and Ω_z to resolve the angular shape of the solution in the problem interior. This can be understood by recalling that, in a diffusive problem, the angular flux is a linear function of angle. To compute the first angular moment of a linear function, we must be able to integrate quadratic polynomials.

B. Second Order Forms

In this section, we will derive three independent second order equations. By this, we mean equations whose streaming operator involves second order spatial derivatives. We note that the even- and odd-parity equations have as their fundamental unknowns the even- and odd-angular components of the angular flux. Thus, in solving these equations we need only consider half of the angular domain. The SAAF equation, on the other hand, has the full range angular flux as its fundamental unknown.

1. The Even- and Odd-Parity Equations

The even- and odd-parity equations have been the basis for a wide variety of numerical transport methods [47, 48, 16, 1, 14, 49, 21, 18, 19, 12, 24, 37, 23, 50]. Our derivation will follow the standard procedure [45] for the most part, though our treatment of boundary conditions follows Adams [1]. We begin the derivation of the parity equations by defining the even-parity angular flux, Ψ^+, and the odd-parity angular flux, Ψ^-, as:

$$\Psi^+(\mathbf{r},\Omega) = [\Psi(\mathbf{r},\Omega) + \Psi(\mathbf{r},-\Omega)], \tag{2.13a}$$

$$\Psi^-(\mathbf{r},\Omega) = [\Psi(\mathbf{r},\Omega) - \Psi(\mathbf{r},-\Omega)]. \tag{2.13b}$$

It is easy to see that the angular flux is simply the sum of the even- and odd-parity fluxes:

$$\Psi(\mathbf{r},\Omega) = \Psi^+(\mathbf{r},\Omega) + \Psi^-(\mathbf{r},\Omega), \tag{2.14}$$

and that the scalar flux and current can be recovered from the parity angular fluxes with the following half-range angular integrals:

$$\Phi(\mathbf{r}) = 2\int_{2\pi} \Psi^+(\mathbf{r},\Omega)\, d\Omega, \tag{2.15a}$$

$$\mathbf{J}(\mathbf{r}) = 2\int_{2\pi} \Omega\Psi^{-}(\mathbf{r},\Omega)\,d\Omega. \tag{2.15b}$$

Now, if we write first order transport equation for the $+\Omega$ direction and the $-\Omega$ direction then add and subtract the results, we obtain the following coupled set of equations:

$$\Omega\cdot\nabla\Psi^{-}(\mathbf{r},\Omega) + \sigma_t(\mathbf{r})\Psi^{+}(\mathbf{r},\Omega) = \frac{\sigma_s(\mathbf{r})\Phi(\mathbf{r}) + Q(\mathbf{r})}{4\pi}, \tag{2.16a}$$

$$\Omega\cdot\nabla\Psi^{+}(\mathbf{r},\Omega) + \sigma_t(\mathbf{r})\Psi^{-}(\mathbf{r},\Omega) = 0. \tag{2.16b}$$

We solve equation (2.16b) for Ψ^{-}:

$$\Psi^{-}(\mathbf{r},\Omega) = -\frac{1}{\sigma_t(\mathbf{r})}\Omega\cdot\nabla\Psi^{+}(\mathbf{r},\Omega), \tag{2.17}$$

and substitute that result into equation (2.16a) to obtain a single equation for Ψ^{+}:

$$-\Omega\cdot\nabla\frac{1}{\sigma_t}\Omega\cdot\nabla\Psi^{+} + \sigma_t\Psi^{+} = \frac{\sigma_s\Phi + Q}{4\pi}. \tag{2.18}$$

Φ can be recovered from the even-parity angular flux via equation (2.15a). Similarly, we can solve equation (2.16a) for Ψ^{+}:

$$\Psi^{+}(\mathbf{r},\Omega) = \frac{\sigma_s(\mathbf{r})\Phi(\mathbf{r}) + Q(\mathbf{r})}{4\pi\sigma_t} - \frac{1}{\sigma_t}\Omega\cdot\nabla\Psi^{-}(\mathbf{r},\Omega), \tag{2.19}$$

and substitute that result into equation (2.16b) to obtain an equation involving both Ψ^{-} and Φ:

$$-\Omega\cdot\nabla\frac{1}{\sigma_t}\Omega\cdot\nabla\Psi^{-} + \sigma_t\Psi^{-} = \Omega\cdot\nabla\Big(\frac{\sigma_s\Phi + Q}{4\pi\sigma_t}\Big). \tag{2.20a}$$

Unlike the even-parity case, here we need another equation to relate Ψ^{-} and Φ. Therefore,

we integrate equation (2.16a) over angle to obtain:

$$\nabla \cdot \mathbf{J} + \sigma_t \Phi = \sigma_s \Phi + Q, \tag{2.20b}$$

where **J** is given by equation (2.15b). Finally, we note that if anisotropic scattering were present we would need a second equation to relate even-parity angular flux to the current.

Now we must address boundary conditions. We manipulate the known incident boundary condition into a form that can be incorporated *naturally* into finite element discretizations. From equations (2.7), (2.14) and (2.17) we see that for $\mathbf{r} \in \partial \mathbf{D_i}$ and $\mathbf{n} \cdot \Omega < 0$:

$$\begin{aligned} \Psi(\mathbf{r},\Omega) &= F(\mathbf{r},\Omega) \\ \Psi^+(\mathbf{r},\Omega) + \Psi^-(\mathbf{r},\Omega) &= F(\mathbf{r},\Omega) \\ \Psi^+(\mathbf{r},\Omega) - \frac{1}{\sigma_t}\Omega \cdot \nabla \Psi^+(\mathbf{r},\Omega) &= F(\mathbf{r},\Omega). \end{aligned} \tag{2.21}$$

For $\mathbf{r} \in \partial \mathbf{D_i}$, it is obvious that:

$$\begin{aligned} \frac{1}{\sigma_t}\Omega \cdot \nabla \Psi^+(\mathbf{r},\Omega) &= \Big[\Psi^+(\mathbf{r},\Omega) - F(\mathbf{r},\Omega)\Big] \quad \text{for } \mathbf{n}\cdot\Omega < 0 \\ &= -\Big[\Psi^+(\mathbf{r},\Omega) - F(\mathbf{r},-\Omega)\Big] \quad \text{for } \mathbf{n}\cdot\Omega > 0. \end{aligned}$$

If we make the even angular extension of $F(\mathbf{r},\Omega)$ for outgoing angles:

$$F^+(\mathbf{r},\Omega) = \begin{cases} F(\mathbf{r},\Omega) & \text{for } \mathbf{n}\cdot\Omega < 0 \\ F(\mathbf{r},-\Omega) & \text{for } \mathbf{n}\cdot\Omega > 0 \end{cases}$$

we can write the boundary condition for all angles in the following compact form:

$$(\mathbf{n}\cdot\Omega)\Big(\frac{1}{\sigma_t}\Omega\cdot\nabla\Psi^+\Big) = -|\mathbf{n}\cdot\Omega|\Big(\Psi^+ - F^+\Big) \quad \text{for } \mathbf{r} \in \partial\mathbf{D_i}. \tag{2.22}$$

We follow a similar procedure to the derive the odd-parity boundary condition. Here,

we have for $\mathbf{r} \in \partial\mathbf{D_i}$:

$$\begin{aligned}\frac{1}{\sigma_t}\Omega\cdot\nabla\Psi^-(\mathbf{r},\Omega)-\frac{\sigma_s\Phi+Q}{4\pi\sigma_t} &= \Big[\Psi^-(\mathbf{r},\Omega)-F(\mathbf{r},\Omega)\Big] \quad \text{for } \mathbf{n}\cdot\Omega<0\\ &= \Big[-\Psi^-(\mathbf{r},\Omega)-F(\mathbf{r},-\Omega)\Big] \quad \text{for } \mathbf{n}\cdot\Omega>0.\end{aligned}$$

Then, if we make the odd angular extension of $F(\mathbf{r},\Omega)$:

$$F^-(\mathbf{r},\Omega)=\begin{cases}F(\mathbf{r},\Omega) & \text{for } \mathbf{n}\cdot\Omega<0\\ -F(\mathbf{r},-\Omega) & \text{for } \mathbf{n}\cdot\Omega>0\end{cases}$$

we obtain the desired form of the odd-parity boundary condition:

$$(\mathbf{n}\cdot\Omega)\Big(\frac{1}{\sigma_t}\Omega\cdot\nabla\Psi^- - \frac{\sigma_s\Phi+Q}{4\pi\sigma_t}\Big) = -|\mathbf{n}\cdot\Omega|(\Psi^- - F^-) \quad \text{for } \mathbf{r}\in\partial\mathbf{D_i}. \tag{2.23}$$

To summarize, we rewrite the even- and odd-parity equations and their boundary conditions. The even-parity system is:

$$-\Omega\cdot\nabla\frac{1}{\sigma_t}\Omega\cdot\nabla\Psi^+ + \sigma_t\Psi^+ = \frac{\sigma_s\Phi+Q}{4\pi}, \tag{2.24a}$$

$$(\mathbf{n}\cdot\Omega)\Big(\frac{1}{\sigma_t}\Omega\cdot\nabla\Psi^+\Big) = -|\mathbf{n}\cdot\Omega|\Big(\Psi^+ - F^+\Big) \quad \text{for } \mathbf{r}\in\partial\mathbf{D}. \tag{2.24b}$$

The odd-parity system is:

$$-\Omega\cdot\nabla\frac{1}{\sigma_t}\Omega\cdot\nabla\Psi^- + \sigma_t\Psi^- = \Omega\cdot\nabla\Big(\frac{\sigma_s\Phi+Q}{4\pi\sigma_t}\Big), \tag{2.25a}$$

$$\nabla\cdot\mathbf{J} + \sigma_t\Phi = \sigma_s\Phi + Q, \tag{2.25b}$$

$$(\mathbf{n}\cdot\Omega)\Big(\frac{1}{\sigma_t}\Omega\cdot\nabla\Psi^- - \frac{\sigma_s\Phi+Q}{4\pi\sigma_t}\Big) = -|\mathbf{n}\cdot\Omega|(\Psi^- - F^-) \quad \text{for } \mathbf{r}\in\partial\mathbf{D}. \tag{2.25c}$$

Equations (2.24) and (2.25) completely specify the parity systems that we will discretize in

Chapter III. Note that we have replaced $\partial\mathbf{D_i}$ with $\partial\mathbf{D}$. That is, we will only consider known incident boundary conditions in the remainder of this work. Reflective boundary conditions result in fully implicit coupling between the incoming and outgoing directions. This is not the case for first order forms of the transport equation and is a significant disadvantage of the parity equations.

2. The Self-Adjoint Angular Flux Equation

The so-called self-adjoint angular flux equation has recently been suggested as a basis for numerical transport methods [4]. Though this equation was initially proposed in the context of improving standard P_1 theory [7] in the early 1960s, it has received little attention. Ackroyd [47] identified the SAAF through a least-squares solution procedure for the first order transport equation. We stress that the fundamental unknown in the SAAF is the full-range angular flux.

The derivation presented by Morel and McGhee [4] is simple. We rearrange the first order transport equation:

$$\Psi = \frac{\sigma_s\Phi + Q}{4\pi\sigma_t} - \frac{1}{\sigma_t}\Omega\cdot\nabla\Psi,$$

and substitute this back into the streaming term of the transport equation to obtain the self-adjoint angular flux equation:

$$-\Omega\cdot\nabla\frac{1}{\sigma_t}\Omega\cdot\nabla\Psi + \sigma_t\Psi = \frac{\sigma_s\Phi + Q}{4\pi} - \Omega\cdot\nabla\left(\frac{\sigma_s\Phi + Q}{4\pi\sigma_t}\right). \tag{2.26}$$

We note that it is of the same basic form as the parity equations. Further, since the fundamental unknown is simply the angular flux, we need not manipulate the boundary conditions. That means that all of the boundary conditions, including reflective boundary conditions, can be implemented in the same way they are for the first order transport equation. We must, however, also specify boundary conditions for *outgoing* angles. We simply

require that the outgoing angular flux on the boundary satisfy the first order form of the transport equation:

$$\Omega \cdot \nabla \Psi(\mathbf{r},\Omega) + \sigma_t \Psi(\mathbf{r},\Omega) = \frac{\sigma_s \Phi(\mathbf{r}) + Q(\mathbf{r})}{4\pi} \quad \text{for } \mathbf{r} \in \partial\mathbf{D} \text{ and } \mathbf{n}\cdot\Omega > 0. \tag{2.27}$$

This is analogous to the extensions of the boundary data we make for the even- and odd-parity equations, and is discussed more fully in the next section.

3. General Properties of Second Order Forms of the Transport Equation

There are several unique characteristics of second order forms of the transport equation that we should be consider before proceeding. As we have already noted, the streaming operators now involve second derivatives. The first order within-group equation is a hyperbolic first order partial differential equation, while the parity equations and SAAF equation are parabolic second order PDEs. This has two important consequences. First, the second order equations actually have more possible solutions than the first order system. For a purely absorbing, within-group slab problem, the first order equation has a solution of the form $Ae^{-\sigma_t x/\mu}$ while the second order forms admit both $Ae^{-\sigma_t x/\mu}$ and $Be^{\sigma_t x/\mu}$. Second, correspondingly more boundary conditions are required to damp the non-physical solutions. This is the reason we must enforce boundary conditions for outgoing angles in second order formulations.

Since the second order systems involve boundary conditions for outgoing directions, it is possible for discretized forms to violate directional causality. That is, it is possible for solutions in one region of a problem to depend non-physically upon downstream information.

The presence of the total cross section in the denominator of the streaming term makes the treatment of voids difficult. This has been considered by Ackroyd, Issa and Riyait [47] with some success. It is clear, however, that this is a significant disadvantage peculiar to

second order forms of the transport equation.

Finally, discretizations of second order forms of the transport equation typically require the inversion of SPD matrices, whereas first order forms often lead to block-lower triangular matrices that can be solved very rapidly by sweeping methods. Whether this is an advantage or disadvantage depends on the type of problem being considered. For example, on an unstructured mesh in 3D, it may be very difficult to sweep the mesh even with serial algorithms. Additionally, efficient parallel implementations of sweeping routines on grids of this type have yet to be developed, so it may, in fact, be more efficient to use well-established parallel iterative methods on the SPD matrices that result from second order transport discretizations.

C. Coupled First Order Forms

We now briefly discuss the coupled first order systems of equations that will be the bases of the mixed finite element transport discretizations that we will develop in Chapter IV. One factor motivating the forms we consider is that they should allow vector current unknowns to be spatially located on cell faces and scalar flux unknowns to be located in cell centers.

1. The Coupled Parity Equations

Our starting point will be the coupled even- and odd-parity system in equations (2.16). We define the odd-parity angular current density to be:

$$\mathbf{G}^{-}(\mathbf{r},\Omega) = \Omega\Psi^{-}(\mathbf{r},\Omega), \tag{2.28}$$

then multiply equation 2.16b by Ω to obtain:

$$\nabla\cdot\mathbf{G}^{-} + \sigma_t\Psi^{+} = \frac{\sigma_s\Phi + Q}{4\pi}, \tag{2.29a}$$

$$\nabla \cdot \Omega\Omega\Psi^{+} + \sigma_t \mathbf{G}^{-} = 0. \tag{2.29b}$$

To obtain the appropriate boundary condition, we simply multiply equation (2.25c) by Ω:

$$(\mathbf{n}\cdot\Omega)\Omega\Big(\frac{1}{\sigma_t}\nabla\cdot\mathbf{G}^{-} - \frac{\sigma_s\Phi + Q}{4\pi\sigma_t}\Big) = -|\mathbf{n}\cdot\Omega|(\mathbf{G}^{-} - \Omega F^{-}) \quad \text{for } \mathbf{r}\in\partial\mathbf{D}. \tag{2.29c}$$

To our knowledge, no numerical transport methods have been based upon equations (2.29). The fundamental unknowns in this system are the even-parity angular flux, Ψ^{+}, and odd-parity angular current density, $\mathbf{G}^{-}$. The odd-parity angular flux can be recovered from $\mathbf{G}^{-}$ with the following relation:

$$\Psi^{-}(\mathbf{r},\Omega) = \Omega\cdot\mathbf{G}^{-}(\mathbf{r},\Omega),$$

since $\Omega\cdot\Omega = 1$.

2. The Angular Flux-Angular Current Density Equations

We now consider a method for recasting the first order transport equation into a coupled system of equations involving a scalar and a vector unknown. First, we rewrite equation (2.2) using the definition of the angular current density in equation (2.5) then we multiply equation (2.2) by Ω to obtain a coupled set of equations with the angular flux and angular current density as their unknowns:

$$\nabla\cdot\mathbf{G} + \sigma_t\Psi = \frac{\sigma_s\Phi + Q}{4\pi} \tag{2.30a}$$

$$\nabla\cdot\Omega\Omega\Psi + \sigma_t\mathbf{G} = \Omega\frac{\sigma_s\Phi + Q}{4\pi} \tag{2.30b}$$

We will refer to equations (2.30) as the angular flux-angular current density (AFACD) equations. We note that if we were to assume that the angular flux was linearly anisotropic and integrate equations (2.30) over angle, we would obtain the standard P_1 equations. The

boundary condition for equation (2.30b) is written in a form that allows us to incorporate it naturally in a finite element system. That is, for $\mathbf{r} \in \partial\mathbf{D}$:

$$\mathbf{G}_b(\mathbf{r},\Omega) = \Omega\Psi(\mathbf{r},\Omega) = \begin{cases} \Omega F(\mathbf{r},\Omega) & \text{for } \mathbf{n}\cdot\Omega < 0 \\ \mathbf{G} & \text{for } \mathbf{n}\cdot\Omega > 0. \end{cases} \tag{2.30c}$$

The condition for $\mathbf{n}\cdot\Omega > 0$ corresponds to requiring the angular flux to satisfy the first order transport equation for outgoing directions. Reflective boundary conditions can be incorporated by simply setting $F(\mathbf{r},\Omega)$ equal to $\Psi(\mathbf{r},\Omega')$ where Ω' is the direction that reflects onto Ω at the point $\mathbf{r}$.

D. The Asymptotic Diffusion Limit of the Transport Equation

The asymptotic behavior of the analytic transport equation for thick diffusive problems is well established [51, 25, 52, 30]. Adams [1] extended analyses of this type to include problems that contain adjacent diffusive and non-diffusive regions. In this section, we will review the properties of the analytic transport equation for problems that contain regions that are optically thick and diffusive.

1. Solution of the Transport Equation in the Diffusion Limit

Let us again consider the first order within-group transport equation with a known incident boundary condition:

$$\Omega\cdot\nabla\Psi + \sigma_t(\mathbf{r})\Psi(\mathbf{r},\Omega) = \frac{\sigma_s(\mathbf{r})\Phi(\mathbf{r}) + Q(\mathbf{r})}{4\pi} \quad \text{for } \mathbf{r}\in\mathbf{D}, \tag{2.31a}$$

$$\Psi(\mathbf{r},\Omega) = F(\mathbf{r},\Omega) \quad \text{for } \mathbf{r}\in\partial\mathbf{D} \text{ and } \mathbf{n}\cdot\Omega < 0. \tag{2.31b}$$

We now introduce the following scaling:

$$\sigma_t \rightarrow \frac{\sigma_t}{\varepsilon} \tag{2.32a}$$

$$\sigma_a \rightarrow \varepsilon\sigma_a \tag{2.32b}$$

$$\sigma_s \rightarrow \frac{\sigma_t}{\varepsilon} - \varepsilon\sigma_a \tag{2.32c}$$

$$Q \rightarrow \varepsilon Q, \tag{2.32d}$$

where σ_t, σ_a and Q are all O(1). Thus, as $\varepsilon \rightarrow 0$ the total cross section becomes very large so that a problem of fixed physical dimensions becomes thick in terms of particle mean free paths. Further, the rates at which particles are added to the system through sources and removed from the system through absorption become small. Physically, we expect these conditions to result in a diffusive particle transport problem. This particular scaling possesses several important properties [29] that make this heuristic argument more precise. First, the infinite medium solution, Q/σ_a, and the diffusion length, $(3\sigma_a\sigma_t)^{-\frac{1}{2}}$, are both O(1). More importantly, the diffusion equation itself is *invariant* under this scaling. Now we apply the above scaling to equation (2.31a):

$$\Omega \cdot \nabla\Psi + \frac{\sigma_t}{\varepsilon}\Psi = \frac{\left(\frac{\sigma_t}{\varepsilon} - \varepsilon\sigma_a\right)\Phi + \varepsilon Q}{4\pi}. \tag{2.33}$$

We propose the following ansatz for our solution:

$$\Psi = \Psi^{[0]} + \varepsilon\Psi^{[1]} + \varepsilon^2\Psi^{[2]} + ..., \tag{2.34a}$$

$$\Phi = \Phi^{[0]} + \varepsilon\Phi^{[1]} + \varepsilon^2\Phi^{[2]} + ... \quad \text{where } \Phi^{[k]} = \int_{4\pi} \Psi^{[k]}\, d\Omega. \tag{2.34b}$$

We insert the ansatz into the scaled transport equation and require the resulting equations to hold for terms of like order. The $O(1/\varepsilon)$ equation is:

$$\sigma_t \Psi^{[0]} = \frac{\sigma_t \Phi^{[0]}}{4\pi}. \tag{2.35}$$

Thus, our first important result is that the leading order angular flux is isotropic. Now, we write the O(1) equation:

$$\Omega \cdot \nabla \Psi^{[0]} + \sigma_t \Psi^{[1]} = \frac{\sigma_t \Phi^{[1]}}{4\pi}, \tag{2.36}$$

and take its first angular moment to obtain *Fick's Law*:

$$\mathbf{J}^{[1]}(\mathbf{r}) = -\frac{1}{3\sigma_t} \nabla \Phi^{[0]}(\mathbf{r}) \quad \text{where we have defined } \mathbf{J}^{[k]} = \int_{4\pi} \Omega \Psi^{[k]} \, d\Omega. \tag{2.37}$$

The $O(\varepsilon)$ equation is:

$$\Omega \cdot \nabla \Psi^{[1]} + \sigma_t \Psi^{[2]} = \frac{\sigma_t \Phi^{[2]} - \sigma_a \Phi^{[0]} + Q}{4\pi}. \tag{2.38}$$

Finally, we take the zeroth angular moment of the $O(\varepsilon)$ equation and use equation (2.37) to find that the leading order scalar flux satisfies the following diffusion equation:

$$-\nabla \cdot \frac{1}{3\sigma_t} \nabla \Phi^{[0]} + \sigma_a \Phi^{[0]} = Q. \tag{2.39a}$$

Equation (2.39a) describes the behavior of the leading order solution in the problem interior. Now, we must determine what boundary condition the leading order equation satisfies. First, we note that there is a complicated boundary layer of thickness $O(\varepsilon)$. We make no attempt, however, to explicitly model the boundary layer. Rather, we derive a boundary value that yields the correct interior solution. This is facilitated by recognizing that the boundary layer in a thick diffusive problem is described by a purely scattering half-space problem [51, 25, 52, 30]. Analytic solutions to such problems do exist [53]. The resulting

boundary condition is given by:

$$\Phi^{[0]}(\mathbf{r}) = 2 \int_{\mathbf{n}\cdot\Omega<0} W(|\mathbf{n}\cdot\Omega|) f(\mathbf{r},\Omega)\, d\Omega \quad \text{for } \mathbf{r} \in \partial\mathbf{D}. \tag{2.39b}$$

$W(|\mathbf{n}\cdot\Omega|)$ depends on Chandrasekhar's H-function and is well approximated by a simple polynomial:

$$W(|\mathbf{n}\cdot\Omega|) = \frac{\sqrt{3}}{2}|\mathbf{n}\cdot\Omega| H(|\mathbf{n}\cdot\Omega|) \simeq |\mathbf{n}\cdot\Omega| + \frac{3}{2}|\mathbf{n}\cdot\Omega|^2. \tag{2.39c}$$

In summary, the leading order solution of the transport equation (a first order hyperbolic equation) satisfies the diffusion equation (a second order elliptic equation) as the scaling parameter $\varepsilon \to 0$. Further, despite the presence of a complicated boundary layer, we can obtain the correct interior solution by using a simple weighted integral of the known incident angular flux. While this is an intuitive result, the implications for discretized problems are significant. A discrete transport solution will not be accurate for thick diffusive problems unless its leading order solution satisfies a reasonable discretization of the diffusion system shown in equations (2.39) [29].

2. Solution of the Transport Equation at an Internal Interface

We now turn our attention to an idealized problem containing adjacent diffusive and non-diffusive regions as shown in Fig. 2. This analysis was originally performed by Adams [1]. We denote the boundary between the two regions as $\partial\mathbf{D}_{dt}$ with a normal $\mathbf{n}_d$ that points out of the diffusive region and into the transport region. We also define $\mathbf{n}_t$ as $-\mathbf{n}_d$, so that it points out of the transport region and into the diffusive region.

We begin by applying the scaling shown in equation (2.34) to the diffusive portion of the problem. We then simply note that our results in the previous section directly apply to

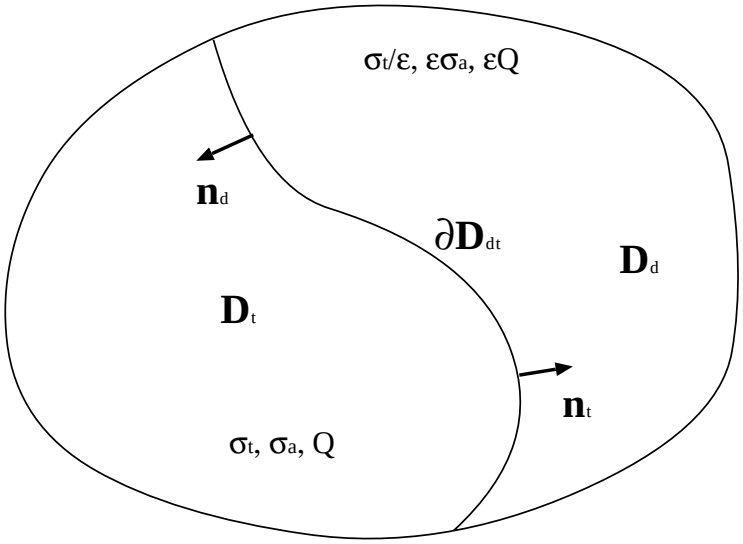

Fig. 2. An arbitrary spatial domain with an internal interface.

the leading order solution in this region. These are:

$$\sigma_t \Psi^{[0]} = \frac{\sigma_t \Phi^{[0]}}{4\pi} \quad \text{for } \mathbf{r} \in \mathbf{D}_d \tag{2.40a}$$

$$-\nabla \cdot \frac{1}{3\sigma_t} \nabla \Phi^{[0]} + \sigma_a \Phi^{[0]} = Q \quad \text{for } \mathbf{r} \in \mathbf{D}_d \tag{2.40b}$$

$$\Phi^{[0]}(\mathbf{r}) = 2 \int\limits_{\mathbf{n}_d \cdot \Omega < 0} W(|\mathbf{n}_d \cdot \Omega|) \Psi^{[0]}(\mathbf{r}, \Omega)\, d\Omega \quad \text{for } \mathbf{r} \in \partial \mathbf{D}_{dt}. \tag{2.40c}$$

In this expression, $\Psi^{[0]}(\mathbf{r}, \Omega)$ is the as yet unknown angular flux leaving the transport region and entering the diffusive region. Now, we consider the transport region. Obviously, since we do not apply the diffusion scaling to the transport equation in this region, the leading order solution satisfies the transport equation. The development of the boundary condition is more involved. Here we must determine the value of the angular flux entering $\mathbf{D}_t$ through $\partial \mathbf{D}_{dt}$ as a function of the flux leaving $\mathbf{D}_t$ through $\partial \mathbf{D}_{dt}$. To leading order this is corresponds to the problem of determining the albedo of a half-space, which has been

solved analytically [43]. Therefore we have:

$$\Omega \cdot \nabla \Psi^{[0]} + \sigma_t \Psi^{[0]} = \frac{\sigma_t \Phi^{[0]} + Q}{4\pi}, \tag{2.41a}$$

subject to an albedo condition for $\mathbf{r} \in \partial \mathbf{D}_{dt}$ and $\mathbf{n}_t \cdot \Omega < 0$

$$\Psi^{[0]}(\mathbf{r}, \Omega) = \frac{1}{2\pi} \int\limits_{\mathbf{n}_t \cdot \Omega' > 0} \alpha(\mu, \mu') \Psi^{[0]}(\mathbf{r}, \Omega')\, d\Omega' \quad \text{where } \mu = |\mathbf{n}_t \cdot \Omega|. \tag{2.41b}$$

The albedo, $\alpha(\mu, \mu')$, is given by:

$$\alpha(\mu, \mu') = \left[\frac{W(\mu')}{\mu + \mu'}\right] \Big/ \left[\int\limits_0^1 \frac{W(y)}{y + \mu}\, dy\right] \quad \text{where } 0 \leq \mu, \mu' \leq 1. \tag{2.42}$$

$W(\mu)$ is the weight function shown equation (2.39c). Note that the albedo boundary condition is a function of both the incoming and outgoing angle.

E. The Within Group Iteration

As we have noted, the transport equation is an integro-differential equation that is usually solved iteratively when $\sigma_s > 0$. In this section, we will discuss issues related to the iterative solutions of such problems.

1. Source Iteration

Let us consider the slab geometry transport equation:

$$\mu \frac{\partial}{\partial x} \Psi + \sigma_t \Psi(x, \mu) = \frac{1}{2} \sigma_s \Phi(x) + \frac{1}{2} Q(x) \quad \text{where } \mu = \Omega \cdot \mathbf{e}_{\mathbf{x}}, \tag{2.43a}$$

$$\Phi(x) = \int_{-1}^{1} \Psi(x, \mu)\, d\mu. \tag{2.43b}$$

A very simple approach for solving equations (2.43) would be to guess the value of the scalar flux ($\Phi^{(0)}(x) = 0$, for example), solve equation (2.43a) for the angular flux, then use

equation (2.43b) to update the scalar flux:

$$\mu\frac{\partial}{\partial x}\Psi^{(\ell+1/2)}+\sigma_t\Psi^{(\ell+1/2)}(x,\mu)=\frac{1}{2}\sigma_s\Phi^{(\ell)}(x)+\frac{1}{2}Q(x), \tag{2.44a}$$

$$\Phi^{(\ell+1)}(x)=\int_{-1}^{1}\Psi^{(\ell+1/2)}(x,\mu)\,d\mu. \tag{2.44b}$$

This process is known as *source iteration* and is closely related to Neumann iteration [44, 45]. When source iteration (SI) is applied to a discretized system, it is, in fact, equivalent to stationary Richardson iteration [54]. We will discuss this in more detail in Chapter V.

The iteration described in equations (2.44) is carried out until some measure of the error is less than a prescribed tolerance. Often, the infinity- or 2-norm of the relative difference between successive iterates is used as the error measure. The rate at which an iterative method converges is governed by the spectral radius, ρ, which is the largest eigenvalue of the iteration operator (or iteration matrix for discretized problems). If $\hat{\Phi}^{(\ell)}=\Phi-\Phi^{(\ell)}$ is the difference between the exact solution and the current iterate, we may write:

$$\rho\sim\frac{\|\hat{\Phi}^{(\ell+1)}\|_2}{\|\hat{\Phi}^{(\ell)}\|_2}\quad\text{for large }\ell. \tag{2.45}$$

In practice, since we do not know the exact solution *a priori*, we will often use the following relation to estimate the spectral radius:

$$\rho\simeq\sqrt{\frac{\|\Phi^{(\ell+1)}-\Phi^{(\ell)}\|_2}{\|\Phi^{(\ell-1)}-\Phi^{(\ell-2)}\|_2}}. \tag{2.46}$$

If we assume that the angular and spatial portions of the solution to equations (2.43) are separable then we can determine the spectral radius of SI analytically with an infinite medium Fourier analysis. We assume constant material properties and define the iteration

errors:

$$\hat{\Psi}^{(\ell+1/2)} = \Psi - \Psi^{(\ell+1/2)}, \tag{2.47a}$$

$$\hat{\Phi}^{(\ell)} = \Phi - \Phi^{(\ell)}, \tag{2.47b}$$

where Ψ and Φ are the converged angular and scalar fluxes, respectively. We now subtract equations (2.44) from (2.43) to obtain:

$$\mu\frac{\partial}{\partial x}\hat{\Psi}^{(\ell+1/2)} + \sigma_t\hat{\Psi}^{(\ell+1/2)}(x,\mu) = \frac{c\sigma_t}{2}\hat{\Phi}^{(\ell)}(x), \tag{2.48a}$$

$$\hat{\Phi}^{(\ell+1)}(x) = \int_{-1}^{1}\hat{\Psi}^{(\ell+1/2)}(x,\mu)\,d\mu, \tag{2.48b}$$

where we have noted that $c\sigma_t = \sigma_s$ At this point, we insert the standard Fourier ansatz:

$$\hat{\Psi}^{(\ell+1/2)} = \omega^{\ell}(\lambda)a(\lambda,\mu)e^{\imath\lambda\sigma_t x}, \tag{2.49a}$$

$$\hat{\Phi}^{(\ell)} = \omega^{\ell}(\lambda)A(\lambda)e^{\imath\lambda\sigma_t x} \tag{2.49b}$$

where

$$\imath = \sqrt{-1} \quad \text{and} \quad -\infty < \lambda < \infty. \tag{2.49c}$$

After substituting the above ansatz into equations (2.48), we find that:

$$a(\lambda,\mu) = \frac{cA(\lambda)}{2}\frac{1}{1+\imath\lambda\mu}, \tag{2.50}$$

and

$$\omega(\lambda) = c\int_0^1 \frac{d\mu}{1+\lambda^2\mu^2}. \tag{2.51}$$

Therefore, the SI spectral radius is:

$$\rho_{si} = \sup_{\lambda} |\omega(\lambda)| = c \quad \text{for } \lambda = 0. \tag{2.52}$$

This means that for highly scattering problems (c close to unity), source iteration can converge very slowly. We note that the $\lambda = 0$ mode is not present in finite problems, so source iteration will converge for $c \leq 1$, though the iteration eigenvalues remain near unity for small values of λ. This analysis also shows that the eigenfunctions associated with the slowest converging modes are nearly linear functions of angle [36]. That is:

$$a(\lambda, \mu) = \frac{cA(\lambda)}{2} \frac{1}{1 + \imath\lambda\mu} \simeq \frac{cA(\lambda)}{2}(1 - \imath\lambda\mu) \quad \text{for } \lambda \text{ near } 0. \tag{2.53}$$

There is an insightful physical principle underlying the convergence behavior of the source iteration system. If we begin our SI solution by guessing $\Phi^{(0)}(x) = 0$, then $\Phi^{(\ell)}(x)$ represents the scalar flux due to particles that have had no more than $\ell - 1$ collisions since birth. For a thick, diffusive problem, particles will undergo many collisions prior to being absorbed or leaking from the system, so we expect ℓ to become very large before $\Phi^{(\ell)}(x)$ reaches the correct solution.

2. Diffusion Synthetic Acceleration

The diffusion synthetic acceleration (DSA) method [32, 33, 34, 35, 55, 56, 36, 57] is a well known and powerful method for accelerating the convergence of the within group iteration. It is motivated by the fact that the slowest converging error modes in equations (2.44) are linear in angle.

We begin be defining the following additive corrections:

$$\gamma^{(\ell+1/2)}(x, \mu) = \Psi(x, \mu) - \Psi^{(\ell+1/2)}(x, \mu), \tag{2.54a}$$

$$\Gamma^{(\ell+1/2)}(x) = \Phi(x) - \Phi^{(\ell+1/2)}(x) \quad \left(= \int_{-1}^{1} \gamma^{(\ell+1/2)}(x,\mu)\, d\mu \right), \tag{2.54b}$$

where

$$\Phi^{(\ell+1/2)}(x) = \int_{-1}^{1} \Psi^{(\ell+1/2)}(x,\mu)\, d\mu.$$

Now, we subtract equation (2.44a) from (2.43a) to obtain an equation for the additive corrections. We stress that this equation is exact and is as difficult to solve as the original problem. We have:

$$\mu \frac{\partial}{\partial x} \gamma^{(\ell+1/2)} + \sigma_t \gamma^{(\ell+1/2)}(x,\mu) - \frac{c\sigma_t}{2} \Gamma^{(\ell+1/2)}(x) = \frac{c\sigma_t}{2} \left[\Phi^{(\ell+1/2)}(x) - \Phi^{(\ell)}(x) \right] \tag{2.55}$$

Now, we make use of the observation in the previous section that the slowest converging error modes are nearly linear in angle. Thus, they would be well approximated by a diffusion solution. This suggests that we simply replace equation (2.55) with its diffusion approximation. The DSA iterative scheme may then be written in the following form:

$$\mu \frac{\partial}{\partial x} \Psi^{(\ell+1/2)} + \sigma_t \Psi^{(\ell+1/2)}(x,\mu) = \frac{1}{2} \sigma_s \Phi^{(\ell)}(x) + \frac{1}{2} Q(x), \tag{2.56a}$$

$$\Phi^{(\ell+1/2)}(x) = \int_{-1}^{1} \Psi^{(\ell+1/2)}(x,\mu)\, d\mu, \tag{2.56b}$$

$$-\frac{\partial}{\partial x} \frac{1}{3\sigma_t} \frac{\partial}{\partial x} \Gamma^{(\ell+1/2)} + \sigma_t (1-c) \Gamma^{(\ell+1/2)}(x) = c\sigma_t \left[\Phi^{(\ell+1/2)}(x) - \Phi^{(\ell)}(x) \right] \tag{2.56c}$$

$$\Phi^{(\ell+1)}(x) = \Phi^{(\ell+1/2)}(x) + \Gamma^{(\ell+1/2)}(x). \tag{2.56d}$$

Equations (2.56) have been analyzed [36] and we will simply report the results:

$$\omega(\lambda) = \frac{\lambda^2 c}{\lambda^2 + 3(1-c)} \int_{-1}^{1} \frac{1-3\mu^2}{1+\lambda^2\mu^2}\, d\mu. \tag{2.57}$$

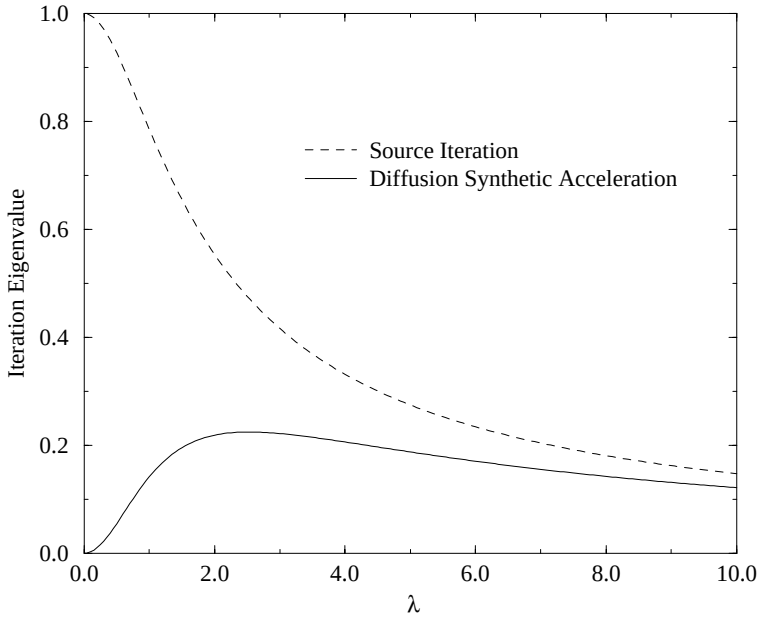

Fig. 3. Slab geometry DSA/SI iteration eigenvalues with c=1.

Therefore, the DSA spectral radius is:

$$\rho_{dsa} = \sup_{\lambda} |\omega(\lambda)| \leq 0.2247c. \tag{2.58}$$

The DSA iteration eigenvalues are shown along with the correspond SI iteration eigenvalues in Fig. 3. Clearly, DSA significantly improves the convergence of the within-group iteration. For example, suppose we have a problem with a scattering ratio of 0.99999. If the error needs to be reduced by a factor of 10^5, then the approximate number for iterations is:

$$N_{si} \simeq \frac{ln(10^{-5})}{ln(0.99999)} = 1,150,000 \text{ iterations.}$$

For the DSA method, the approximate number of iterations is:

$$N_{dsa} \simeq \frac{ln(10^{-5})}{ln(0.2247)} = 8 \text{ iterations.}$$

Clearly, DSA can be an extremely powerful acceleration scheme, reducing the number of iterations in our example by 5 orders of magnitude.

Adams and Wareing [57] have analyzed DSA for more general multidimensional spatially analytic problems. They found that in 2D and 3D, the DSA spectral radius is bounded by 0.5. Further, they found that DSA becomes unstable for highly forward peaked scattering or if the angular quadrature set does not exactly integrate linear functions of angle. Finally, if the within-group problem is symmetric positive definite under some norm, established methods like the preconditioned conjugate gradient method can be successfully applied.

In this chapter we have discussed the properties of the first order form of the transport equation and derived the second order forms that we discretize in Chapters III and IV. We have also discussed the behavior of the transport equation in thick diffusive problems and outlined the iterative solution techniques used for the within-group problem. We now prepared to begin our discretization and analysis.

CHAPTER III

CONTINUOUS FINITE ELEMENT DISCRETIZATION AND ANALYSIS

In this chapter, we develop the continuous finite element approximations to the parity equations and the SAAF equation. For each system, we begin in general 3D Cartesian geometry then reduce to slab geometry. We then show that the sum of the discretized parity equations is algebraically equivalent to the discretized SAAF equation in the problem interior. Further, we derive the relationship between the SAAF system and the parity equations on boundaries. The behavior of the discretized systems is analyzed in the thick diffusion limit for both completely diffusive problems and problems with adjacent diffusive and non-diffusive regions. We conclude this chapter with a discussion of several issues that arise during implementation and partially motivate the mixed finite element discretization we discuss in Chapter IV.

We use upper case $F(\mathbf{r},\Omega)$ and $Q(\mathbf{r},\Omega)$ for the analytic known incident boundary condition and source. In this chapter, the lower case $f(\mathbf{r},\Omega)$ and $q(\mathbf{r},\Omega)$ denote the projections of these functions onto the appropriate finite element spaces. It is important to expand $q(\mathbf{r},\Omega)$ in the same space as the within-group scattering source since it can contain inscattering information from other energy groups.

A. Even-Parity

We now use the weighted residual method to develop the even-parity CFEM discretization. This involves multiplying the analytic even-parity equation by a set of weight functions then requiring the resulting systems to hold in an integral sense over the problem domain. We then expand the analytic unknowns in a series of basis functions, which ultimately reduces our original problem to a system of linear equations. Recall the analytic within-

group even-parity equation and its boundary condition, as shown in equation (2.24):

$$-\Omega\cdot\nabla\frac{1}{\sigma_t}\Omega\cdot\nabla\Psi^+ + \sigma_t\Psi^+ = \frac{\sigma_s\Phi+Q}{4\pi}, \tag{3.1a}$$

$$(\mathbf{n}\cdot\Omega)\left(\frac{1}{\sigma_t}\Omega\cdot\nabla\Psi^+\right) = -|\mathbf{n}\cdot\Omega|\left(\Psi^+ - F^+\right) \quad \text{for } \mathbf{r}\in\partial\mathbf{D}. \tag{3.1b}$$

Here, Ψ^+ and Φ will naturally exist in the same finite element space upon discretization.

1. XYZ Geometry

We begin by multiplying equation (3.1a) by a set of linearly independent weight functions $(w_i^+(\mathbf{r}), 1\le i\le I)$. We then integrate over the problem domain $\mathbf{D}$. For each weight function, we obtain an equation of the form:

$$-\int_{\mathbf{D}}\Omega\cdot\nabla\frac{1}{\sigma_t}\Omega\cdot\nabla\Psi^+ w_i^+\,dV + \int_{\mathbf{D}}\sigma_t\Psi^+ w_i^+\,dV = \int_{\mathbf{D}}\frac{\sigma_s\Phi+Q}{4\pi}w_i^+\,dV. \tag{3.2}$$

We now apply the vector identity

$$\nabla\cdot\left(f\mathbf{A}\right) = f\left(\nabla\cdot\mathbf{A}\right) + \mathbf{A}\cdot\left(\nabla f\right), \tag{3.3}$$

to the streaming term of equation (3.2) to get:

$$-\int_{\mathbf{D}}\nabla\cdot\left(w_i^+\Omega\frac{1}{\sigma_t}\Omega\cdot\nabla\Psi^+\right)dV + \int_{\mathbf{D}}(\Omega\cdot\nabla w_i^+)\frac{1}{\sigma_t}(\Omega\cdot\nabla\Psi^+)\,dV + \int_{\mathbf{D}}\sigma_t\Psi^+ w_i^+\,dV = \int_{\mathbf{D}}\frac{\sigma_s\Phi+Q}{4\pi}w_i^+\,dV. \tag{3.4}$$

Green's theorem can be used on the first term of equation (3.4) to obtain:

$$-\int_{\partial\mathbf{D}}(\mathbf{n}\cdot\Omega)\frac{1}{\sigma_t}\Omega\cdot\nabla\Psi^+ w_i^+\,dS+\int_{\mathbf{D}}(\Omega\cdot\nabla w_i^+)\frac{1}{\sigma_t}(\Omega\cdot\nabla\Psi^+)\,dV+\int_{\mathbf{D}}\sigma_t\Psi^+ w_i^+\,dV = \int_{\mathbf{D}}\frac{\sigma_s\Phi+Q}{4\pi}w_i^+\,dV. \quad (3.5)$$

Now, we can incorporate the boundary condition, equation (3.1b), naturally:

$$\int_{\partial\mathbf{D}}|\mathbf{n}\cdot\Omega|\left(\Psi^+-F^+\right)w_i^+\,dS+\int_{\mathbf{D}}(\Omega\cdot\nabla w_i^+)\frac{1}{\sigma_t}(\Omega\cdot\nabla\Psi^+)\,dV+\int_{\mathbf{D}}\sigma_t\Psi^+ w_i^+\,dV = \int_{\mathbf{D}}\frac{\sigma_s\Phi+Q}{4\pi}w_i^+\,dV. \quad (3.6)$$

We expand the analytic unknowns in series of basis functions $(b_j(\mathbf{r}), 1\le j\le I)$

$$\Psi^+(\mathbf{r},\Omega)\simeq\psi^+(\mathbf{r},\Omega)=\sum_{j=1}^{I}\psi_j^+(\Omega)b_j^+(\mathbf{r}), \quad (3.7a)$$

$$\Phi(\mathbf{r})\simeq\phi^+(\mathbf{r})=\sum_{j=1}^{I}\phi_j^+ b_j^+(\mathbf{r}) \quad \text{where } \phi_j^+=2\int_{2\pi}\psi_j^+(\Omega)\,d\Omega, \quad (3.7b)$$

and substitute them into equation 3.6. Thus we arrive at the even-parity CFEM system which is a system of I linear equations for the unkowns $(\psi_i^+, 1\le i\le I)$:

$$\int_{\partial\mathbf{D}}|\mathbf{n}\cdot\Omega|(\psi^+-f^+)w_i^+\,dS+\int_{\mathbf{D}}(\Omega\cdot\nabla w_i^+)\frac{1}{\sigma_t}(\Omega\cdot\nabla\psi^+)\,dV+\int_{\mathbf{D}}\sigma_t\psi^+ w_i^+\,dV = \int_{\mathbf{D}}\frac{\sigma_s\phi^++q^+}{4\pi}w_i^+\,dV \quad \text{for } i=1..I. \quad (3.8)$$

For each direction, Ω, this system has a sparse, symmetric coefficient matrix. We also consider the important simplification known as *mass matrix lumping* [58]. This is a procedure where the collision (or *mass*) term in equation (3.8) is diagonalized. In general, mass lumping results in more robust linear systems, though at the cost of a slight decrease in

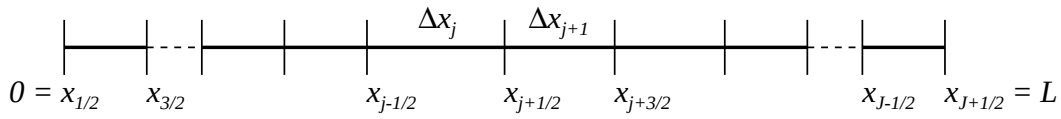

Fig. 4. A slab geometry spatial mesh.

accuracy. We stress, however, that the order of the truncation error does not change. In this approximation, we have:

$$\int_{\mathbf{D}} \sigma_t \psi^+ w_i^+ \, dV \to \psi_i^+ \int_{\mathbf{D}} \sigma_t w_i^+ \, dV,$$

and

$$\int_{\mathbf{D}} \frac{\sigma_s \phi^+}{4\pi} w_i^+ \, dV \to \phi_i^+ \int_{\mathbf{D}} \frac{\sigma_s}{4\pi} w_i^+ \, dV.$$

2. Slab Geometry

As a concrete example, we evaluate the above system for the slab geometry case using linear continuous finite elements and Galerkin weighting. That is, we use the well known *tent functions* on the mesh shown in Figure 4 as our basis and weight functions. They are given by:

$$w_{j+1/2}^+ = b_{j+1/2}^+ = \begin{cases} (x_{j+3/2} - x)/(x_{j+3/2} - x_{j+1/2}) & \text{for } x \in (x_{j+1/2}, x_{j+3/2}) \\ (x - x_{j-1/2})/(x_{j+1/2} - x_{j-1/2}) & \text{for } x \in (x_{j-1/2}, x_{j+1/2}) \\ 0 & \text{otherwise} \end{cases}$$

First, we consider the left and right boundary cells:

$$|\mu|(\psi_{1/2}^+ - f_l^+) - \mu^2 \left(\frac{\psi_{3/2}^+ - \psi_{1/2}^+}{\sigma_{t1}\Delta x_1} \right) + \frac{\sigma_{t1}\Delta x_1}{3} \psi_{1/2}^+ + \frac{\sigma_{t1}\Delta x_1}{6} \psi_{3/2}^+ = \frac{\sigma_{s1}\Delta x_1}{6} \phi_{1/2}^+ + \frac{\sigma_{s1}\Delta x_1}{12} \phi_{3/2}^+ + \frac{\Delta x_1}{6} q_{1/2}^+ + \frac{\Delta x_1}{12} q_{3/2}^+ \quad \text{for } j = 1, \quad (3.9a)$$

and

$$|\mu|(\psi^+_{J+1/2}-f^+_r)+\mu^2\Big(\frac{\psi^+_{J+1/2}-\psi^+_{J-1/2}}{\sigma_{t1}\Delta x_1}\Big)+\frac{\sigma_{tJ}\Delta x_J}{6}\psi^+_{J-1/2}+\frac{\sigma_{tJ}\Delta x_J}{3}\psi^+_{J+1/2}$$
$$=\frac{\sigma_{sJ}\Delta x_J}{12}\phi^+_{J-1/2}+\frac{\sigma_{sJ}\Delta x_J}{6}\phi^+_{J+1/2}+\frac{\Delta x_J}{12}q^+_{J-1/2}+\frac{\Delta x_J}{6}q^+_{J+1/2}\quad\text{for } j=J. \quad (3.9b)$$

The interior cells are described by:

$$-\mu^2\Big(\frac{\psi^+_{j+3/2}-\psi^+_{j+1/2}}{\sigma_{tj+1}\Delta x_{j+1}}-\frac{\psi^+_{j+1/2}-\psi^+_{j-1/2}}{\sigma_{tj}\Delta x_{tj}}\Big)$$
$$+\frac{\sigma_{tj}\Delta x_j}{6}\psi^+_{j-1/2}+\Big(\frac{\sigma_{tj}\Delta x_j}{3}+\frac{\sigma_{tj+1}\Delta x_{j+1}}{3}\Big)\psi^+_{j+1/2}+\frac{\sigma_{tj+1}\Delta x_{j+1}}{6}\psi^+_{j+3/2}$$
$$=\frac{\sigma_{sj}\Delta x_j}{12}\phi^+_{j-1/2}+\Big(\frac{\sigma_{sj}\Delta x_j}{6}+\frac{\sigma_{sj+1}\Delta x_{j+1}}{6}\Big)\phi^+_{j+1/2}+\frac{\sigma_{sj+1}\Delta x_{j+1}}{12}\phi^+_{j+3/2}$$
$$+\frac{\Delta x_j}{12}q^+_{j-1/2}+\Big(\frac{\Delta x_j}{6}+\frac{\Delta x_{j+1}}{6}\Big)q^+_{j+1/2}+\frac{\Delta x_{j+1}}{12}q^+_{j+3/2}\quad\text{for } j=2..J-1. \quad (3.9c)$$

With mass matrix lumping, we obtain for the boundary cells:

$$|\mu|(\psi^+_{1/2}-f^+_l)-\mu^2\Big(\frac{\psi^+_{3/2}-\psi^+_{1/2}}{\sigma_{t1}\Delta x_1}\Big)+\frac{\sigma_{t1}\Delta x_1}{2}\psi^+_{1/2}$$
$$=\frac{\sigma_{s1}\Delta x_1}{4}\phi^+_{1/2}+\frac{\Delta x_1}{4}q^+_{1/2}\quad\text{for } j=1, \quad (3.10a)$$

and

$$|\mu|(\psi^+_{J+1/2}-f^+_r)+\mu^2\Big(\frac{\psi^+_{J+1/2}-\psi^+_{J-1/2}}{\sigma_{t1}\Delta x_1}\Big)+\frac{\sigma_{tJ}\Delta x_J}{2}\psi^+_{J+1/2}$$
$$=\frac{\sigma_{sJ}\Delta x_J}{4}\phi^+_{J+1/2}+\frac{\Delta x_J}{4}q^+_{J+1/2}\quad\text{for } j=J. \quad (3.10b)$$

In the problem interior, the lumped LCFEM system is:

$$-\mu^2\Big(\frac{\psi^+_{j+3/2}-\psi^+_{j+1/2}}{\sigma_{tj+1}\Delta x_{j+1}}-\frac{\psi^+_{j+1/2}-\psi^+_{j-1/2}}{\sigma_{tj}\Delta x_j}\Big)$$
$$+\Big(\frac{\sigma_{tj}\Delta x_j+\sigma_{tj+1}\Delta x_{j+1}}{2}\Big)\psi^+_{j+1/2}=\Big(\frac{\sigma_{sj}\Delta x_j+\sigma_{sj+1}\Delta x_{j+1}}{4}\Big)\phi^+_{j+1/2}$$
$$+\Big(\frac{\Delta x_j+\Delta x_{j+1}}{4}\Big)q^+_{j+1/2}\quad\text{for } j=2..J-1. \quad (3.10c)$$

For both the lumped and unlumped cases, these equations form a symmetric, tridiagonal matrix problem.

B. Odd-Parity

We now apply the weighted residual procedure to the odd-parity system, which we reproduce here:

$$-\Omega\cdot\nabla\frac{1}{\sigma_t}\Omega\cdot\nabla\Psi^- + \sigma_t\Psi^- = \Omega\cdot\nabla\Big(\frac{\sigma_s\Phi+Q}{4\pi\sigma_t}\Big), \tag{3.11a}$$

$$\nabla\cdot\Big(2\int_{2\pi}\Omega\Psi^- d\Omega\Big) + \sigma_t\Phi = \sigma_s\Phi + Q, \tag{3.11b}$$

$$(\mathbf{n}\cdot\Omega)\Big(\frac{1}{\sigma_t}\Omega\cdot\nabla\Psi^- - \frac{\sigma_s\Phi+Q}{4\pi\sigma_t}\Big) = -|\mathbf{n}\cdot\Omega|(\Psi^- - F^-) \quad \text{for } \mathbf{r}\in\partial\mathbf{D}. \tag{3.11c}$$

In this case, we note that the analytic odd-parity system implies that the most natural finite element space for the scalar flux is the space generated by the gradient of the odd-parity angular flux space. We, therefore, propose different weight and basis functions for Ψ^- and Φ.

1. XYZ Geometry

We begin by multiplying equation (3.11a) by a set of weight functions $(w_i^-(\mathbf{r}), 1\le i\le I)$ and equation (3.11b) by a different set of weight functions $(v_k^-(\mathbf{r}), 1\le k\le K)$. We then integrate over the problem domain and obtain equations of the form:

$$-\int_{\mathbf{D}}\Omega\cdot\nabla\Big(\frac{1}{\sigma_t}\Omega\cdot\nabla\Psi^- - \frac{\sigma_s\Phi+Q}{4\pi\sigma_t}\Big)w_i^- dV + \int_{\mathbf{D}}\sigma_t\Psi^- w_i^- dV = 0, \tag{3.12a}$$

$$\int_{\mathbf{D}} \nabla\cdot\Big(2\int_{2\pi}\Omega\Psi^{-}\,d\Omega\Big)v_k^{-}\,dV+\int_{\mathbf{D}}\sigma_t\Phi v_k^{-}\,dV=\int_{\mathbf{D}}(\sigma_s\Phi+Q)v_k^{-}\,dV, \tag{3.12b}$$

for each value of i and k. Equation (3.12b) is in its final form. However, we must work on equation (3.12a) in order to insert the boundary condition, equation (3.11c), naturally. This procedure is identical to the one we followed in developing the even-parity CFEM system. Using identity 3.3 on the streaming term, we obtain:

$$-\int_{\mathbf{D}}\nabla\cdot\Big[w_i^{-}\Omega\Big(\frac{1}{\sigma_t}\Omega\cdot\nabla\Psi^{-}-\frac{\sigma_s\Phi+Q}{4\pi\sigma_t}\Big)\Big]\,dV+\int_{\mathbf{D}}(\Omega\cdot\nabla w_i^{-})\Big(\frac{1}{\sigma_t}\Omega\cdot\nabla\Psi^{-}-\frac{\sigma_s\Phi+Q}{4\pi\sigma_t}\Big)\,dV$$
$$+\int_{\mathbf{D}}\sigma_t\Psi^{-}w_i^{-}\,dV=0. \tag{3.13}$$

Now, we use Green's Theorem to transform the first term in equation (3.13) into a surface integral:

$$-\int_{\partial\mathbf{D}}(\mathbf{n}\cdot\Omega)\Big(\frac{1}{\sigma_t}\Omega\cdot\nabla\Psi^{-}-\frac{\sigma_s\Phi+Q}{4\pi\sigma_t}\Big)w_i^{-}\,dS+\int_{\mathbf{D}}(\Omega\cdot\nabla w_i^{-})\Big(\frac{1}{\sigma_t}\Omega\cdot\nabla\Psi^{-}-\frac{\sigma_s\Phi+Q}{4\pi\sigma_t}\Big)\,dV$$
$$+\int_{\mathbf{D}}\sigma_t\Psi^{-}w_i^{-}\,dV=0. \tag{3.14}$$

We insert the boundary condition:

$$\int_{\partial\mathbf{D}}|\mathbf{n}\cdot\Omega|(\Psi^{-}-F^{-})w_i^{-}\,dS+\int_{\mathbf{D}}(\Omega\cdot\nabla w_i^{-})\frac{1}{\sigma_t}(\Omega\cdot\nabla\Psi^{-})\,dV+\int_{\mathbf{D}}\sigma_t\Psi^{-}w_i^{-}\,dV$$
$$=\int_{\mathbf{D}}(\Omega\cdot\nabla w_i^{-})\Big(\frac{\sigma_s\Phi+Q}{4\pi\sigma_t}\Big)\,dV, \tag{3.15}$$

then expand Ψ^{-} and Φ in two set of linearly independent basis functions:

$$\Psi^{-}(\mathbf{r},\Omega)\simeq\psi^{-}(\mathbf{r},\Omega)=\sum_{j=1}^{I}\psi_j^{-}(\Omega)b_j^{-}(\mathbf{r}), \tag{3.16a}$$

and

$$\Phi(\mathbf{r}) \simeq \phi^-(\mathbf{r}) = \sum_{l=1}^{K} \phi_l^- d_l^-(\mathbf{r}). \tag{3.16b}$$

Hence, we obtain:

$$\int_{\partial \mathbf{D}} |\mathbf{n}\cdot\Omega|(\psi^- - f^-)w_i^- \, dS + \int_{\mathbf{D}} (\Omega\cdot\nabla w_i^-)\frac{1}{\sigma_t}(\Omega\cdot\nabla\psi^-)\, dV + \int_{\mathbf{D}} \sigma_t \psi^- w_i^- \, dV$$
$$= \int_{\mathbf{D}} (\Omega\cdot\nabla w_i^-)\frac{\sigma_s\phi^- + q^-}{4\pi\sigma_t}\, dV \quad \text{for } i = 1..I, \tag{3.17a}$$

and

$$\int_{\mathbf{D}} \nabla\cdot\Big(2\int_{2\pi} \Omega\psi^-\, d\Omega\Big) v_k^- \, dV + \int_{\mathbf{D}} \sigma_t\phi^- v_k^- \, dV$$
$$= \int_{\mathbf{D}} (\sigma_s\phi^- + q^-)v_k^- \, dV \quad \text{for } k = 1..K. \tag{3.17b}$$

Thus, we have arrived at a system of I linear equations for the unknowns $(\psi_i^-, 1 \le i \le I)$ coupled to a system of K linear equations for the unknowns $(\phi_l^-, 1 \le l \le K)$. While we refer to this as the CFEM discretization of the odd-parity system, it is actually a mixed finite element method. The reason we term this a CFEM approximation is that the odd-parity angular flux is expanded in a continuous finite element basis.

2. Slab Geometry

Again, we present the slab geometry linear continuous finite element equations. In this case, the odd-parity angular fluxes are expanded in the standard tent function basis, while

the scalar fluxes are piecewise constants in each cell:

$$w^-_{j+1/2} = b^-_{j+1/2} = \begin{cases} (x_{j+3/2} - x)/(x_{j+3/2} - x_{j+1/2}) & \text{for } x \in (x_{j+1/2}, x_{j+3/2}) \\ (x - x_{j-1/2})/(x_{j+1/2} - x_{j-1/2}) & \text{for } x \in (x_{j-1/2}, x_{j+1/2}) \\ 0 & \text{otherwise,} \end{cases}$$

$$v^-_j = d^-_j = \begin{cases} 1 & \text{for } x \in (x_{j-1/2}, x_{j+1/2}) \\ 0 & \text{otherwise.} \end{cases}$$

The equations governing the boundary cells are:

$$|\mu|(\psi^-_{1/2} - f^-_l) - \mu^2\Big(\frac{\psi^-_{3/2} - \psi^-_{1/2}}{\sigma_{t1}\Delta x_1}\Big) + \frac{\sigma_{t1}\Delta x_1}{3}\psi^-_{1/2} + \frac{\sigma_{t1}\Delta x_1}{6}\psi^-_{3/2} = -\frac{\mu}{2}\Big(\frac{\sigma_{s1}\phi^-_1 + q^-_1}{\sigma_{t1}}\Big) \quad \text{for } j = 1, \quad (3.18a)$$

and

$$|\mu|(\psi^-_{J+1/2} - f^-_r) + \mu^2\Big(\frac{\psi^-_{J+1/2} - \psi^-_{J-1/2}}{\sigma_{t1}\Delta x_1}\Big) + \frac{\sigma_{tJ}\Delta x_J}{6}\psi^-_{J-1/2} + \frac{\sigma_{tJ}\Delta x_J}{3}\psi^-_{J+1/2} = \frac{\mu}{2}\Big(\frac{\sigma_{sJ}\phi^-_J + q^-_J}{\sigma_{tJ}}\Big) \quad \text{for } j = J. \quad (3.18b)$$

For the interior cells, we have:

$$-\mu^2\Big(\frac{\psi^-_{j+3/2} - \psi^-_{j+1/2}}{\sigma_{tj+1}\Delta x_{j+1}} - \frac{\psi^-_{j+1/2} - \psi^-_{j-1/2}}{\sigma_{tj}\Delta x_{tj}}\Big) + \frac{\sigma_{tj}\Delta x_j}{6}\psi^-_{j-1/2} + \Big(\frac{\sigma_{tj}\Delta x_j}{3} + \frac{\sigma_{tj+1}\Delta x_{j+1}}{3}\Big)\psi^-_{j+1/2} + \frac{\sigma_{tj+1}\Delta x_{j+1}}{6}\psi^-_{j+3/2} = -\frac{\mu}{2}\Big(\frac{\sigma_{sj+1}\phi^-_{j+1} + q^-_{j+1}}{\sigma_{tj+1}} - \frac{\sigma_{sj}\phi^-_j + q^-_j}{\sigma_{tj}}\Big) \quad \text{for } j = 2..J-1. \quad (3.18c)$$

Finally, using piecewise constant finite elements to evaluate equation (3.17b), we obtain the following cell centered balance equation:

$$2\int_0^1 \mu(\psi^-_{j+1/2}-\psi^-_{j-1/2})\,d\mu+\sigma_{tj}\Delta x_j\phi^-_j=\Delta x_j(\sigma_{sj}\phi^-_j+q^-_j)\quad \text{for } j=1..J. \tag{3.18d}$$

Again, we can lump the mass terms. The boundary cells are then described by:

$$|\mu|(\psi^-_{1/2}-f^-_l)-\mu^2\Big(\frac{\psi^-_{3/2}-\psi^-_{1/2}}{\sigma_{t1}\Delta x_1}\Big)+\frac{\sigma_{t1}\Delta x_1}{2}\psi^-_{1/2} = -\frac{\mu}{2}\Big(\frac{\sigma_{s1}\phi^-_1+q^-_1}{\sigma_{t1}}\Big)\quad \text{for } j=1, \tag{3.19a}$$

and

$$|\mu|(\psi^-_{J+1/2}-f^-_r)+\mu^2\Big(\frac{\psi^-_{J+1/2}-\psi^-_{J-1/2}}{\sigma_{tJ}\Delta x_J}\Big)+\frac{\sigma_{tJ}\Delta x_J}{2}\psi^-_{J+1/2} = \frac{\mu}{2}\Big(\frac{\sigma_{sJ}\phi^-_J+q^-_J}{\sigma_{tJ}}\Big)\quad \text{for } j=J. \tag{3.19b}$$

In the interior, we obtain:

$$-\mu^2\Big(\frac{\psi^-_{j+3/2}-\psi^-_{j+1/2}}{\sigma_{tj+1}\Delta x_{j+1}}-\frac{\psi^-_{j+1/2}-\psi^-_{j-1/2}}{\sigma_{tj}\Delta x_{tj}}\Big)+\Big(\frac{\sigma_{tj}\Delta x_j+\sigma_{tj+1}\Delta x_{j+1}}{2}\Big)\psi^-_{j+1/2} = -\frac{\mu}{2}\Big(\frac{\sigma_{sj+1}\phi^-_{j+1}+q^-_{j+1}}{\sigma_{tj+1}}-\frac{\sigma_{sj}\phi^-_j+q^-_j}{\sigma_{tj}}\Big)\quad \text{for } j=2..J-1. \tag{3.19c}$$

The cell centered balance equation remains unchanged:

$$2\int_0^1 \mu(\psi^-_{j+1/2}-\psi^-_{j-1/2})\,d\mu+\sigma_{tj}\Delta x_j\phi^-_j=\Delta x_j(\sigma_{sj}\phi^-_j+q^-_j)\quad \text{for } j=1..J. \tag{3.19d}$$

Both the lumped and unlumped odd-parity systems consist of symmetric tridiagonal matrix problems for each angle coupled to a cell centered balance equation.

C. Self Adjoint Angular Flux

We rewrite the SAAF system of equations here:

$$-\Omega\cdot\nabla\frac{1}{\sigma_t}\Omega\cdot\nabla\Psi+\sigma_t\Psi=\frac{\sigma_s\Phi+Q}{4\pi}-\Omega\cdot\nabla\Big(\frac{\sigma_s\Phi+Q}{4\pi\sigma_t}\Big), \tag{3.20a}$$

$$\Omega\cdot\nabla\Psi+\sigma_t\Psi=\frac{\sigma_s\Phi+Q}{4\pi}, \tag{3.20b}$$

and define the boundary condition for $\mathbf{r}\in\partial\mathbf{D}$ to be:

$$\Psi_b(\mathbf{r},\Omega)=\begin{cases}F(\mathbf{r},\Omega) & \text{for } \mathbf{n}\cdot\Omega<0\\ \Psi(\mathbf{r},\Omega) & \text{for } \mathbf{n}\cdot\Omega>0.\end{cases} \tag{3.20c}$$

As in the odd-parity system, we have a problem where the solutions naturally exist in different finite element spaces.

1. XYZ Geometry

We begin by multiplying equation (3.20a) by a set of weight functions $(w_i(\mathbf{r}),1\le i\le I)$ and equation (3.20b) by a different set of weight functions $(v_k(\mathbf{r}),1\le k\le K)$. We then integrate over the problem domain and obtain equations of the form:

$$-\int_{\mathbf{D}}\Omega\cdot\nabla\Big(\frac{1}{\sigma_t}\Omega\cdot\nabla\Psi-\frac{\sigma_s\Phi+Q}{4\pi\sigma_t}\Big)w_i\,dV+\int_{\mathbf{D}}\sigma_t\Psi w_i\,dV = \int_{\mathbf{D}}\frac{\sigma_s\Phi+Q}{4\pi}w_i\,dV, \tag{3.21a}$$

and

$$\int_{\mathbf{D}}\Omega\cdot\nabla\Psi v_k\,dV+\int_{\mathbf{D}}\sigma_t\Psi v_k\,dV=\int_{\mathbf{D}}\frac{\sigma_s\Phi+Q}{4\pi}v_k\,dV, \tag{3.21b}$$

for each value of i and k. We must manipulate equation (3.21a) so that we can apply the boundary condition. First, we use identity (3.3) to get:

$$-\int_{\mathbf{D}} \nabla\cdot\Big[w_i\Omega\Big(\frac{1}{\sigma_t}\Omega\cdot\nabla\Psi-\frac{\sigma_s\Phi+Q}{4\pi\sigma_t}\Big)\Big]\,dV+\int_{\mathbf{D}}(\Omega\cdot\nabla w_i)\Big(\frac{1}{\sigma_t}\Omega\cdot\nabla\Psi-\frac{\sigma_s\Phi+Q}{4\pi\sigma_t}\Big)\,dV + \int_{\mathbf{D}}\sigma_t\Psi w_i\,dV=\int_{\mathbf{D}}\frac{\sigma_s\Phi+Q}{4\pi}w_i\,dV. \quad (3.22)$$

Now we apply Green's theorem to the first term in equation (3.22) to arrive at:

$$\int_{\partial\mathbf{D}}(\mathbf{n}\cdot\Omega)\underbrace{\Big(-\frac{1}{\sigma_t}\Omega\cdot\nabla\Psi+\frac{\sigma_s\Phi+Q}{4\pi\sigma_t}\Big)}_{\Psi_b}w_i\,dS+\int_{\mathbf{D}}(\Omega\cdot\nabla w_i)\Big(\frac{1}{\sigma_t}\Omega\cdot\nabla\Psi-\frac{\sigma_s\Phi+Q}{4\pi\sigma_t}\Big)\,dV + \int_{\mathbf{D}}\sigma_t\Psi w_i\,dV=\int_{\mathbf{D}}\frac{\sigma_s\Phi+Q}{4\pi}w_i\,dV. \quad (3.23)$$

We recognize that the parenthetical term in the boundary integral of equation (3.23) is, by equation (3.20b), the value of the angular flux on the boundary. This allows us to incorporate equation (3.20c), naturally:

$$\int_{\partial\mathbf{D}}(\mathbf{n}\cdot\Omega)\Psi_b w_i\,dS+\int_{\mathbf{D}}(\Omega\cdot\nabla w_i)\frac{1}{\sigma_t}\Omega\cdot\nabla\Psi\,dV+\int_{\mathbf{D}}\sigma_t\Psi w_i\,dV = \int_{\mathbf{D}}\frac{\sigma_s\Phi+Q}{4\pi}w_i\,dV+\int_{\mathbf{D}}(\Omega\cdot\nabla w_i)\frac{\sigma_s\Phi+Q}{4\pi\sigma_t}\,dV. \quad (3.24)$$

Up to this point, we have made no assumptions about the form of the analytic variables. That is, we are free to chose the finite element bases that we judge to be most appealing. With this in mind, we rewrite the weighted residual equations in the following form:

$$\int_{\partial\mathbf{D}}(\mathbf{n}\cdot\Omega)\Psi_b w_i\,dS+\int_{\mathbf{D}}(\Omega\cdot\nabla w_i)\frac{1}{\sigma_t}\Omega\cdot\nabla\Psi\,dV+\int_{\mathbf{D}}\sigma_t\Psi w_i\,dV = \int_{\mathbf{D}}\frac{\sigma_s\Phi+Q}{4\pi}w_i\,dV+\int_{\mathbf{D}}(\Omega\cdot\nabla w_i)\frac{\sigma_s\tilde{\Phi}+\tilde{Q}}{4\pi\sigma_t}\,dV, \quad (3.25a)$$

$$\int_{\mathbf{D}} \Omega \cdot \nabla \Psi v_k \, dV + \int_{\mathbf{D}} \sigma_t \tilde{\Psi} v_k \, dV = \int_{\mathbf{D}} \frac{\sigma_s \tilde{\Phi} + \tilde{Q}}{4\pi} v_k \, dV. \tag{3.25b}$$

Finally, we approximate the analytic unknowns with the following basis function expansions:

$$\Psi(\mathbf{r},\Omega) \simeq \psi(\mathbf{r},\Omega) = \sum_{j=1}^{I} \psi_j(\Omega) b_j(\mathbf{r}), \tag{3.26a}$$

$$\Phi(\mathbf{r}) \simeq \phi(\mathbf{r}) = \sum_{j=1}^{I} \phi_j b_j(\mathbf{r}) \quad \text{where } \phi_j = \int_{4\pi} \psi_j(\Omega) \, d\Omega, \tag{3.26b}$$

$$\tilde{\Psi}(\mathbf{r},\Omega) \simeq \tilde{\psi}(\mathbf{r},\Omega) = \sum_{l=1}^{K} \tilde{\psi}_l(\Omega) d_l(\mathbf{r}), \tag{3.26c}$$

$$\tilde{\Phi}(\mathbf{r}) \simeq \tilde{\phi}(\mathbf{r}) = \sum_{l=1}^{K} \tilde{\phi}_l d_l(\mathbf{r}) \quad \text{where } \tilde{\phi_j} = \int_{4\pi} \tilde{\psi}_j(\Omega) \, d\Omega. \tag{3.26d}$$

to obtain the SAAF CFEM system:

$$\int_{\partial\mathbf{D}} (\mathbf{n} \cdot \Omega) \psi_b w_i \, dS + \int_{\mathbf{D}} (\Omega \cdot \nabla w_i) \frac{1}{\sigma_t} \Omega \cdot \nabla \psi \, dV + \int_{\mathbf{D}} \sigma_t \psi w_i \, dV$$
$$= \int_{\mathbf{D}} \frac{\sigma_s \phi + q}{4\pi} w_i \, dV + \int_{\mathbf{D}} (\Omega \cdot \nabla w_i) \frac{\sigma_s \tilde{\phi} + \tilde{q}}{4\pi\sigma_t} \, dV \quad \text{for } i = 1..I. \tag{3.27a}$$

$$\int_{\mathbf{D}} \Omega \cdot \nabla \psi v_k \, dV + \int_{\mathbf{D}} \sigma_t \tilde{\psi} v_k \, dV = \int_{\mathbf{D}} \frac{\sigma_s \tilde{\phi} + \tilde{q}}{4\pi} v_k \, dV \quad \text{for } k = 1..K. \tag{3.27b}$$

$$\psi_b(\mathbf{r},\Omega) = \begin{cases} f(\mathbf{r},\Omega) & \text{for } \mathbf{n} \cdot \Omega < 0 \\ \psi(\mathbf{r},\Omega) & \text{for } \mathbf{n} \cdot \Omega > 0 \end{cases} \tag{3.27c}$$

Like the odd-parity system, this is a CFEM approximation only in the sense that the angular flux, ψ, is described with a continuous finite element basis. Equations (3.27) are, in fact, a mixed finite element system.

2. Slab Geometry

The LCFEM discretization of the SAAF system involves angular and scalar flux unknowns from two different spaces. We expand ψ and ϕ in the linear continuous basis, while $\tilde{\psi}$ and $\tilde{\phi}$ are piecewise constants:

$$w_{j+1/2} = b_{j+1/2} = \begin{cases} (x_{j+3/2} - x)/(x_{j+3/2} - x_{j+1/2}) & \text{for } x \in (x_{j+1/2}, x_{j+3/2}) \\ (x - x_{j-1/2})/(x_{j+1/2} - x_{j-1/2}) & \text{for } x \in (x_{j-1/2}, x_{j+1/2}) \\ 0 & \text{otherwise,} \end{cases}$$

$$v_j = d_j = \begin{cases} 1 & \text{for } x \in (x_{j-1/2}, x_{j+1/2}) \\ 0 & \text{otherwise.} \end{cases}$$

For the boundary cells we obtain:

$$\begin{aligned} -\mu\psi_l - \mu^2\left(\frac{\psi_{3/2} - \psi_{1/2}}{\sigma_{t1}\Delta x_1}\right) + \frac{\sigma_{t1}\Delta x_1}{3}\psi_{1/2} + \frac{\sigma_{t1}\Delta x_1}{6}\psi_{3/2} \\ = \frac{\sigma_{s1}\Delta x_1}{6}\phi_{1/2} + \frac{\sigma_{s1}\Delta x_1}{12}\phi_{3/2} \\ + \frac{\Delta x_1}{6}q_{1/2} + \frac{\Delta x_1}{12}q_{3/2} - \frac{\mu}{2}\left(\frac{\sigma_{s1}\tilde{\phi}_1 + \tilde{q}_1}{\sigma_{t1}}\right) \quad \text{for } j = 1, \end{aligned} \tag{3.28a}$$

and

$$\mu\psi_r + \mu^2\Big(\frac{\psi_{J+1/2}-\psi_{J-1/2}}{\sigma_{tJ}\Delta x_J}\Big) + \frac{\sigma_{tJ}\Delta x_J}{6}\psi_{J-1/2} + \frac{\sigma_{tJ}\Delta x_J}{3}\psi_{J+1/2}$$
$$= \frac{\sigma_{sJ}\Delta x_J}{6}\phi_{J+1/2} + \frac{\sigma_{sJ}\Delta x_J}{12}\phi_{J-3/2}$$
$$+ \frac{\Delta x_J}{6}q_{J+1/2} + \frac{\Delta x_J}{12}q_{J-3/2} + \frac{\mu}{2}\Big(\frac{\sigma_{sJ}\tilde{\phi}_J + \tilde{q}_J}{\sigma_{tJ}}\Big) \quad \text{for } j = J, \quad (3.28b)$$

where the boundary fluxes, ψ_l and ψ_r are given by:

$$\psi_l = \begin{cases} f_l & \text{for } \mu > 0 \\ \psi_{1/2} & \text{for } \mu < 0, \end{cases} \qquad \psi_r = \begin{cases} \psi_{J+1/2} & \text{for } \mu > 0 \\ f_r & \text{for } \mu < 0. \end{cases} \quad (3.28c)$$

In the interior, we have:

$$-\mu^2\Big(\frac{\psi_{j+3/2}-\psi_{j+1/2}}{\sigma_{tj+1}\Delta x_{j+1}} - \frac{\psi_{j+1/2}-\psi_{j-1/2}}{\sigma_{tj}\Delta x_{tj}}\Big)$$
$$+ \frac{\sigma_{tj}\Delta x_j}{6}\psi_{j-1/2} + \Big(\frac{\sigma_{tj}\Delta x_j}{3} + \frac{\sigma_{tj+1}\Delta x_{j+1}}{3}\Big)\psi_{j+1/2} + \frac{\sigma_{tj+1}\Delta x_{j+1}}{6}\psi_{j+3/2}$$
$$= \frac{\sigma_{sj}\Delta x_j}{12}\phi_{j-1/2} + \Big(\frac{\sigma_{sj}\Delta x_j}{6} + \frac{\sigma_{sj+1}\Delta x_{j+1}}{6}\Big)\phi_{j+1/2} + \frac{\sigma_{sj+1}\Delta x_{j+1}}{12}\phi_{j+3/2}$$
$$+ \frac{\Delta x_j}{12}q_{j-1/2} + \Big(\frac{\Delta x_j}{6} + \frac{\Delta x_{j+1}}{6}\Big)q_{j+1/2} + \frac{\Delta x_{j+1}}{12}q_{j+3/2}$$
$$- \frac{\mu}{2}\Big(\frac{\sigma_{sj+1}\tilde{\phi}_{j+1} + \tilde{q}_{j+1}}{\sigma_{tj+1}} - \frac{\sigma_{sj}\tilde{\phi}_j + \tilde{q}_j}{\sigma_{tj}}\Big) \quad \text{for } j = 2..J-1. \quad (3.28d)$$

Finally, equation (3.27b) is evaluated with piecewise constant finite elements to arrive at the SAAF cell centered balance equation:

$$\mu(\psi_{j+1/2} - \psi_{j-1/2}) + \sigma_{tj}\Delta x_j\tilde{\psi}_j = \Delta x_j\Big(\frac{\sigma_{sj}\tilde{\phi}_j + \tilde{q}_j}{2}\Big) \quad \text{for } j = 1..J. \quad (3.28e)$$

With mass matrix lumping, we arrive at the following equations for the boundary cells:

$$-\mu\psi_l - \mu^2\Big(\frac{\psi_{3/2}-\psi_{1/2}}{\sigma_{t1}\Delta x_1}\Big) + \frac{\sigma_{t1}\Delta x_1}{2}\psi_{1/2} = \frac{\sigma_{s1}\Delta x_1}{4}\phi_{1/2} + \frac{\Delta x_1}{4}q_{1/2} - \frac{\mu}{2}\Big(\frac{\sigma_{s1}\tilde{\phi}_1+\tilde{q}_1}{\sigma_{t1}}\Big) \quad \text{for } j=1, \quad (3.29a)$$

and

$$\mu\psi_r + \mu^2\Big(\frac{\psi_{J+1/2}-\psi_{J-1/2}}{\sigma_{tJ}\Delta x_J}\Big) + \frac{\sigma_{tJ}\Delta x_J}{2}\psi_{J+1/2} = \frac{\sigma_{sJ}\Delta x_J}{4}\phi_{J+1/2} + \frac{\Delta x_J}{4}q_{J+1/2} + \frac{\mu}{2}\Big(\frac{\sigma_{sJ}\tilde{\phi}_J+\tilde{q}_J}{\sigma_{tJ}}\Big) \quad \text{for } j=J. \quad (3.29b)$$

In the interior, we have:

$$-\mu^2\Big(\frac{\psi_{j+3/2}-\psi_{j+1/2}}{\sigma_{tj+1}\Delta x_{j+1}} - \frac{\psi_{j+1/2}-\psi_{j-1/2}}{\sigma_{tj}\Delta x_{tj}}\Big) + \Big(\frac{\sigma_{tj}\Delta x_j + \sigma_{tj+1}\Delta x_{j+1}}{2}\Big)\psi_{j+1/2} = \Big(\frac{\sigma_{sj}\Delta x_j + \sigma_{sj+1}\Delta x_{j+1}}{4}\Big)\phi_{j+1/2} + \Big(\frac{\Delta x_j + \Delta x_{j+1}}{4}\Big)q_{j+1/2} - \frac{\mu}{2}\Big(\frac{\sigma_{sj+1}\tilde{\phi}_{j+1}+\tilde{q}_{j+1}}{\sigma_{tj+1}} - \frac{\sigma_{sj}\tilde{\phi}_j+\tilde{q}_j}{\sigma_{tj}}\Big) \quad \text{for } j=2..J-1. \quad (3.29c)$$

The cell centered balance equation remains the same:

$$\mu(\psi_{j+1/2}-\psi_{j-1/2}) + \sigma_{tj}\Delta x_j\tilde{\psi}_j = \Delta x_j\Big(\frac{\sigma_{sj}\tilde{\phi}_j+\tilde{q}_j}{2}\Big) \quad \text{for } j=1..J. \quad (3.29d)$$

As in the odd-parity case, the slab geometry SAAF system consists of a symmetric tridiagonal matrix problem for each angle coupled to a cell centered balance equation.

At this point, some additional discussion regarding the external fixed source is necessary. We noted above that the inscattering source should exist in the same finite element space as the within-group scattering source. In the case of the SAAF systems, we have two separate within-group scattering sources, so it is necessary to have two separate fixed sources so that the inscattering sources from both finite element spaces can be properly accounted for. The external fixed source, however, need only be defined for one space. The

value for the other space can be obtained by simply taking the appropriate average of the source already defined. We define the external fixed source for the cell centered unknowns.

Finally, we observe that for both the parity and SAAF slab geometry systems the mass matrix lumped LCFEM approximation is identical to the edge centered finite difference approximation.

D. Relationship Between the Parity Equations and the SAAF Equation

Morel and McGhee [4] have shown that solving the P_1 SAAF equations is equivalent to solving both the even- and odd-parity P_1 equations that are independent in the problem interior, but coupled on the boundaries. In fact, a more general relationship can be developed. Consider the CFEM discretizations of the even- and odd-parity equations shown in equations (3.8) and (3.17). If we set $w_i^+ = w_i^- = w_i$ and $v_k^- = v_k$, then, since these are linear systems, we can simply add them to obtain:

$$\int_{\partial \mathbf{D}} |\mathbf{n}\cdot\Omega|\left(\psi - f^+ - f^-\right) w_i \, dS + \int_{\mathbf{D}} (\Omega\cdot\nabla w_i)\frac{1}{\sigma_t}\Omega\cdot\nabla\psi, dV + \int_{\mathbf{D}} \sigma_t \psi w_i \, dV$$
$$= \int_{\mathbf{D}} \frac{\sigma_s\phi^+ + q^+}{4\pi} w_i \, dV + \int_{\mathbf{D}} (\Omega\cdot\nabla w_i)\frac{\sigma_s\phi^- + q^-}{4\pi\sigma_t} dV \quad \text{for } i = 1..I, \quad (3.30a)$$

and

$$\int_{\mathbf{D}} \nabla\cdot\left(2\int_{2\pi} \Omega\psi^- \, d\Omega\right) v_k \, dV + \int_{\mathbf{D}} \sigma_t\phi^- v_k \, dV$$
$$= \int_{\mathbf{D}} (\sigma_s\phi^- + q^-) v_k \, dV \quad \text{for } k = 1..K. \quad (3.30b)$$

Equations (3.30) are nearly identical to the SAAF CFEM system shown in equations (3.27). There is, however, one important difference. Using the definition of $f^{+/-}$, we see that the

sum of the even- and odd- parity equations satisfies the following boundary condition:

$$|\mathbf{n}\cdot\Omega|\left(\psi - f^{+} - f^{-}\right) = \begin{cases} (\mathbf{n}\cdot\Omega)(2f-\psi) & \text{for } \mathbf{n}\cdot\Omega < 0 \\ (\mathbf{n}\cdot\Omega)\psi & \text{for } \mathbf{n}\cdot\Omega > 0, \end{cases} \tag{3.31}$$

while the SAAF systems satisfies:

$$(\mathbf{n}\cdot\Omega)\psi_b = \begin{cases} (\mathbf{n}\cdot\Omega)f & \text{for } \mathbf{n}\cdot\Omega < 0 \\ (\mathbf{n}\cdot\Omega)\psi & \text{for } \mathbf{n}\cdot\Omega > 0. \end{cases} \tag{3.32}$$

Thus, the only difference in the finite element formulations is in the boundary term. If we were to substitute the boundary condition $(\mathbf{n}\cdot\Omega)(2f-\psi)$ in place of $(\mathbf{n}\cdot\Omega)f$ in the SAAF system, we would expect to obtain results identical to the average of the even- and odd-parity solutions. If we redefine the SAAF boundary condition, equation (3.27c), as:

$$\psi_b(\mathbf{r},\Omega) = \begin{cases} \theta f(\mathbf{r},\Omega) + (1-\theta)\psi(\mathbf{r},\Omega) & \text{for } \mathbf{n}\cdot\Omega < 0 \\ \psi(\mathbf{r},\Omega) & \text{for } \mathbf{n}\cdot\Omega > 0 \end{cases} \tag{3.33}$$

we obtain standard SAAF boundary condition with $\theta = 1$ and a boundary condition that yields solutions identical to the even- and odd-parity CFEM solutions with $\theta = 2$.

E. Discrete Diffusion Limit Analysis

We now commence with a thick diffusion limit analysis of the CFEM discretization we have developed. We note that Adams has previously published analyses for the even- and odd-parity systems [1, 2]. We review those results, then proceed to an analysis of the SAAF system. Our procedure is to introduce the diffusion limit scaling discussed in Chapter II into each discretization then require the resulting equations to hold for like powers of the scaling parameter ε.

1. Even-Parity

We begin by applying the diffusion limit scaling, equation (2.32), to the even-parity CFEM system, equation (3.8). This results in the scaled even-parity CFEM equation:

$$\int_{\partial \mathbf{D}} |\mathbf{n}\cdot\Omega|(\psi^+ - f^+)w_i^+\,dS + \int_{\mathbf{D}} (\Omega\cdot\nabla w_i^+)\frac{\varepsilon}{\sigma_t}(\Omega\cdot\nabla\psi^+)\,dV + \int_{\mathbf{D}} \frac{\sigma_t}{\varepsilon}\psi^+ w_i^+\,dV = \int_{\mathbf{D}} \frac{(\frac{\sigma_t}{\varepsilon} - \varepsilon\sigma_a)\phi^+ + \varepsilon q^+}{4\pi} w_i^+\,dV. \quad (3.34)$$

We introduce the ansatz:

$$\psi^+ = \psi^{+[0]} + \varepsilon\psi^{+[1]} + \varepsilon^2\psi^{+[2]} + ..., \quad (3.35a)$$

$$\phi^+ = \phi^{+[0]} + \varepsilon\phi^{+[1]} + \varepsilon^2\phi^{+[2]} + ... \quad \text{where } \phi^{+[k]} = \int_{4\pi} \psi^{+[k]}\,d\Omega, \quad (3.35b)$$

into equation (3.34) and group terms of like order. The $O(1/\varepsilon)$ equation:

$$\int_{\mathbf{D}} \sigma_t\psi^{+[0]} w_i^+\,dV = \int_{\mathbf{D}} \frac{\sigma_t\phi^{+[0]}}{4\pi} w_i^+\,dV, \quad (3.36)$$

shows that the leading order even-parity angular flux is isotropic if the mass matrix is invertible (which we would expect for any CFEM):

$$\psi^{+[0]} = \frac{\phi^{+[0]}}{4\pi}. \quad (3.37)$$

The O(1) equation,

$$\int_{\partial \mathbf{D}} |\mathbf{n}\cdot\Omega|(\psi^{+[0]} - f^+)w_i^+\,dS + \int_{\mathbf{D}} \sigma_t\psi^{+[1]} w_i^+\,dV = \int_{\mathbf{D}} \frac{\sigma_t\phi^{+[1]}}{4\pi} w_i^+\,dV, \quad (3.38)$$

can be integrated over angle (after substituting $\psi^{+[0]} = \phi^{+[0]}/4\pi$) to obtain an expression for the leading order scalar flux on the boundary:

$$\int_{\partial \mathbf{D}} \phi^{+[0]} w_i^+ \, dS = \int_{\partial \mathbf{D}} \left(2 \int_{\mathbf{n}\cdot\Omega<0} 2|\mathbf{n}\cdot\Omega| f^+ \, d\Omega \right) w_i^+ \, dS. \tag{3.39}$$

Finally, we write the O(ε) equation:

$$\int_{\partial \mathbf{D}} |\mathbf{n}\cdot\Omega| \psi^{+[1]} w_i^+ \, dS + \int_{\mathbf{D}} (\Omega\cdot\nabla w_i^+) \frac{1}{\sigma_t} (\Omega\cdot\nabla\psi^{+[0]}) \, dV + \int_{\mathbf{D}} \sigma_t \psi^{+[2]} w_i^+ \, dV = \int_{\mathbf{D}} \frac{\sigma_t \phi^{+[2]} - \sigma_a \phi^{+[0]} + q^+}{4\pi} w_i^+ \, dV. \tag{3.40}$$

After integrating this over angle, we obtain:

$$\int_{\partial \mathbf{D}} \left(\int_{4\pi} |\mathbf{n}\cdot\Omega| \psi^{+[1]} \, d\Omega \right) w_i^+ \, dS + \int_{\mathbf{D}} \frac{1}{3\sigma_t} (\nabla w_i^+) \cdot (\nabla \phi^{+[0]}) \, dV + \int_{\mathbf{D}} \sigma_a \phi^{+[0]} w_i^+ \, dV = \int_{\mathbf{D}} q^+ w_i^+ \, dV, \tag{3.41}$$

where we have noted that

$$\int_{4\pi} \Omega\Omega \, d\Omega = \frac{4\pi}{3}\mathbf{I} \quad \text{where } \mathbf{I} \text{ is the identity tensor.}$$

Clearly, the appropriate system that specifies the leading order even-parity scalar flux is the CFEM approximation to the diffusion equation:

$$\int_{\mathbf{D}} \frac{1}{3\sigma_t} (\nabla w_i^+) \cdot (\nabla \phi^{+[0]}) \, dV + \int_{\mathbf{D}} \sigma_a \phi^{+[0]} w_i^+ \, dV = \int_{\mathbf{D}} q^+ w_i^+ \, dV. \tag{3.42a}$$

subject to a Marshak boundary condition:

$$\int_{\partial \mathbf{D}} \phi^{+[0]} w_i^+ \, dS = \int_{\partial \mathbf{D}} \left(2 \int_{\mathbf{n}\cdot\Omega<0} 2|\mathbf{n}\cdot\Omega| f^+ \, d\Omega \right) w_i^+ \, dS = \int_{\partial \mathbf{D}} \phi_b^+ w_i^+ \, dS. \tag{3.42b}$$

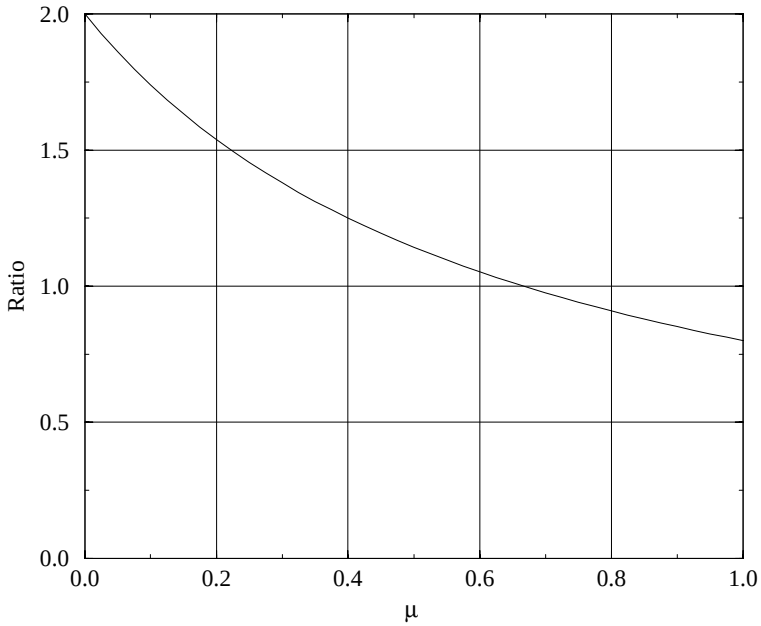

Fig. 5. Ratio of the even-parity boundary weighting function to $\mu + \frac{3}{2}\mu^2$.

Note that this is an essential boundary condition, whereas the even-parity transport equation is subject to a natural boundary condition.

Whether this is an accurate discretization of the diffusion equation depends on both the accuracy of the underlying diffusion discretization and on how well the Marshak boundary condition approximates the exact boundary condition. While the accuracy of the CFEM diffusion approximation depends on the spatial grid and choice of weight and basis functions, it is well understood. We do not pursue this issue further, and simply assume that the weight and basis functions have been selected so that equations (3.42) yield an accurate solution of the diffusion equation.

The remaining question is whether or not equation (3.42b) is an accurate representation of the exact boundary condition, equation (2.39b). In general, it is not. We plot the ratio of even-parity boundary weighting function to the polynomial approximation of the

exact boundary weighting function,

$$\frac{2|\mathbf{n}\cdot\Omega|}{|\mathbf{n}\cdot\Omega|+\frac{3}{2}|\mathbf{n}\cdot\Omega|^2}\rightarrow\frac{2}{1+\frac{3}{2}|\mathbf{n}\cdot\Omega|},$$

in Fig. 5. For a thick diffusive problem driven by a grazing incoming angular flux ($|\mathbf{n}\cdot\Omega|$ very small) we would expect the leading order even-parity solution to be higher than the correct solution by a factor of approximately two.

2. Odd-Parity

Now we apply the diffusion limit scaling, equation (2.32), to the odd-parity CFEM system, equations (3.17). This results in the scaled odd-parity CFEM system:

$$\int_{\partial\mathbf{D}}|\mathbf{n}\cdot\Omega|(\psi^- - f^-)w_i^-\,dS+\int_{\mathbf{D}}(\Omega\cdot\nabla w_i^-)\frac{\varepsilon}{\sigma_t}(\Omega\cdot\nabla\psi^-)\,dV+\int_{\mathbf{D}}\frac{\sigma_t}{\varepsilon}\psi^- w_i^-\,dV = \int_{\mathbf{D}}(\Omega\cdot\nabla w_i^-)\frac{(\sigma_t-\varepsilon^2\sigma_a)\phi^- +\varepsilon^2 q^-}{4\pi\sigma_t}\,dV, \quad (3.43a)$$

$$\int_{\mathbf{D}}\nabla\cdot\Big(2\int_{2\pi}\Omega\psi^-\,d\Omega\Big)v_k^-\,dV+\int_{\mathbf{D}}\frac{\sigma_t}{\varepsilon}\phi^- v_k^-\,dV = \int_{\mathbf{D}}\Big[(\frac{\sigma_t}{\varepsilon}-\varepsilon\sigma_a)\phi^- +\varepsilon q^-\Big]v_k^-\,dV. \quad (3.43b)$$

We substitute the following ansatz:

$$\psi^- = \psi^{-[0]}+\varepsilon\psi^{-[1]}+\varepsilon^2\psi^{-[2]}+..., \quad (3.44a)$$

$$\phi^- = \phi^{-[0]}+\varepsilon\phi^{-[1]}+\varepsilon^2\phi^{-[2]}+..., \quad (3.44b)$$

into the scaled equations then require that the resulting systems hold for each power of ε. The $O(1/\varepsilon)$ term in equation (3.43a) is:

$$\int_{\mathbf{D}} \frac{\sigma_t}{\varepsilon} \psi^{-[0]} w_i^- \, dV = 0. \tag{3.45}$$

This implies (assuming that the mass matrix is invertible) that

$$\psi^{-[0]} = 0. \tag{3.46}$$

The O(1) part of equation (3.43a),

$$\int_{\partial\mathbf{D}} |\mathbf{n}\cdot\Omega|(\psi^{-[0]} - f^-) w_i^- \, dS + \int_{\mathbf{D}} \sigma_t \psi^{-[1]} w_i^- \, dV = \int_{\mathbf{D}} (\Omega\cdot\nabla w_i^-) \frac{\sigma_t \phi^{-[0]}}{4\pi\sigma_t} \, dV, \tag{3.47}$$

can be multiplied by Ω and integrated over angle to obtain:

$$\frac{1}{3}\int_{\partial\mathbf{D}} \mathbf{n}\cdot\Big(2\int_{\mathbf{n}\cdot\Omega<0} 3\Omega\Omega f^- \, d\Omega\Big) w_i^- \, dS - \frac{1}{3}\int_{\mathbf{D}} \phi^{-[0]} \nabla w_i^- \, dV + \int_{\mathbf{D}} \sigma_t \Big(2\int_{2\pi} \Omega\psi^{-[1]} \, d\Omega\Big) w_i^- \, dV = 0, \tag{3.48}$$

where we have noted that:

$$\int_{4\pi} 3\Omega|\mathbf{n}\cdot\Omega| f^- \, d\Omega = -\mathbf{n}\cdot\Big(2\int_{\mathbf{n}\cdot\Omega<0} 3\Omega\Omega f^- \, d\Omega\Big).$$

Now, we turn our attention to equation (3.43b). The $O(\varepsilon)$ equation is:

$$\int_{\mathbf{D}} \nabla\cdot\Big(2\int_{2\pi} \Omega\psi^{-[1]} \, d\Omega\Big) v_k^- \, dV + \int_{\mathbf{D}} \sigma_a \phi^{-[0]} v_k^- \, dV = \int_{\mathbf{D}} q^- v_k^- \, dV. \tag{3.49}$$

Hence, we find that in the thick diffusive limit, the leading order odd-parity solution satisfies the following coupled systems of equations:

$$\frac{1}{3}\int_{\partial\mathbf{D}} \mathbf{n}\cdot\Big(2\int_{\mathbf{n}\cdot\Omega<0} 3\Omega\Omega f^{-}\,d\Omega\Big)w_i^{-}\,dS - \frac{1}{3}\int_{\mathbf{D}} \phi^{-[0]}\nabla w_i^{-}\,dV + \int_{\mathbf{D}} \sigma_t\Big(2\int_{2\pi}\Omega\psi^{-[1]}\,d\Omega\Big)w_i^{-}\,dV = 0, \quad (3.50a)$$

$$\int_{\mathbf{D}} \nabla\cdot\Big(2\int_{2\pi}\Omega\psi^{-[1]}\,d\Omega\Big)v_k^{-}\,dV + \int_{\mathbf{D}} \sigma_a\phi^{-[0]}v_k^{-}\,dV = \int_{\mathbf{D}} q^{-}v_k^{-}\,dV. \quad (3.50b)$$

If f^{-} is symmetric about the outward normal, then:

$$\mathbf{n}\cdot\Big(2\int_{\mathbf{n}\cdot\Omega<0} 3\Omega\Omega f^{-}\,d\Omega\Big) = \mathbf{n}\Big(2\int_{\mathbf{n}\cdot\Omega<0} 3|\mathbf{n}\cdot\Omega|^2 f^{-}\,d\Omega\Big) = \mathbf{n}\phi_b^{-}. \quad (3.50c)$$

Equations (3.50) constitute a *dual mixed variational* finite element discretization of the diffusion equation. We can easily obtain a single diffusion equation if we mass lump (3.50a) and apply Green's theorem to (3.50b). The resulting system is interesting in that the scalar flux in a particular cell is coupled to the scalar fluxes in every other cell that shares a common vertex with the cell in question. We note that, even with the assumption of an azimuthally symmetric incoming angular flux, equation (3.50c) is not, in general, a good approximation to equation (2.39b). The ratio between the odd-parity boundary weighting function and the polynomial approximation to the exact boundary weighting function,

$$\frac{3|\mathbf{n}\cdot\Omega|^2}{|\mathbf{n}\cdot\Omega| + \frac{3}{2}|\mathbf{n}\cdot\Omega|^2} \rightarrow \frac{3|\mathbf{n}\cdot\Omega|}{1+\frac{3}{2}|\mathbf{n}\cdot\Omega|},$$

is shown in Fig. 6. In this case, for a thick diffusive problem driven by a grazing incoming angular flux, we would expect the odd-parity solution to be significantly lower than the correct solution.

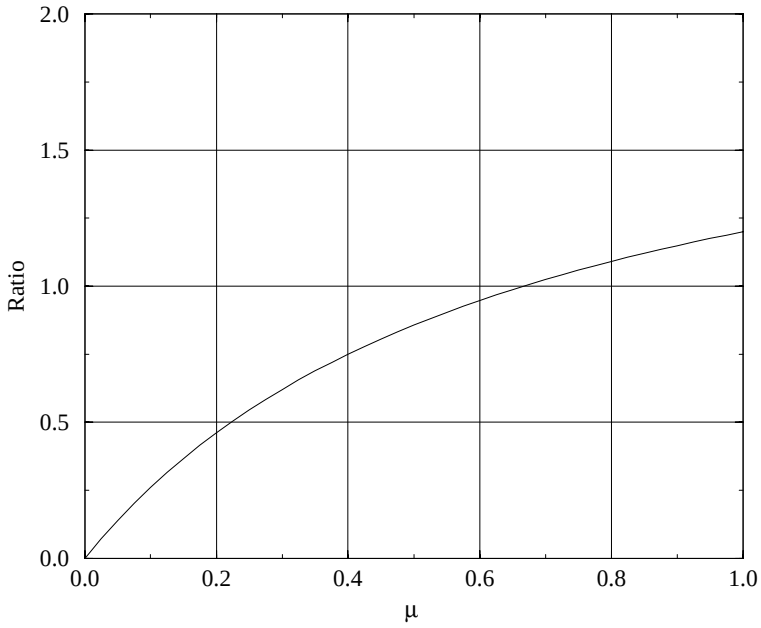

Fig. 6. Ratio of the odd-parity boundary weighting function to $\mu+\frac{3}{2}\mu^2$.

3. A Hybrid-Parity Method

If we examine the leading-order even- and odd-parity boundary conditions in the diffusion limit, it is obvious that their average would be a very good approximation to the exact boundary condition (at least if the incoming angular flux is azimuthally symmetric). That is:

$$\frac{\phi_b^+ + \phi_b^-}{2} = 2 \int\limits_{\mathbf{n}\cdot\Omega<0} \left(|\mathbf{n}\cdot\Omega| + \frac{3}{2}|\mathbf{n}\cdot\Omega|^2 \right) f(\mathbf{r},\Omega)\, d\Omega$$

$$\simeq 2 \int\limits_{\mathbf{n}\cdot\Omega<0} W(|\mathbf{n}\cdot\Omega|)\, f(\mathbf{r},\Omega)\, d\Omega. \quad (3.51)$$

Therefore, if we select appropriate weight functions, basis functions and a spatial grid for a specific diffusion problem, then the average of the even- and odd-parity solutions should be accurate for thick diffusive transport problems. We test this prediction in Chapter VI. A similar result has been observed for certain reactor physics problems [31].

4. SAAF

We now apply the diffusion limit scaling to the SAAF system with the standard boundary condition ($\theta = 1$). If we were to set $\theta = 2$ then we would expect to obtain the even- and odd-parity results. That is, ϕ would satisfy a Marshak boundary condition and $\tilde{\phi}$ a $3\mu^2$ boundary condition in the thick diffusion limit. The scaled equations are:

$$\int_{\partial \mathbf{D}} (\mathbf{n}\cdot\Omega)\psi_b w_i \, dS + \int_{\mathbf{D}} (\Omega\cdot\nabla w_i)\frac{\varepsilon}{\sigma_t}\Omega\cdot\nabla\psi \, dV + \int_{\mathbf{D}} \frac{\sigma_t}{\varepsilon}\psi w_i \, dV = \int_{\mathbf{D}} \frac{(\frac{\sigma_t}{\varepsilon} - \varepsilon\sigma_a)\phi + \varepsilon q}{4\pi} w_i \, dV + \int_{\mathbf{D}} (\Omega\cdot\nabla w_i)\frac{(\sigma_t - \varepsilon^2\sigma_a)\tilde{\phi} + \varepsilon^2\tilde{q}}{4\pi\sigma_t} \, dV, \quad (3.52a)$$

$$\int_{\mathbf{D}} \Omega\cdot\nabla\psi v_k \, dV + \int_{\mathbf{D}} \frac{\sigma_t}{\varepsilon}\tilde{\psi} v_k \, dV = \int_{\mathbf{D}} \frac{(\frac{\sigma_t}{\varepsilon} - \varepsilon\sigma_a)\tilde{\phi} + \varepsilon\tilde{q}}{4\pi} v_k \, dV, \quad (3.52b)$$

$$\psi_b(\mathbf{r},\Omega) = \begin{cases} f(\mathbf{r},\Omega) & \text{for } \mathbf{n}\cdot\Omega < 0 \\ \psi(\mathbf{r},\Omega) & \text{for } \mathbf{n}\cdot\Omega > 0. \end{cases} \quad (3.52c)$$

We introduce the following ansatz:

$$\psi = \psi^{[0]} + \varepsilon\psi^{[1]} + \varepsilon^2\psi^{[2]} + \ldots, \quad (3.53a)$$

$$\phi = \phi^{[0]} + \varepsilon\phi^{[1]} + \varepsilon^2\phi^{[2]} + \ldots \quad \text{where } \phi^{[k]} = \int_{4\pi} \psi^{[k]} \, d\Omega, \quad (3.53b)$$

$$\tilde{\psi} = \tilde{\psi}^{[0]} + \varepsilon\tilde{\psi}^{[1]} + \varepsilon^2\tilde{\psi}^{[2]} + \ldots, \quad (3.53c)$$

$$\tilde{\phi} = \tilde{\phi}^{[0]} + \varepsilon\tilde{\phi}^{[1]} + \varepsilon^2\tilde{\phi}^{[2]} + \ldots \quad \text{where } \tilde{\phi}^{[k]} = \int_{4\pi} \tilde{\psi}^{[k]} \, d\Omega, \quad (3.53d)$$

into the scaled equations. The $O(1/\varepsilon)$ portions of equations (3.52a) and (3.52b) are, respectively:

$$\int_{\mathbf{D}} \sigma_t \psi^{[0]} w_i \, dV = \int_{\mathbf{D}} \frac{\sigma_t \phi^{[0]}}{4\pi} w_i \, dV, \tag{3.54a}$$

and

$$\int_{\mathbf{D}} \sigma_t \tilde{\psi}^{[0]} v_k \, dV = \int_{\mathbf{D}} \frac{\sigma_t \tilde{\phi}^{[0]}}{4\pi} v_k \, dV. \tag{3.54b}$$

These equations imply, under the assumption of invertible mass matrices, that the leading order angular fluxes are isotropic:

$$\psi^{[0]} = \frac{\phi^{[0]}}{4\pi}, \tag{3.55a}$$

and

$$\tilde{\psi}^{[0]} = \frac{\tilde{\phi}^{[0]}}{4\pi}. \tag{3.55b}$$

Now we consider the O(1) terms of equation (3.52a):

$$\int_{\partial\mathbf{D}} (\mathbf{n}\cdot\Omega)\psi_b w_i \, dS + \int_{\mathbf{D}} \sigma_t \psi^{[1]} w_i \, dV = \int_{\mathbf{D}} \frac{\sigma_t \phi^{[1]}}{4\pi} w_i \, dV + \int_{\mathbf{D}} (\Omega\cdot\nabla w_i) \frac{\sigma_t \tilde{\phi}^{[0]}}{4\pi\sigma_t} \, dV. \tag{3.56}$$

Integrating over angle, we arrive at:

$$\int_{\partial\mathbf{D}} \Big(\int_{4\pi} (\mathbf{n}\cdot\Omega)\psi_b \, d\Omega \Big) w_i \, dS = 0. \tag{3.57}$$

If we have continuous weight and basis functions, and apply lumping on the surface terms so that the surface coefficient matrix is invertible, we have:

$$\int_{4\pi} (\mathbf{n}\cdot\Omega)\psi_b \, d\Omega = \int_{\mathbf{n}\cdot\Omega<0} (\mathbf{n}\cdot\Omega) f \, d\Omega + \int_{\mathbf{n}\cdot\Omega>0} (\mathbf{n}\cdot\Omega)\psi^{[0]} \, d\Omega = 0 \quad \text{for } \mathbf{r} \in \partial\mathbf{D}.$$

We have already shown that the leading order angular flux is isotropic throughout the entire problem, thus:

$$\int_{\mathbf{n}\cdot\Omega<0} (\mathbf{n}\cdot\Omega) f \, d\Omega + \int_{\mathbf{n}\cdot\Omega>0} (\mathbf{n}\cdot\Omega) \frac{\phi^{[0]}}{4\pi} \, d\Omega = 0 \quad \text{for } \mathbf{r} \in \partial\mathbf{D}.$$

We move the leading order scalar flux outside the integral to obtain:

$$\phi_i^{[0]} = \frac{4\pi \int_{\mathbf{n}\cdot\Omega<0} |\mathbf{n}\cdot\Omega| f \, d\Omega}{\int_{\mathbf{n}\cdot\Omega>0} (\mathbf{n}\cdot\Omega) \, d\Omega} \quad \text{for } \mathbf{r} \in \partial\mathbf{D}.$$

Evaluating the integrals, we find that:

$$\phi_i^{[0]}(\mathbf{r}) = 2 \int_{\mathbf{n}\cdot\Omega<0} 2|\mathbf{n}\cdot\Omega| f \, d\Omega \quad \text{for } \mathbf{r} \in \partial\mathbf{D}. \tag{3.58}$$

Thus, to leading order, $\phi^{[0]}$ satisfies a Marshak boundary condition. Let us take the first angular moment of equation (3.52a) to obtain:

$$\int_{\partial\mathbf{D}} \Big(\int_{4\pi} (\mathbf{n}\cdot\Omega)\Omega\psi_b \, d\Omega \Big) w_i \, dS + \int_{\mathbf{D}} \Big(\int_{4\pi} \sigma_t \Omega \psi^{[1]} \, d\Omega \Big) w_i \, dV = \frac{1}{3} \int_{\mathbf{D}} \tilde{\phi}^{[0]} \nabla w_i \, dV. \tag{3.59}$$

We now work on the boundary term. We again make use of equation (3.52c) to split this integral into two parts:

$$\int_{4\pi} (\mathbf{n}\cdot\Omega)\Omega\psi_b \, d\Omega = \int_{\mathbf{n}\cdot\Omega<0} (\mathbf{n}\cdot\Omega)\Omega f \, d\Omega + \int_{\mathbf{n}\cdot\Omega>0} (\mathbf{n}\cdot\Omega)\Omega\psi^{[0]} \, d\Omega.$$

However, we have already determined that the magnitude of $\phi^{[0]}$ on the boundary is equal to the Marshak weighting of the known incident angular flux. Since we also know that the

leading order scalar flux on the boundary is isotropic we can write:

$$\begin{aligned}\int\limits_{\mathbf{n}\cdot\Omega>0} (\mathbf{n}\cdot\Omega)\Omega\psi^{[0]}\,d\Omega &= \Big(\frac{1}{\pi}\int\limits_{\mathbf{n}\cdot\Omega<0} |\mathbf{n}\cdot\Omega|\,f\,d\Omega\Big)\Big(\int\limits_{\mathbf{n}\cdot\Omega>0} (\mathbf{n}\cdot\Omega)\Omega\,d\Omega\Big)\\ &= \Big(\frac{1}{\pi}\int\limits_{\mathbf{n}\cdot\Omega<0} |\mathbf{n}\cdot\Omega|\,f\,d\Omega\Big)\Big(\mathbf{n}\frac{2\pi}{3}\Big)\\ &= \frac{2\mathbf{n}}{3}\int\limits_{\mathbf{n}\cdot\Omega<0} |\mathbf{n}\cdot\Omega|\,f\,d\Omega.\end{aligned}$$

Therefore, the boundary term in equation (3.59) becomes:

$$\frac{1}{3}\int\limits_{\partial\mathbf{D}}\Big(2\mathbf{n}\int\limits_{\mathbf{n}\cdot\Omega<0} |\mathbf{n}\cdot\Omega|\,f\,d\Omega+\mathbf{n}\cdot\int\limits_{\mathbf{n}\cdot\Omega<0} 3\Omega\Omega\,f\,d\Omega\Big)w_i\,dS$$

The O(ε) coefficients from equation (3.52b) give:

$$\int\limits_{\mathbf{D}}\Omega\cdot\nabla\psi^{[1]}v_k\,dV+\int\limits_{\mathbf{D}}\sigma_t\tilde{\psi}^{[2]}v_k\,dV=\int\limits_{\mathbf{D}}\frac{\sigma_t\tilde{\phi}^{[2]}-\sigma_a\tilde{\phi}^{[0]}+\tilde{q}}{4\pi}v_k\,dV. \tag{3.60}$$

We integrate this over angle find that the leading order SAAF solution satisfies the following coupled diffusion system:

$$\begin{aligned}\frac{1}{3}\int\limits_{\partial\mathbf{D}}\Big(2\mathbf{n}\int\limits_{\mathbf{n}\cdot\Omega<0} |\mathbf{n}\cdot\Omega|\,f\,d\Omega+\mathbf{n}\cdot\int\limits_{\mathbf{n}\cdot\Omega<0} 3\Omega\Omega\,f\,d\Omega\Big)w_i\,dS&\\ -\frac{1}{3}\int\limits_{\mathbf{D}}\tilde{\phi}^{[0]}\nabla w_i\,dV+\int\limits_{\mathbf{D}}\sigma_t\Big(\int\limits_{4\pi}\Omega\psi^{[1]}\,d\Omega\Big)w_i\,dV=0.&\end{aligned} \tag{3.61a}$$

$$\int\limits_{\mathbf{D}}\nabla\cdot\Big(\int\limits_{4\pi}\Omega\psi^{[1]}\,d\Omega\Big)v_k\,dV+\int\limits_{\mathbf{D}}\sigma_a\tilde{\phi}^{[0]}v_k\,dV=\int\limits_{\mathbf{D}}\tilde{q}v_k\,dV. \tag{3.61b}$$

If the incoming angular flux is azimuthally symmetric, we can simplify the first term in the boundary integral:

$$\frac{1}{3}\int_{\partial\mathbf{D}} \mathbf{n}\Big(2\int_{\mathbf{n}\cdot\Omega<0}(|\mathbf{n}\cdot\Omega|+\frac{3}{2}|\mathbf{n}\cdot\Omega|^2)\,f\,d\Omega\Big)w_i\,dS$$
$$-\frac{1}{3}\int_{\mathbf{D}}\tilde{\phi}^{[0]}\nabla w_i\,dV+\int_{\mathbf{D}}\sigma_t\Big(\int_{4\pi}\Omega\psi^{[1]}\,d\Omega\Big)w_i\,dV=0. \quad (3.62a)$$

$$\int_{\mathbf{D}}\nabla\cdot\Big(\int_{4\pi}\Omega\psi^{[1]}\,d\Omega\Big)v_k\,dV+\int_{\mathbf{D}}\sigma_a\tilde{\phi}^{[0]}v_k\,dV=\int_{\mathbf{D}}\tilde{q}v_k\,dV. \quad (3.62b)$$

Equations (3.62) are a dual mixed variational finite element approximation to the diffusion equation. We can very simply obtain a single diffusion equation if we mass lump (3.62a) and apply Green's theorem to (3.62b). Thus, the coupling between cells is identical to the odd-parity system, equations (3.50). With the assumption of an azimuthally symmetric incoming angular flux, the SAAF boundary condition for $\tilde{\phi}$ should be an excellent approximation to equation (2.39b).

F. Internal Interface Analysis

In the previous section, we analyzed problems that were entirely diffusive. In this section, we consider problems with adjacent diffusive and non-diffusive regions. Adams [1] has analyzed the even-parity CFEM system for problems like this in general 3D geometry with unspecified weight and basis functions. However, there is an minor error in that analysis that invalidates a portion of the results.

In this section, we restrict our analysis to the case of lumped linear continuous finite element discretizations in slab geometry. Fortunately, a great deal of insight can be gained through such analyses because many of the important features of this problem are predominately one-dimensional.

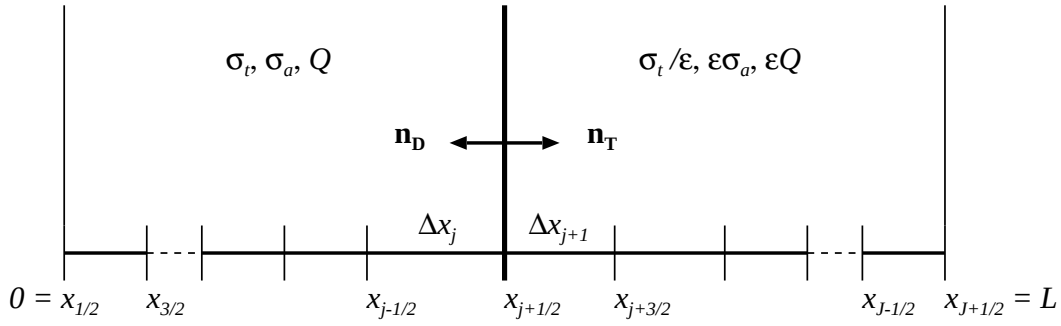

Fig. 7. Slab geometry spatial mesh with an internal interface.

Consider the spatial mesh shown in Fig. 7. The problem we consider consists of a *transport* region to the left of $x_{j+1/2}$ and a *thick diffusive* region to the right of $x_{j+1/2}$. The unscaled transport equation holds in cells 1 to j (of course, it also holds throughout the entire problem). The diffusion limit results from the previous sections hold for the cells right of, but not including $j+1$. Thus, our task is to find the leading order solution to the discretized transport equation in the two cells immediately adjacent to the interface, that is cells j and $j+1$. The outward normal $\mathbf{n}_T$ points out of the transport region and into the diffusive region, while $\mathbf{n}_D$ points out of the diffusive region and into the transport region.

First, we determine the magnitude of the scalar flux on the boundary assuming the angular flux incident on the diffusive region from the transport region is known. We then find the angular flux that exits from the diffusive region back into the transport region.

1. Even-Parity

The scaled equation that governs the solution at the interface is:

$$-\mu^2\left(\varepsilon\frac{\psi^+_{j+3/2}-\psi^+_{j+1/2}}{\sigma_{tj+1}\Delta x_{j+1}}-\frac{\psi^+_{j+1/2}-\psi^+_{j-1/2}}{\sigma_{tj}\Delta x_j}\right)$$
$$+\left(\frac{\sigma_{tj}\Delta x_j}{2}+\frac{\sigma_{tj+1}\Delta x_{j+1}}{2\varepsilon}\right)\psi^+_{j+1/2}=\frac{1}{4}\left[\sigma_{sj}\Delta x_j+(\frac{\sigma_{tj+1}}{\varepsilon}-\varepsilon\sigma_{aj+1})\Delta x_{j+1}\right]\phi^+_{j+1/2}$$
$$+\left(\frac{\Delta x_j}{4}+\frac{\varepsilon\Delta x_{j+1}}{4}\right)q^+_{j+1/2}. \quad (3.63)$$

The $O(1/\varepsilon)$ equation shows that the leading order even-parity angular flux is isotropic on the boundary between the diffusive and transport regions:

$$\psi^{+[0]}_{j+1/2} = \frac{1}{2}\phi^{+[0]}_{j+1/2}. \tag{3.64}$$

The O(1) terms are:

$$\mu^2\left(\frac{\psi^{+[0]}_{j+1/2} - \psi^{+[0]}_{j-1/2}}{\sigma_{tj}\Delta x_j}\right) + \frac{\sigma_{tj}\Delta x_j}{2}\psi^{+[0]}_{j+1/2} + \frac{\sigma_{tj+1}\Delta x_{j+1}}{2}\psi^{+[1]}_{j+1/2} = \frac{\sigma_{sj}\Delta x_j}{4}\phi^{+[0]}_{j+1/2} + \frac{\sigma_{tj+1}\Delta x_{j+1}}{4}\phi^{+[1]}_{j+1/2} + \frac{\Delta x_j}{4}q^{+}_{j+1/2}. \tag{3.65}$$

The zeroth moment of equation (3.65) produces:

$$\int_{-1}^{1}\frac{\mu^2}{\sigma_{tj}}\left(\frac{\psi^{+[0]}_{j+1/2} - \psi^{+[0]}_{j-1/2}}{\Delta x_j}\right)d\mu + \frac{\sigma_{aj}\Delta x_j}{2}\phi^{+[0]}_{j+1/2} = \frac{\Delta x_j}{2}q^{+}_{j+1/2}. \tag{3.66}$$

The first term in even in angle, so we can write:

$$\int_{0}^{1}2\frac{\mu^2}{\sigma_{tj}}\left(\frac{\psi^{+[0]}_{j+1/2} - \psi^{+[0]}_{j-1/2}}{\Delta x_j}\right)d\mu + \frac{\sigma_{aj}\Delta x_j}{2}\phi^{+[0]}_{j+1/2} = \frac{\Delta x_j}{2}q^{+}_{j+1/2}. \tag{3.67}$$

We now add and subtract $\mu\psi^{+[0]}_{j+1/2}$ to obtain:

$$-\int_{0}^{1}2\mu\left(\psi^{+[0]}_{j+1/2} - \frac{\mu}{\sigma_{tj}}\frac{\psi^{+[0]}_{j+1/2} - \psi^{+[0]}_{j-1/2}}{\Delta x_j}\right)d\mu + 2\int_{0}^{1}\mu\psi^{+[0]}_{j+1/2}d\mu + \frac{\sigma_{aj}\Delta x_j}{2}\phi^{+[0]}_{j+1/2} = \frac{\Delta x_j}{2}q^{+}_{j+1/2}. \tag{3.68}$$

Thus, we find that:

$$\phi^{+[0]}_{j+1/2} = \frac{\int_{0}^{1}2\mu\left(\psi^{+[0]}_{j+1/2} - \frac{\mu}{\sigma_{tj}}\frac{\psi^{+[0]}_{j+1/2} - \psi^{+[0]}_{j-1/2}}{\Delta x_j}\right)d\mu + \Delta x_j q^{+}_{j+1/2}}{1 + \sigma_{aj}\Delta x_j} \tag{3.69}$$

However, if we assume that the transport region is finely zoned ($\Delta x_j \to 0$), then,

$$\frac{\psi^{+[0]}_{j+1/2} - \psi^{+[0]}_{j-1/2}}{\Delta x_j} \to \left.\frac{d\psi^{+[0]}}{dx}\right|_j . \tag{3.70}$$

We then identify,

$$\psi^{e[0]}_{j+1/2} = \psi^{+[0]}_{j+1/2} - \left.\frac{\mu}{\sigma_{tj}}\frac{d\psi^{+[0]}}{dx}\right|_j$$

as the even-parity approximation to the full range angular flux. Thus:

$$\phi^{+[0]}_{j+1/2} = 2\int_0^1 2\mu\psi^{e[0]}_{j+1/2}\,d\mu. \tag{3.71}$$

That is, the magnitude of the scalar flux on the interface is simply a Marshak weighting of $\psi^{e[0]}_{j+1/2}$, the even-parity approximation to the full range angular flux on the interface.

Now, we must consider the problem of determining what returns from the diffusive region back into the transport region. Recall that in Chapter II, we showed that the exact solution satisfies the complicated albedo shown in equation (2.42). Our goal here is to find the corresponding albedo for the even-parity system.

It is straightforward to show that at a boundary for $\mu < 0$:

$$\psi^e(x_b,\mu) = 2\psi^+(x_b,\mu) - f(x_b,-\mu),$$

where $f(x_b,-\mu)$ is the angular flux incident upon that boundary. We have just shown that the even-parity angular flux on the interface between the diffusive and transport region is

isotropic. Using equation (3.71), we find that for $\mu < 0$:

$$\begin{aligned}
\psi^{e[0]}_{j+1/2}(\mu) &= 2\psi^{+[0]}_{j+1/2}(\mu) - f(-\mu) && \text{(3.72a)}\\
&= \phi^{+[0]}_{j+1/2} - \psi^{e[0]}_{j+1/2}(-\mu)\\
&= 2\int_0^1 2\mu'\psi^{e[0]}_{j+1/2}(\mu')\,d\mu' - \psi^{e[0]}_{j+1/2}(-\mu)\\
&= \int_0^1 \alpha^e(\mu,\mu')\psi^{e[0]}_{x_{j+1/2}}(\mu')\,d\mu'
\end{aligned}$$

where we have defined the albedo, $\alpha^e(\mu,\mu')$, as:

$$\alpha^e(\mu,\mu') = 4\mu' - \delta(\mu'+\mu). \qquad \text{(3.72b)}$$

We have also identified $f(-\mu)$ as $\psi^{e[0]}_{j+1/2}(-\mu)$, which is appropriate for the albedo problem we are considering. To summarize, we can now say that the leading order transport solution in a problem with an internal interface satisfies:

- the discrete even-parity transport equation for all the cells from the left boundary to the interface, subject to the albedo boundary condition shown in equation (3.72), and
- the discrete diffusion limit even-parity system for all the cells from the interface to the right boundary, subject to equation (3.71).

2. Odd-Parity

At the interface, the scaled odd-parity lumped linear finite element equations are:

$$\begin{aligned}
-\mu^2\Big(\varepsilon\frac{\psi^-_{j+3/2}-\psi^-_{j+1/2}}{\sigma_{tj+1}\Delta x_{j+1}} - \frac{\psi^-_{j+1/2}-\psi^-_{j-1/2}}{\sigma_{tj}\Delta x_{tj}}\Big) + \Big(\frac{\sigma_{tj}\Delta x_j}{2} + \frac{\sigma_{tj+1}\Delta x_{j+1}}{2\varepsilon}\Big)\psi^-_{j+1/2}&\\
= -\frac{\mu}{2}\Big(\frac{(\sigma_{tj+1}-\varepsilon^2\sigma_{aj+1})\phi^-_{j+1}+\varepsilon^2 q^-_{j+1}}{\sigma_{tj+1}} - \frac{\sigma_{sj}\phi^{-]}_j + q^-_j}{\sigma_{tj}}\Big), \qquad \text{(3.73a)}&
\end{aligned}$$

$$2\int_0^1 \mu(\psi^-_{j+1/2}-\psi^-_{j-1/2})\,d\mu+\sigma_{aj}\Delta x_j\phi^-_j=\Delta x_j q^-_j\,, \tag{3.73b}$$

$$2\int_0^1 \mu(\psi^-_{j+3/2}-\psi^-_{j+1/2})\,d\mu+\varepsilon\sigma_{aj+1}\Delta x_{j+1}\phi^-_{j+1}=\varepsilon\Delta x_{j+1}q^-_{j+1}. \tag{3.73c}$$

The O$(1/\varepsilon)$ equation shows that the leading order odd-parity angular flux is zero:

$$\psi^{-[0]}_{j+1/2}=0. \tag{3.74}$$

The O(1) terms of equation (3.73a) are:

$$\mu^2\Big(\frac{\psi^{-[0]}_{j+1/2}-\psi^{-[0]}_{j-1/2}}{\sigma_{tj}\Delta x_{tj}}\Big)+\frac{\sigma_{tj+1}\Delta x_{j+1}}{2}\psi^{-[1]}_{j+1/2}=-\frac{\mu}{2}\Big(\phi^{-[0]}_{j+1}-\frac{\sigma_{sj}\phi^{-[0]}_j+q^-_j}{\sigma_{tj}}\Big), \tag{3.75}$$

where we have used the O$(1/\varepsilon)$ result. We solve for $\psi^{-[1]}_{j+1/2}$ and take the μ moment to find:

$$\begin{aligned}\frac{\sigma_{tj+1}\Delta x_{j+1}}{2}&\int_{-1}^1 \mu\psi^{-[1]}_{j+1/2}\,d\mu\\ &=-\frac{1}{3}\phi^{-[0]}_{j+1}+\int_0^1 2\mu^2\Big(-\mu\frac{\psi^{-[0]}_{j+1/2}-\psi^{-[0]}_{j-1/2}}{\sigma_{tj}\Delta x_{tj}}+\frac{\sigma_{sj}\phi^{-[0]}_j+q^-_j}{\sigma_{tj}}\Big)\,d\mu.\end{aligned} \tag{3.76}$$

If we again assume that the transport region is finely zoned ($\Delta x_j\to 0$), then,

$$\frac{\psi^{-[0]}_{j+1/2}-\psi^{-[0]}_{j-1/2}}{\Delta x_j}\to\left.\frac{d\psi^{-[0]}}{dx}\right|_j, \tag{3.77}$$

and we have, by definition:

$$\psi^{o[0]}_{j+1/2}=\psi^{-[0]}_{j+1/2}-\frac{\mu}{\sigma_{tj}}\left.\frac{d\psi^{-[0]}}{dx}\right|_j+\frac{\sigma_{sj}\phi^{-[0]}_j+q^-_j}{\sigma_{tj}}.$$

Here, ψ^o the odd-parity approximation to the full range angular flux. Since the leading order odd-parity angular flux is zero, we have:

$$\int_{-1}^{1} \mu \psi_{j+1/2}^{-[1]} d\mu = -\frac{1}{3} \frac{\phi_{j+1}^{-[0]} - 2\int_0^1 3\mu^2 \psi_{j+1/2}^{o[0]} d\mu}{(\sigma_{tj+1}\Delta x_{j+1}/2)}. \tag{3.78}$$

Finally, we take the zeroth moment of the O(1) terms in equation (3.73c) to obtain:

$$-\frac{1}{3}\Big[\frac{\phi_{j+2}^{-[0]} - \phi_{j+1}^{-[0]}}{(\sigma_{tj+2}\Delta x_{j+2} + \sigma_{tj+1}\Delta x_{j+1})/2} - \frac{\phi_{j+1}^{-[0]} - \phi_{j+1/2}^{-[0]}}{(\sigma_{tj+1}\Delta x_{j+1}/2)}\Big] + \sigma_{aj+1}\Delta x_{j+1}\phi_{j+1}^{-[0]}$$
$$= \Delta x_{j+1} q_{j+1}^{-}, \tag{3.79a}$$

where,

$$\phi_{j+1/2}^{-[0]} = 2\int_0^1 3\mu^2 \psi_{j+1/2}^{o[0]} d\mu. \tag{3.79b}$$

We have used the interior analysis results to evaluate the μ moment of $\psi_{j+3/2}^{-[1]}$. Thus, the magnitude of the leading order scalar flux in the first diffusive cell is the $3\mu^2$ moment of the odd-parity approximation to the incident flux from the transport region.

Now, we must find the angular flux that returns from the diffusive region back into the transport region. At a boundary for $\mu < 0$ we can write:

$$\psi^o(x_b, \mu) = 2\psi^-(x_b, \mu) + f(x_b, -\mu),$$

The leading order odd-parity angular flux on the interface between the diffusive and trans-

port region is zero, thus for $\mu < 0$:

$$\begin{aligned} \psi^{o[0]}_{j+1/2}(\mu) &= f(-\mu) \\ &= \psi^{o[0]}_{j+1/2}(-\mu) \\ &= \int_0^1 \alpha^o(\mu,\mu')\psi^{o[0]}_{x_{j+1/2}}(\mu')\,d\mu' \end{aligned} \tag{3.80a}$$

where we have defined the albedo, $\alpha^o(\mu,\mu')$, as:

$$\alpha^o(\mu,\mu') = \delta(\mu'+\mu). \tag{3.80b}$$

- the discrete odd-parity transport system for all the cells from the left boundary to the interface, subject to albedo boundary condition shown in equation (3.80), and
- the discrete diffusion limit odd-parity system for all the cells from the interface to the right boundary, subject to equation (3.79b).

3. Hybrid-Parity

Just as in an entirely diffusive problem, it appears that the average the even- and odd-parity solutions would lead to the correct weighted boundary condition for the diffusive portion of the problem. Specifically,

$$\frac{\phi^{-[0]}_{j+1/2} + \phi^{+[0]}_{j+1/2}}{2} = 2\Big(\int_0^1 \mu\psi^{e[0]}_{j+1/2}\,d\mu + \int_0^1 \frac{3}{2}\mu^2\psi^{o[0]}_{j+1/2}\,d\mu\Big).$$

If the transport region is zoned finely enough to resolve the solution in both the even- and odd-parity cases,

$$\psi^{e[0]}_{j+1/2}(\mu) \simeq \psi^{o[0]}_{j+1/2}(\mu) \simeq \psi^{[0]}_{j+1/2}(\mu) \tag{3.81}$$

then we have,

$$\frac{\phi^{-[0]}_{j+1/2}+\phi^{+[0]}_{j+1/2}}{2}=2\int_0^1(\mu+\frac{3}{2}\mu^2)\psi^{[0]}_{j+1/2}\,d\mu. \tag{3.82}$$

This is a desirable, though not unexpected, result. Again, we see that the average of the parity scalar fluxes should be very accurate for diffusive portions of the problem, assuming that the transport portions are zoned finely enough so that equation (3.81) holds.

A more difficult question to answer is whether or not the average of the even- and odd-parity solutions results in the correct angular flux returning into the transport region. Let us consider the average of the parity albedo conditions. We have:

$$\frac{\alpha^e(\mu,\mu')+\alpha^o(\mu,\mu')}{2}=\frac{1}{2}\Big[4\mu'-\delta(\mu'+\mu)+\delta(\mu'+\mu)\Big]=2\mu'. \tag{3.83}$$

This is an interesting result for two reasons. First, we see that this albedo is not a function of returning angle. The particles returning back into the transport region are isotropically distributed in angle. Second, particles are conserved by the μ' weighting of the incoming angular flux.

The exact albedo boundary, however, not only conserves particles but also returns particles back into the transport region anisotropically. In Figure 8 we plot the exact albedo and the hybrid- parity albedo for various values of μ' as a function of the returning angle. We see from the figure that the largest discrepancies occur for small angles, which have the least impact on the returning solution. In the numerical results section, we verify this behavior and show that the average of the even- and odd-parity solutions is indeed very accurate for problems of this type.

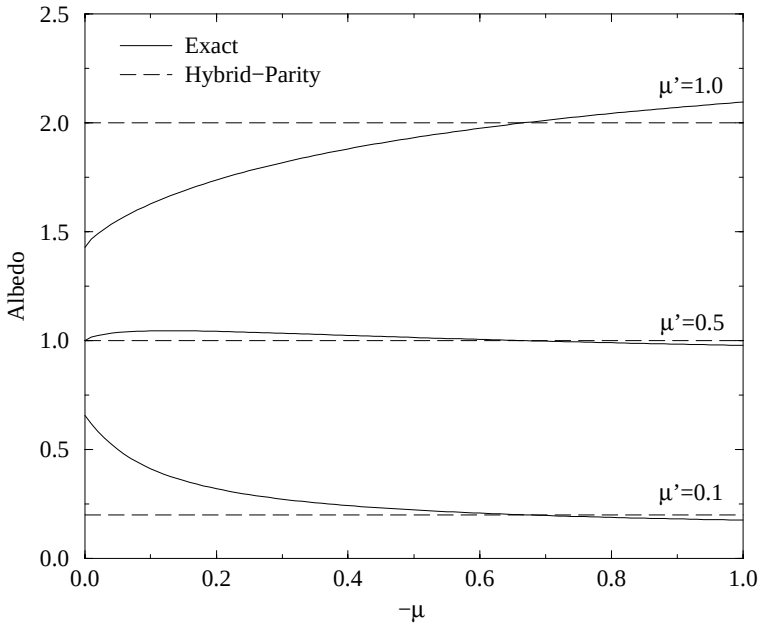

Fig. 8. Exact and hybrid-parity albedo weighting functions.

4. SAAF

We have shown that the SAAF equation is identical to the average of the even- and odd-parity equations in the problem interior. Thus, our simple analysis of the hybrid-parity method applies directly to the SAAF. The leading order solutions satisfy the same discrete equations in the problem interior.

However, they may satisfy different discrete boundary conditions. If we use the standard SAAF boundary condition, equation (3.27c), we do not expect the SAAF solutions to exactly agree with the hybrid parity solution. If, on the other hand, we use equation (3.31), we expect exact agreement. We verify this in the numerical results section.

This behavior is unusual. Using the standard SAAF boundary condition, $\tilde{\phi}$ satisfies a $\mu + \frac{3}{2}\mu^2$ weighting on outer boundaries, but a $3\mu^2$ interface condition on internal interfaces. Again, if we were to replace the standard SAAF boundary condition with equation (3.31), we would expect $\tilde{\phi}$ to satisfy a $3\mu^2$ weighting on both outer boundaries and on internal

interface. Note that ϕ satisfies a 2μ weighting on both outer boundaries and on internal interfaces for *both* forms of the SAAF boundary condition. Thus, the average of $\tilde{\phi}$ and ϕ from a SAAF calculation will satisfy a $\mu + \frac{3}{2}\mu^2$ weighted boundary condition on both external boundaries and internal interfaces.

G. Implemenational Considerations

The linear continuous finite element method (LCFEM) on triangular and tetrahedral meshes is an attractive method to consider for the even-parity equation. This method exhibits second order accuracy for the diffusion equation and allows a high degree of geometric flexibility with a relatively small number of spatial unknowns. However, it may not be appropriate for the odd-parity equation. In fact, this discretization of the odd-parity equation violates the discrete *inf-sup* condition [5]. The easiest way to see this is to consider the linear system that results from equations (3.17).

From equation (3.17b) we see that the natural function space for the scalar fluxes is the one generated by the gradient of the odd-parity angular flux basis functions. On a triangular mesh with a linear continuous basis for ψ^-, the scalar fluxes are then piecewise constants within each cell. The number of scalar fluxes is, therefore, roughly twice the number of odd-parity angular fluxes. The right hand side of equation (3.17a) consists of an N_I x N_K matrix operating on a scalar flux vector of length N_K (where N_I and N_K are the number of vertices and cells, respectively). Since $N_I < N_K$, this matrix has a non-zero null-space. Thus, there are certain non-zero flux vectors that result in a zero right hand side. This has at least two undesirable consequences. First, any scalar flux components that are in the null-space are completely ignored by equation (3.17a). Second, the magnitude of such scalar flux components are meaningless because they are not be damped by the leakage operator.

However, it appears that these undamped null-space modes are not usually present in

realistic problems on *regular meshes*. In fact, all of our odd-parity XY numerical results are calculated with a LCFEM implementation on triangular grids. On the other hand, we have been able to obtain non-physical solutions by contriving problems that contain these modes. Clearly, the LCFEM odd-parity system should be used only with great caution.

In order to understand why it is ever possible to obtain accurate odd-parity LCFEM solutions on triangles, consider the odd-parity CFEM system written in matrix form:

$$L(\Omega)\psi(\Omega) = W_t\phi + F_t q, \tag{3.84a}$$

$$\mathbf{J} = 2\int_{2\pi} \Omega\psi(\Omega)\, d\Omega, \tag{3.84b}$$

$$\mathbf{D}\cdot\mathbf{J} + M\phi = W_d\phi + F_d q. \tag{3.84c}$$

When the odd-parity system is discretized with linear continuous finite elements on a triangular grid, L is a N_I x N_I symmetric positive definite matrix operating on an odd-parity angular flux vector of length N_I; and W_t is a N_I x N_K matrix operating on a scalar flux vector of length N_K (where N_I and N_K are the number of vertices and cells, respectively). Since $N_I < N_K$, W_t has a non-zero null-space.

When we attempt to evaluate equation (3.84c) with with no absorption ($M = W_d$), then the matrix equation for ϕ is $A\phi = b$ where,

$$A = \mathbf{D}\cdot 2\int_{2\pi} \Omega L^{-1}(\Omega) W_t\, d\Omega.$$

Though we do not prove it, we note that A itself is symmetric. In this case, $L(\Omega)$ is symmetric positive definite, so that $L^{-1}(\Omega)$ is non-singular. The matrix A, therefore, has the same null-space as the N_I x N_K matrix W_t. By the Fredholm Alternative theorem, $Au = b$ has a solution if and only if $< b, z >= 0$ for each z such that $A^* z = 0$. Since $A = A^*$ this

implies that our fixed source vector must be orthogonal to the null-space vectors for a particular mesh for a solution to exist. As we show in Chapter VI, these null-space vectors are symmetric and oscillate between positive and negative values on the regular meshes we use for many of our calculations. We suggest that this unusual relation between the fixed source and null-space of A may hold on certain regular meshes, though it is not clear how to prove or disprove this postulate. Finally, we stress that the odd-parity angular flux is not subject to this problem. By that we mean that there is always a solution to equation (3.84a), regardless of the details of the mesh and fixed source. We only face this issue only when we attempt to solve equation (3.84c) for the scalar flux.

The SAAF LCFEM system is clearly also suceptible to undamped null-space error modes via the $\tilde{\phi}$ term on the right hand side of equation (3.27a). If anisotropic scattering was present, then the LCFEM even-parity discretization would also be subject to this problem. This is because the even-parity approximation to the current has the same functional form as the odd-parity approximation to the scalar flux; piecewise constants within each cell.

On a quadrilateral or hexahedral mesh, this discretization would not violate the discrete inf-sup condition. However, these meshes do not allow the geometric flexibility of the triangular and tetrahedral meshes.

Finally, let N be the number of angles and K the number of spatial cells on a triangular mesh. Then, the LCFEM discretization of the even- or odd- parity method has $\frac{1}{4}NK$ unknowns, so that the hybrid parity solution has a total of $\frac{1}{2}NK$. The LCFEM SAAF system, like hybrid-parity, also has $\frac{1}{2}NK$ unknowns.

CHAPTER IV

MIXED FINITE ELEMENT DISCRETIZATION AND ANALYSIS

A more satisfying but correspondingly more costly resolution to the odd-parity *inf-sup* violation involves reformulating the problem. We first note that it is physically appealing to locate vector current unknowns on cell surfaces and scalar flux unknowns in cell centers. While the fundamental unknown in the transport equation is, of course, a scalar function, we can reformulate the even- and odd-parity equations as a coupled system of first-order equations with a scalar and a vector unknown. Our reformulation allows us to employ powerful MFEM methods to transport problems, and represents a significant departure from conventional FEM transport discretizations.

In this chapter, we develop the mixed finite element method (MFEM) discretization of the coupled parity equations and the coupled angular flux/angular current density (AFCD) equations discussed in Chapter II. For each system, we begin in general 3D Cartesian geometry then reduce to slab geometry. We analyze the discretized equations in the thick diffusion limit for both problems that are entirely diffusive and for problems that contain adjacent diffusive and non-diffusive regions. We conclude with a discussion about the details of implementing specific mixed finite element methods and the properties of those methods.

A. Coupled Even- and Odd-Parity System

We now use the wieghted residual method to form the coupled even- and odd- parity MFEM discretization. First we multiply the analytic equations by weight functions, then we integrate over the problem domain. The analytic unknowns can then be replaced with functional expansions, which reduces the original problem to that of sovling a system of linear

equations. The coupled parity system is given by:

$$\nabla \cdot \Omega\Omega\Psi^+ + \sigma_t \mathbf{G}^- = 0. \tag{4.1a}$$

$$\nabla \cdot \mathbf{G}^- + \sigma_t \Psi^+ = \frac{\sigma_s \Phi + Q}{4\pi}, \tag{4.1b}$$

along with its boundary condition,

$$(\mathbf{n}\cdot\Omega)\Omega \underbrace{\left(\frac{1}{\sigma_t}\nabla\cdot\mathbf{G}^- - \frac{\sigma_s\Phi+Q}{4\pi\sigma_t}\right)}_{-\Psi^+} = -|\mathbf{n}\cdot\Omega|(\mathbf{G}^- - \Omega F^-) \quad \text{for } \mathbf{r}\in\partial\mathbf{D}. \tag{4.1c}$$

Recall that we have previously defined $\mathbf{G}^-$ to be $\Omega\Psi^-$.

1. XYZ Geometry

To begin, we dot equation (4.1a) with a set of vector weight functions $(\mathbf{w}_i^-(\mathbf{r}), 1 \le i \le I)$ and integrate the result over the domain. Then, we multiply equation (4.1b) by a set of scalar weight functions $(v_k^+(\mathbf{r}), 1 \le k \le K)$ and integrate the result over the domain. We obtain equations of the form:

$$\int_{\mathbf{D}} \nabla\cdot\Omega\Omega\Psi^+ \cdot \mathbf{w}_i^- \, dV + \int_{\mathbf{D}} \sigma_t \mathbf{G}^- \cdot \mathbf{w}_i^- \, dV = 0. \tag{4.2a}$$

and

$$\int_{\mathbf{D}} \nabla\cdot\mathbf{G}^- v_k^+ \, dV + \int_{\mathbf{D}} \sigma_t \Psi^+ v_k^+ \, dV = \int_{\mathbf{D}} \frac{\sigma_s\Phi+Q}{4\pi} v_k^+ \, dV, \tag{4.2b}$$

for each value of i and k. We now manipulate equation (4.2a) so that we can incorporate the boundary condition, equation (4.1c), naturally. We use identity (3.3) to obtain:

$$\int_{\mathbf{D}} \nabla \cdot \left[(\Omega \cdot \mathbf{w}_i^-)(\Omega \Psi^+) \right] dV - \int_{\mathbf{D}} \Psi^+ \nabla \cdot \Omega (\Omega \cdot \mathbf{w}_i^-) \, dV + \int_{\mathbf{D}} \sigma_t \mathbf{G}^- \cdot \mathbf{w}_i^- \, dV = 0. \quad (4.3)$$

We apply Green's theorem to the first term in equation (4.3) to obtain:

$$\int_{\partial \mathbf{D}} (\mathbf{n} \cdot \Omega)(\Omega \Psi^+) \cdot \mathbf{w}_i^- \, dS - \int_{\mathbf{D}} \Psi^+ \nabla \cdot \Omega (\Omega \cdot \mathbf{w}_i^-) \, dV + \int_{\mathbf{D}} \sigma_t \mathbf{G}^- \cdot \mathbf{w}_i^- \, dV = 0. \quad (4.4)$$

After inserting equation (4.1c) into the surface integral, we arrive at:

$$\int_{\partial \mathbf{D}} |\mathbf{n} \cdot \Omega| (\mathbf{G}^- - \Omega F^-) \cdot \mathbf{w}_i^- \, dS - \int_{\mathbf{D}} \Psi^+ \nabla \cdot \Omega (\Omega \cdot \mathbf{w}_i^-) \, dV + \int_{\mathbf{D}} \sigma_t \mathbf{G}^- \cdot \mathbf{w}_i^- \, dV = 0. \quad (4.5)$$

Now we expand the analytic unknowns with the following basis funcitions:

$$\mathbf{G}^-(\mathbf{r}, \Omega) \simeq \mathbf{g}^-(\mathbf{r}, \Omega) = \sum_{j=1}^{I} g_j^-(\Omega) \mathbf{b}_j^-(\mathbf{r}), \quad (4.6a)$$

$$\Psi^+(\mathbf{r}, \Omega) \simeq \psi^+(\mathbf{r}, \Omega) = \sum_{l=1}^{K} \psi_l^+(\Omega) d_l^+(\mathbf{r}), \quad (4.6b)$$

and

$$\Phi^+(\mathbf{r}) \simeq \phi^+(\mathbf{r}) = \sum_{l=1}^{K} \phi_l^+ d_l^+(\mathbf{r}) \quad \text{where } \phi_l^+ = 2 \int_{2\pi} \psi_l^+(\Omega) \, d\Omega, \quad (4.6c)$$

to obtain:

$$\int_{\partial\mathbf{D}} |\mathbf{n}\cdot\Omega|(\mathbf{g}^- - \Omega f^-)\cdot\mathbf{w}_i^- \, dS - \int_{\mathbf{D}} \psi^+ \nabla\cdot\Omega(\Omega\cdot\mathbf{w}_i^-)\, dV + \int_{\mathbf{D}} \sigma_t \mathbf{g}^- \cdot \mathbf{w}_i^- \, dV = 0, \quad (4.7a)$$

$$\int_{\mathbf{D}} (\nabla\cdot\mathbf{g}^-) v_k^+ \, dV + \int_{\mathbf{D}} \sigma_t \psi^+ v_k^+ \, dV = \int_{\mathbf{D}} \frac{\sigma_s\phi^+ + q^+}{4\pi} v_k^+ \, dV. \quad (4.7b)$$

We know of no *a priori* reason we cannot mass lump either equation (4.7a) or (4.7b).

2. Slab Geometry

In this section, we develop a slab geometry discretization for equations (4.7). We use a one-dimensional analog of the lowest order Raviart-Thomas [40] elements on the grid shown in Fig. 4. In this approximation, the normal component of the vector unknown is continuous across cell edges and the scalar unknown is constant within each cell. We apply Galerkin weighing and expand g^- with linear continuous elments and ψ^+ with piecewise constants:

$$w_{j+1/2}^- = b_{j+1/2}^- = \begin{cases} (x_{j+3/2} - x)/(x_{j+3/2} - x_{j+1/2}) & \text{for } x \in (x_{j+1/2}, x_{j+3/2}) \\ (x - x_{j-1/2})/(x_{j+1/2} - x_{j-1/2}) & \text{for } x \in (x_{j-1/2}, x_{j+1/2}) \\ 0 & \text{otherwise,} \end{cases}$$

$$v_j^+ = d_j^+ = \begin{cases} 1 & \text{for } x \in (x_{j-1/2}, x_{j+1/2}) \\ 0 & \text{otherwise.} \end{cases}$$

The equations governing the boundary cells are:

$$|\mu|(g_{1/2}^- - \mu f_l^-) + \mu^2 \psi_1^+ + \frac{\sigma_{t1}\Delta x_1}{3} g_{1/2}^- + \frac{\sigma_{t1}\Delta x_1}{6} g_{3/2}^- = 0 \quad \text{for } j = 1, \quad (4.8a)$$

and

$$|\mu|(g^-_{J+1/2}-\mu f^-_r)-\mu^2\psi^+_J+\frac{\sigma_{t1}\Delta x_1}{6}g^-_{J-1/2}+\frac{\sigma_{t1}\Delta x_1}{3}g^-_{J+1/2}=0 \quad \text{for } j=J. \tag{4.8b}$$

For the interior cells we have:

$$\mu^2(\psi^+_{j+1}-\psi^+_j)+\frac{\sigma_{tj}\Delta x_j}{6}g^-_{j-1/2}+\Big(\frac{\sigma_{tj}\Delta x_j}{3}+\frac{\sigma_{tj+1}\Delta x_{j+1}}{3}\Big)g^-_{j+1/2} + \frac{\sigma_{tj+1}\Delta x_{j+1}}{6}g^-_{j+3/2}=0 \quad \text{for } j=2..J-1. \tag{4.8c}$$

We also have the following cell centered balance equation that holds for all cells:

$$(g^-_{j+1/2}-g^-_{j-1/2})+\sigma_{tj}\Delta x_j\psi^+_j=\frac{\Delta x_j}{2}(\sigma_{sj}\phi^+_j+q^+_j) \quad \text{for } j=1..J. \tag{4.8d}$$

With mass matrix lumping we arrive at the following equations for the boundary cells:

$$|\mu|(g^-_{1/2}-\mu f^-_l)+\mu^2\psi^+_1+\frac{\sigma_{t1}\Delta x_1}{2}g^-_{1/2}=0 \quad \text{for } j=1, \tag{4.9a}$$

and

$$|\mu|(g^-_{J+1/2}-\mu f^-_r)-\mu^2\psi^+_J+\frac{\sigma_{t1}\Delta x_1}{2}g^-_{J+1/2}=0 \quad \text{for } j=J. \tag{4.9b}$$

In the interior, we have:

$$\mu^2(\psi^+_{j+1}-\psi^+_j)+\Big(\frac{\sigma_{tj}\Delta x_j}{2}+\frac{\sigma_{tj+1}\Delta x_{j+1}}{2}\Big)g^-_{j+1/2}=0 \quad \text{for } j=2..J-1, \tag{4.9c}$$

and the cell centered balance equation is unchanged.

We note that both the lumped and unlumped slab geometry coupled parity discretizations are equivalent to their odd-parity CFEM counterparts developed in Chapter III. This is not the case in multidimensional geometry, however.

B. Angular Flux/Current Density System

Now we apply the weighted residual method to the coupled AFCD equations which we rewrite here:

$$\nabla \cdot \Omega\Omega\Psi + \sigma_t \mathbf{G} = \Omega \frac{\sigma_s \Phi + Q}{4\pi}, \tag{4.10a}$$

$$\nabla \cdot \mathbf{G} + \sigma_t \Psi = \frac{\sigma_s \Phi + Q}{4\pi}, \tag{4.10b}$$

$$\mathbf{G}_b(\mathbf{r},\Omega) \quad \text{for } \mathbf{r} \in \partial\mathbf{D} = \begin{cases} \Omega F(\mathbf{r},\Omega) & \text{for } \mathbf{n}\cdot\Omega < 0 \\ \mathbf{G} & \text{for } \mathbf{n}\cdot\Omega > 0. \end{cases} \tag{4.10c}$$

1. XYZ Geometry

We dot equation (4.10a) with a set of vector weight functions $(\mathbf{w}_i(\mathbf{r}), 1 \le i \le I)$and integrate over the domain. Then we multiply equation (4.10b) by a set of scalar weight functions $(v_k(\mathbf{r}), 1 \le k \le K)$ and integrate the result over the domain. We obtain equations of the form:

$$\int_{\mathbf{D}} \nabla \cdot \Omega\Omega\Psi \cdot \mathbf{w}_i \, dV + \int_{\mathbf{D}} \sigma_t \mathbf{G} \cdot \mathbf{w}_i \, dV = \int_{\mathbf{D}} \frac{\sigma_s \Phi + Q}{4\pi} (\Omega \cdot \mathbf{w}_i) \, dV, \tag{4.11a}$$

$$\int_{\mathbf{D}} \nabla \cdot \mathbf{G} v_k \, dV + \int_{\mathbf{D}} \sigma_t \Psi v_k \, dV = \int_{\mathbf{D}} \frac{\sigma_s \Phi + Q}{4\pi} v_k \, dV. \tag{4.11b}$$

We apply identity (3.3) to the streaming term of equation (4.11a) to obtain:

$$\int_{\mathbf{D}} \nabla \cdot \left[(\Omega\Psi)(\Omega \cdot \mathbf{w}_i) \right] dV - \int_{\mathbf{D}} \Psi \nabla \cdot \Omega (\Omega \cdot \mathbf{w}_i) \, dV + \int_{\mathbf{D}} \sigma_t \mathbf{G} \cdot \mathbf{w}_i \, dV = \int_{\mathbf{D}} \frac{\sigma_s \Phi + Q}{4\pi} (\Omega \cdot \mathbf{w}_i) \, dV. \tag{4.12}$$

Using Green's theorem on the first term in equation (4.12) allows us to replace $\Omega\Psi$ with $\mathbf{G}_b$ to obtain:

$$\int_{\partial\mathbf{D}} (\mathbf{n}\cdot\Omega)\mathbf{G}_b\cdot\mathbf{w}_i\,dS - \int_{\mathbf{D}} \Psi\nabla\cdot\Omega(\Omega\cdot\mathbf{w}_i)\,dV + \int_{\mathbf{D}} \sigma_t\mathbf{G}\cdot\mathbf{w}_i\,dV = \int_{\mathbf{D}} \frac{\sigma_s\Phi+Q}{4\pi}(\Omega\cdot\mathbf{w}_i)\,dV. \quad (4.13)$$

Now we expand the analytic unknowns:

$$\mathbf{G}(\mathbf{r},\Omega) \simeq \mathbf{g}(\mathbf{r},\Omega) = \sum_{j=1}^{I} g_j(\Omega)\mathbf{b}_j(\mathbf{r}), \quad (4.14a)$$

$$\Psi(\mathbf{r},\Omega) \simeq \psi(\mathbf{r},\Omega) = \sum_{l=1}^{K} \psi_l(\Omega)d_l(\mathbf{r}), \quad (4.14b)$$

and

$$\Phi(\mathbf{r}) \simeq \phi(\mathbf{r}) = \sum_{l=1}^{K} \phi_l d_l(\mathbf{r}) \quad \text{where } \phi_l = \int_{4\pi} \psi_l(\Omega)\,d\Omega, \quad (4.14c)$$

to arrive at:

$$\int_{\partial\mathbf{D}} (\mathbf{n}\cdot\Omega)\mathbf{g}_b\cdot\mathbf{w}_i\,dS - \int_{\mathbf{D}} \psi\nabla\cdot\Omega(\Omega\cdot\mathbf{w}_i)\,dV + \int_{\mathbf{D}} \sigma_t\mathbf{g}\cdot\mathbf{w}_i\,dV = \int_{\mathbf{D}} \frac{\sigma_s\phi+q}{4\pi}(\Omega\cdot\mathbf{w}_i)\,dV, \quad (4.15a)$$

$$\int_{\mathbf{D}} \nabla\cdot\mathbf{g}v_k\,dV + \int_{\mathbf{D}} \sigma_t\psi v_k\,dV = \int_{\mathbf{D}} \frac{\sigma_s\phi+q}{4\pi}v_k\,dV, \quad (4.15b)$$

where,

$$\mathbf{g}_b(\mathbf{r},\Omega) \quad \text{for } \mathbf{r}\in\partial\mathbf{D} = \begin{cases} \Omega f(\mathbf{r},\Omega) & \text{for } \mathbf{n}\cdot\Omega < 0 \\ \mathbf{g} & \text{for } \mathbf{n}\cdot\Omega > 0. \end{cases} \quad (4.15c)$$

2. Slab Geometry

Now we apply the same slab geometry discretization as we did for the coupled parity equations:

$$w_{j+1/2} = b_{j+1/2} = \begin{cases} (x_{j+3/2} - x)/(x_{j+3/2} - x_{j+1/2}) & \text{for } x \in (x_{j+1/2}, x_{j+3/2}) \\ (x - x_{j-1/2})/(x_{j+1/2} - x_{j-1/2}) & \text{for } x \in (x_{j-1/2}, x_{j+1/2}) \\ 0 & \text{otherwise,} \end{cases}$$

$$v_j = d_j = \begin{cases} 1 & \text{for } x \in (x_{j-1/2}, x_{j+1/2}) \\ 0 & \text{otherwise.} \end{cases}$$

The boundary cells equations are:

$$-\mu g_l + \mu^2 \psi_1 + \frac{\sigma_{t1}\Delta x_1}{3} g_{1/2} + \frac{\sigma_{t1}\Delta x_1}{6} g_{3/2} = \frac{\mu}{4}(\sigma_{s1}\Delta x_1 \phi_1 + \Delta x_1 q_1) \quad \text{for } j = 1, \quad (4.16a)$$

and

$$\mu g_r - \mu^2 \psi_J + \frac{\sigma_{tJ}\Delta x_J}{6} g_{J-1/2} + \frac{\sigma_{tJ}\Delta x_J}{3} g_{J+1/2} = \frac{\mu}{4}(\sigma_{sJ}\Delta x_J \phi_J + \Delta x_J q_J) \quad \text{for } j = J, \quad (4.16b)$$

where,

$$g_l = \begin{cases} \mu f_l & \text{for } \mu > 0 \\ g_{1/2} & \text{for } \mu < 0, \end{cases} \qquad g_r = \begin{cases} g_{J+1/2} & \text{for } \mu > 0 \\ \mu f_r & \text{for } \mu < 0. \end{cases} \quad (4.16c)$$

For the interior cells we have:

$$\mu^2(\psi_{j+1}-\psi_j) + \frac{\sigma_{tj}\Delta x_j}{6}g_{j-1/2} + \left(\frac{\sigma_{tj}\Delta x_j}{3}+\frac{\sigma_{tj+1}\Delta x_{j+1}}{3}\right)g_{j+1/2} + \frac{\sigma_{tj+1}\Delta x_{j+1}}{6}g_{j+3/2} = \frac{\mu}{4}\left[(\sigma_{sj}\Delta x_j\phi_j+\Delta x_j q_j)+(\sigma_{sj+1}\Delta x_{j+1}\phi_{j+1}+\Delta x_{j+1}q_{j+1})\right] \quad \text{for } j=2..J-1. \quad (4.16d)$$

We also have a cell centered balance equation:

$$(g_{j+1/2}-g_{j-1/2})+\sigma_{tj}\Delta x_j\psi_j = \frac{\Delta x_j}{2}(\sigma_{sj}\phi_j+q_j) \quad \text{for } j=1..J. \quad (4.16e)$$

We can again lump the mass matrix:

$$-\mu g_l + \mu^2\psi_1 + \frac{\sigma_{t1}\Delta x_1}{2}g_{1/2} = \frac{\mu}{4}(\sigma_{s1}\Delta x_1\phi_1+\Delta x_1 q_1) \quad \text{for } j=1, \quad (4.17a)$$

and

$$\mu g_r - \mu^2\psi_J + \frac{\sigma_{tJ}\Delta x_J}{2}g_{J+1/2} = \frac{\mu}{4}(\sigma_{sJ}\Delta x_J\phi_J+\Delta x_J q_J) \quad \text{for } j=J. \quad (4.17b)$$

For the interior cells mass matrix lumping produces:

$$\mu^2(\psi_{j+1}-\psi_j)+\left(\frac{\sigma_{tj}\Delta x_j}{2}+\frac{\sigma_{tj+1}\Delta x_{j+1}}{2}\right)g_{j+1/2} = \frac{\mu}{4}\left[(\sigma_{sj}\Delta x_j\phi_j+\Delta x_j q_j)+(\sigma_{sj+1}\Delta x_{j+1}\phi_{j+1}+\Delta x_{j+1}q_{j+1})\right] \quad \text{for } j=2..J-1. \quad (4.17c)$$

The cell centered balance equation is unchanged by lumping.

By solving equation (4.16e) for ψ_j, we can replace the cell centered unknowns in equation (4.17c) with cell edge unknowns. The resulting system is very nearly identical to the slab geometry SAAF equations. However, there is one important difference. In the case

of the SAAF system, a scalar flux is explicitly defined for cell edge quantities. Here, the term that corresponds to the cell edge SAAF scalar flux is the average of the two adjacent cell centered scalar fluxes.

C. Discrete Diffusion Limit Analysis

We now analyze the behavior of equations (4.7) and (4.15) in the thick diffusion limit. Our procedure involves scaling the discretized equations as in equation (2.32), then requiring the resulting equations to hold form like powers of the scaling parameter ε.

1. Coupled Parity

We introduce the scaling shown in equation (2.32) into the coupled parity system to obtain:

$$\int_{\partial \mathbf{D}} |\mathbf{n}\cdot\Omega|(\mathbf{g}^- - \Omega f^-)\cdot \mathbf{w}_i^- \, dS - \int_{\mathbf{D}} \psi^+ \nabla\cdot\Omega(\Omega\cdot\mathbf{w}_i^-)\, dV + \int_{\mathbf{D}} \frac{\sigma_t}{\varepsilon}\mathbf{g}^-\cdot\mathbf{w}_i^- \, dV = 0, \quad (4.18a)$$

$$\int_{\mathbf{D}} (\nabla\cdot\mathbf{g}^-)v_k^+ \, dV + \int_{\mathbf{D}} \frac{\sigma_t}{\varepsilon}\psi^+ v_k^+ \, dV = \int_{\mathbf{D}} \frac{(\frac{\sigma_t}{\varepsilon} - \varepsilon\sigma_a)\phi^+ + \varepsilon q^+}{4\pi} v_k^+ \, dV. \quad (4.18b)$$

We introduce the following ansatz:

$$\mathbf{g}^- = \mathbf{g}^{-[0]} + \varepsilon\mathbf{g}^{-[1]} + \varepsilon^2\mathbf{g}^{-[2]} + ..., \quad (4.19a)$$

$$\psi^+ = \psi^{+[0]} + \varepsilon\psi^{+[1]} + \varepsilon^2\psi^{+[2]} + ..., \quad (4.19b)$$

$$\phi^+ = \phi^{+[0]} + \varepsilon\phi^{+[1]} + \varepsilon^2\phi^{+[2]} + ... \quad \text{where } \phi^{+[k]} = \int_{4\pi} \psi^{+[k]} \, d\Omega, \quad (4.19c)$$

into the scaled systems then require that the resulting systems hold for each power of ε. The O(1/ε) terms in equations (4.18a) and (4.18b) are:

$$\int_{\mathbf{D}} \sigma_t \mathbf{g}^{-[0]} \cdot \mathbf{w}_i^- \, dV = 0 \tag{4.20a}$$

$$\int_{\mathbf{D}} \sigma_t \psi^{+[0]} v_k^+ \, dV = \int_{\mathbf{D}} \frac{\sigma_t \phi^{+[0]}}{4\pi} v_k^+ \, dV. \tag{4.20b}$$

Under the assumption of invertible mass matrices, these equations imply that the leading order angular current density is zero,

$$\mathbf{g}^{-[0]} = 0, \tag{4.21a}$$

and that the leading order even-parity angular flux is isotropic,

$$\psi^{+[0]} = \frac{\phi^{+[0]}}{4\pi}. \tag{4.21b}$$

Now, we consider the O(1) terms in equation (4.18a):

$$\int_{\partial\mathbf{D}} |\mathbf{n}\cdot\Omega|(\mathbf{g}^{-[0]} - \Omega f^-) \cdot \mathbf{w}_i^- \, dS - \int_{\mathbf{D}} \psi^{+[0]} \nabla\cdot\Omega(\Omega\cdot\mathbf{w}_i^-) \, dV + \int_{\mathbf{D}} \sigma_t \mathbf{g}^{-[1]} \cdot \mathbf{w}_i^- \, dV = 0, \tag{4.22}$$

Using the results from equations (4.21a) and (4.21b) we can integrate over angle to arrive at:

$$\frac{1}{3}\int_{\partial\mathbf{D}} \left(2\mathbf{n}\cdot \int_{\mathbf{n}\cdot\Omega<0} 3\Omega\Omega f^- \, d\Omega\right) \cdot \mathbf{w}_i^- \, dS - \frac{1}{3}\int_{\mathbf{D}} \phi^{+[0]} \nabla\cdot\mathbf{w}_i^- \, dV + \int_{\mathbf{D}} \sigma_t \left(2\int_{2\pi} \mathbf{g}^{-[1]} \, d\Omega\right) \cdot \mathbf{w}_i^- \, dV = 0, \tag{4.23}$$

We turn our attention to the O(ε) terms in equation (4.18b):

$$\int_{\mathbf{D}} (\nabla \cdot \mathbf{g}^{-[1]}) v_k^+ \, dV + \int_{\mathbf{D}} \sigma_t \psi^{+[2]} v_k^+ \, dV = \int_{\mathbf{D}} \frac{\sigma_t \phi^{+[2]} - \sigma_a \phi^{+[0]} + q^+}{4\pi} v_k^+ \, dV. \tag{4.24}$$

We integrate equation (4.24) over angle to find that:

$$\int_{\mathbf{D}} \nabla \cdot \Big(\int_{2\pi} \mathbf{g}^{-[1]} \, d\Omega \Big) v_k^+ \, dV + \int_{\mathbf{D}} \sigma_a \phi^{+[0]} v_k^+ \, dV = \int_{\mathbf{D}} q^+ v_k^+ \, dV. \tag{4.25}$$

Thus, we find that the leading order coupled parity solution satisfies the following coupled diffusion system in the thick diffusive limit:

$$\frac{1}{3} \int_{\partial \mathbf{D}} \Big(2\mathbf{n} \cdot \int_{\mathbf{n}\cdot\Omega<0} 3\Omega\Omega f^- \, d\Omega \Big) \cdot \mathbf{w}_i^- \, dS - \frac{1}{3} \int_{\mathbf{D}} \phi^{+[0]} \nabla \cdot \mathbf{w}_i^- \, dV + \int_{\mathbf{D}} \sigma_t \Big(2 \int_{2\pi} \mathbf{g}^{-[1]} \, d\Omega \Big) \cdot \mathbf{w}_i^- \, dV = 0, \tag{4.26a}$$

$$\int_{\mathbf{D}} \nabla \cdot \Big(\int_{2\pi} \mathbf{g}^{-[1]} \, d\Omega \Big) v_k^+ \, dV + \int_{\mathbf{D}} \sigma_a \phi^{+[0]} v_k^+ \, dV = \int_{\mathbf{D}} q^+ v_k^+ \, dV. \tag{4.26b}$$

If Raviart-Thomas elements are used to discretize equations (4.26) then f^- need not be be symmetric about the outward normal for us to have:

$$\mathbf{n} \cdot \Big(2 \int_{\mathbf{n}\cdot\Omega<0} 3\Omega\Omega f^- \, d\Omega \Big) = \mathbf{n} \Big(2 \int_{\mathbf{n}\cdot\Omega<0} 3|\mathbf{n}\cdot\Omega|^2 f^- \, d\Omega \Big) = \mathbf{n} \phi_b^{rt}. \tag{4.26c}$$

since the RT_0 weight and basis functions are normal to cell faces. This system is simply a mixed finite element discretization to the diffusion equation subject to a potentially inaccurate boundary condition. The weighting function is identical the odd-parity weighing function shown in Fig. 6, therefore, we expect the average of CFEM even- parity results and MFEM odd-parity results to be accurate for thick diffusive problems.

2. AFCD

We now consider the diffusion limit of the discrete AFCD equations. We find that it does indeed limit to a MFEM discretization of the diffusion equation with a complex boundary condition. However, unlike the other discretizations we have examineded, in order to interpret the boundary condition, we are forced to consider the slab geometry case. Though this is not as rigorous, we fully expect that the essential characteristics of this method are sufficiently characterized in slab geometry, given that diffusive boundaries are essentially one-dimensional. By that, we mean in a thick, diffusive problem the curvature of the boundary is an order ε quantity and should not affect the leading order solution.

We scale the discrete AFCD system in the standard way,

$$\int_{\partial\mathbf{D}} (\mathbf{n}\cdot\Omega)\mathbf{g}_b\cdot\mathbf{w}_i\,dS - \int_{\mathbf{D}} \psi\nabla\cdot\Omega(\Omega\cdot\mathbf{w}_i)\,dV + \int_{\mathbf{D}} \frac{\sigma_t}{\varepsilon}\mathbf{g}\cdot\mathbf{w}_i\,dV = \int_{\mathbf{D}} \frac{(\frac{\sigma_t}{\varepsilon}-\varepsilon\sigma_a)\phi+q}{4\pi}(\Omega\cdot\mathbf{w}_i)\,dV, \quad (4.27a)$$

$$\int_{\mathbf{D}} \nabla\cdot\mathbf{g}v_k\,dV + \int_{\mathbf{D}} \frac{\sigma_t}{\varepsilon}\psi v_k\,dV = \int_{\mathbf{D}} \frac{(\frac{\sigma_t}{\varepsilon}-\varepsilon\sigma_a)\phi+q}{4\pi}v_k\,dV, \quad (4.27b)$$

and introduce the ansatz:

$$\mathbf{g} = \mathbf{g}^{[0]} + \varepsilon\mathbf{g}^{[1]} + \varepsilon^2\mathbf{g}^{[2]} + \ldots, \quad (4.28a)$$

$$\psi = \psi^{[0]} + \varepsilon\psi^{[1]} + \varepsilon^2\psi^{[2]} + \ldots, \quad (4.28b)$$

$$\phi = \phi^{[0]} + \varepsilon\phi^{[1]} + \varepsilon^2\phi^{[2]} + \ldots \quad \text{where } \phi^{[k]} = \int_{4\pi} \psi^{[k]}\,d\Omega, \quad (4.28c)$$

and require the scaled equations to hold for each power of ε. The O(1/ε) equations are:

$$\int_{\mathbf{D}} \sigma_t \mathbf{g}^{[0]} \cdot \mathbf{w_i}\, dV = \int_{\mathbf{D}} \frac{\sigma_t \phi^{[0]}}{4\pi} (\Omega \cdot \mathbf{w_i})\, dV, \tag{4.29a}$$

and

$$\int_{\mathbf{D}} \sigma_t \psi^{[0]} v_k\, dV = \int_{\mathbf{D}} \frac{\sigma_t \phi^{[0]}}{4\pi} v_k\, dV. \tag{4.29b}$$

Equation (4.29b) implies that the leading order angular flux is isotropic, as expected. The O(1) terms of equation (4.27a) are:

$$\int_{\partial\mathbf{D}} (\mathbf{n} \cdot \Omega) \mathbf{g}_b^{[0]} \cdot \mathbf{w_i}\, dS - \int_{\mathbf{D}} \psi^{[0]} \nabla \cdot \Omega (\Omega \cdot \mathbf{w_i})\, dV + \int_{\mathbf{D}} \sigma_t \mathbf{g}^{[1]} \cdot \mathbf{w_i}\, dV = \int_{\mathbf{D}} \frac{\sigma_t \phi^{[1]}}{4\pi} (\Omega \cdot \mathbf{w_i})\, dV. \tag{4.30}$$

Making use of the fact that the leading order angular flux is isotropic, we integrate this over angle to obtain:

$$\int_{\partial\mathbf{D}} \mathbf{n} \cdot \left(\int_{4\pi} \Omega \mathbf{g}_b^{[0]}\, d\Omega \right) \cdot \mathbf{w_i}\, dS - \frac{1}{3} \int_{\mathbf{D}} \phi^{[0]} \nabla \cdot \mathbf{w_i}\, dV + \int_{\mathbf{D}} \sigma_t \left(\int_{4\pi} \mathbf{g}^{[1]}\, d\Omega \right) \cdot \mathbf{w_i}\, dV = 0. \tag{4.31}$$

Now, we examine the O(ε) terms in equation (4.27b). If we integrate this over angle, we obtain another equation relating $\phi^{[0]}$ and $\mathbf{g}^{[1]}$. Hence, we find that our leading order scalar flux satisfies the following diffusion discretization in the thick diffusion limit:

$$\int_{\partial\mathbf{D}} \mathbf{n} \cdot \left(\int_{4\pi} \Omega \mathbf{g}_b^{[0]}\, d\Omega \right) \cdot \mathbf{w_i}\, dS - \frac{1}{3} \int_{\mathbf{D}} \phi^{[0]} \nabla \cdot \mathbf{w_i}\, dV + \int_{\mathbf{D}} \sigma_t \left(\int_{4\pi} \mathbf{g}^{[1]}\, d\Omega \right) \cdot \mathbf{w_i}\, dV = 0. \tag{4.32a}$$

$$\int_{\mathbf{D}} \nabla \cdot \Big(\int_{4\pi} \mathbf{g}^{[1]}\, d\Omega \Big) v_j\, dV + \int_{\mathbf{D}} \sigma_a \phi^{[0]} v_j\, dV = \int_{\mathbf{D}} q v_k\, dV. \tag{4.32b}$$

Finally, we examine the boundary integral in equation (4.32a) in more detail. We have found that proceeding with this analysis in three dimensions with generic weight and basis functions is intractable. Therefore, we continue in slab geometry with lumped linear finite elements. On the left boundary we have:

$$-\mu g_l^{[0]} + \mu^2 \psi_1^{[0]} + \frac{\sigma_{t1}\Delta x_1}{2} g_{1/2}^{[1]} = \frac{\mu}{4} \sigma_{t1} \Delta x_1 \phi_1^{[1]}, \tag{4.33a}$$

where

$$g_l = \begin{cases} \mu f_l & \text{for } \mu > 0 \\ g_{1/2}^{[0]} & \text{for } \mu < 0. \end{cases} \tag{4.33b}$$

We take the zeroth moment of equation (4.33) to arrive at:

$$-\int_{-1}^{1} \mu g_l^{[0]}\, d\mu + \frac{1}{3}\phi_1^{[0]} + \frac{\sigma_{t1}\Delta x_1}{2} \int_{-1}^{1} g_{1/2}^{[1]}\, d\mu = 0. \tag{4.34}$$

Substituting for $g_l^{[0]}$:

$$-\Big(\int_{-1}^{0} \mu g_{1/2}^{[0]}\, d\mu + \int_{0}^{1} \mu^2 f_l\, d\mu \Big) + \frac{1}{3}\phi_1^{[0]} + \frac{\sigma_{t1}\Delta x_1}{2} \int_{-1}^{1} g_{1/2}^{[1]}\, d\mu = 0. \tag{4.35}$$

In slab geometry, equation (4.29a) reduces to $g_{1/2}^{[0]} = \mu\phi_1^{[0]}/2$ so that we have:

$$-\frac{1}{3}\Big(\frac{\phi_1^{[0]}}{2} + \int_{0}^{1} 3\mu^2 f_l\, d\mu \Big) + \frac{1}{3}\phi_1^{[0]} + \frac{\sigma_{t1}\Delta x_1}{2} \int_{-1}^{1} g_{1/2}^{[1]}\, d\mu = 0. \tag{4.36}$$

Thus,

$$\int_{-1}^{1} g_{1/2}^{[1]}\, d\mu = -\frac{1}{3}\frac{\phi_1^{[0]} - 2\int_0^1 3\mu^2 f_l\, d\mu}{\sigma_{t1}\Delta x_1}. \tag{4.37}$$

The above equation represents a $3\mu^2$ weighting of the incoming angular flux spatially located *one half cell to the left of the physical boundary*. In the odd-parity system, the corresponding relation is:

$$\int_{-1}^{1} g_{1/2}^{-[1]}\, d\mu = -\frac{1}{3}\frac{\phi_1^{-[0]} - 2\int_0^1 3\mu^2 f_l\, d\mu}{(\sigma_{t1}\Delta x_1/2)}. \tag{4.38}$$

Thus, the odd-parity boundary flux is located on the actual left boundary. This means that for thick diffusive problems driven by incoming angular fluxes, we expect the AFCD boundary scalar flux to be lower than the odd-parity result. However, if the first cell were made thin, then both methods should agree. We confirm this behavior in the numerical results section.

D. Internal Interface Analysis

1. Coupled Parity

As we noted above, the slab geometry linear finite element approximation of the coupled parity equations is equivalent to the corresponding discretization of the odd-parity equations. Thus, those results directly hold here.

2. AFCD

Our ability to analyze the internal interface problem is due, in large part, to our solid understanding of the even- and odd-parity systems. They are unique in that we can derive explicit

expressions for both the mangitude of the scalar flux on the transport/diffusive interface, and for the angular shape and magnitude of the flux that returns back into the transport region.

Our attempts to analyze the AFCD system have thus far been fruitless. Inevitably, we arrive at systems that couple both upstream and downstream unknowns, making it impossible to derive simple, closed form expressions for the quantities we desire. We confess that we do not fully understand the behavior of the AFCD system at an internal interface.

However, we conjecture that, because of the fact that the AFCD system behaves much like the odd-parity system at external boundaries, the AFCD solution at an internal interface should be similar to the odd-parity solution. We test this prediction in the numerical results section, and find that it appears warranted.

E. Implementational Considerations

An attractive discretization to consider is the lowest order Raviart-Thomas (RT_0) method. It is derived in such a way that the normal component of the vector unknown is continuous (and, in fact, constant) on each face. The scalar unknown lives in the finite element space generated by the gradient of the vector basis functions. In the RT_0 case on triangles, the scalar flux would be piecewise constant within each element. The vector basis functions have the following form:

$$\mathbf{b}(\mathbf{r}) = (a + cx)\mathbf{i} + (b + cy)\mathbf{j}. \tag{4.39}$$

This method is well established for triangles, rectangles and tetrahedra [59, 5]. Recently, several researchers have developed methods for logically rectangular grids that reduce to the Raviart-Thomas discretization on an orthogonal mesh [60, 61].

The vector unknown exhibits first order convergence, but the scalar unknown is second

order. In terms of unknowns, the RT_0 method has a vector unknown on each face and a scalar unknown in each cell. On the downside, the linear systems that result from this type of mixed FEM are symmetric but possibly indefinite. They are of the form:

$$\begin{bmatrix} \mathbf{A} & \mathbf{B} \\ \mathbf{B}^T & \mathbf{C} \end{bmatrix} \begin{bmatrix} \mathbf{g} \\ \psi \end{bmatrix} = \begin{bmatrix} \mathbf{S} \\ \mathbf{Q} \end{bmatrix},$$

where ψ represents a vector of scalar unknowns and $\mathbf{g}$ is a vector of *vector* unknowns. Since mixed FEM methods have become so popular of late, efficient iterative methods for saddle point problems like this have been developed [62]. Finally, we note that the RT_0 method has an unknown on each cell face and an unknown in each cell center so that the CP discretization will have $5NK/4$ total unknowns and the AFCD discretization $5NK/2$ unknowns where N and K are again the number of angles and cells, respectively. We note that if we use the RT_0 coupled-parity method along with the CFEM even-parity method to form a hybrid-parity solution, there are a total of $3NK/2$ unknowns.

CHAPTER V

ITERATIVE METHODS

In this chapter we discuss the iterative methods used to solve the within-group scattering problem. Historically, the source iteration (SI) method has been the most frequently used technique. However, it is well known that SI can converge arbitrarily slowly for problems that are dominated by scattering.

Many methods have been proposed to solve the within-group problem more efficiently. Synthetic acceleration [32, 33, 34, 35, 55, 56, 36, 57, 63], coarse mesh rebalance [64], quasi-diffusion [65, 66, 67], and boundary projection acceleration [68] have all been implemented with various degrees of success, though no method has emerged as the best choice for all problems.

Here, we focus on developing DSA schemes for our discretizations. Because of their underlying form (self-adjoint, second order transport operators) we expect that successful implementation of multidimensional DSA will be straightforward, whereas this is notoriously difficult for discretizations of the first order transport equation. Our procedure consists of the following steps.

1. Subtract the discrete source iteration equations from the converged equations to form discrete *correction* equations.

2. Take the zeroth and first moments of the correction equations, assuming that the corrections are linearly anisotropic in angle.

3. Eliminate the first moments to obtain a single diffusion equation.

These steps are equivalent to Larsen's 4-step procedure. We note that it may not be possible, or desirable, to form a single diffusion equation for all of the discretizations we consider.

For each method we first present the source iteration scheme, then derive discrete DSA systems.

Finally, we note that if the within-group problem can be cast in a form that is symmetric positive definite under some norm, the conjugate gradient (CG) method [69, 54, 70] can be used. The CFEM even- and odd-parity operators are symmetric positive definite under the following *scattering* inner product:

$$\langle \mathbf{u}, \mathbf{v} \rangle_s = \sum_{i=1}^{I} \sigma_{si} u_i v_i V_i \tag{5.1}$$

where V_i is the volume of the i^{th} cell.

A. Even-Parity DSA

The source iteration scheme for the even-parity system is given by:

$$\int_{\partial \mathbf{D}} |\mathbf{n}\cdot\Omega| (\psi^{+(\ell+1/2)} - f^{+}) w_i^{+}\, dS + \int_{\mathbf{D}} (\Omega\cdot\nabla w_i^{+}) \frac{1}{\sigma_t} (\Omega\cdot\nabla \psi^{+(\ell+1/2)})\, dV + \int_{\mathbf{D}} \sigma_t \psi^{+(\ell+1/2)} w_i^{+}\, dV = \int_{\mathbf{D}} \frac{\sigma_s \phi^{+(\ell)} + q^{+}}{4\pi} w_i^{+}\, dV, \tag{5.2a}$$

$$\phi^{+(\ell+1)} = \phi^{+(\ell+1/2)} = 2\int_{2\pi} \psi^{+(\ell+1/2)}\, d\Omega, \tag{5.2b}$$

If we define the additive corrections:

$$\gamma^{+(\ell+1/2)} = \psi^{+} - \psi^{+(\ell+1/2)}, \tag{5.3a}$$

and

$$\Gamma^{+(\ell+1/2)} = \phi^{+} - \phi^{+(\ell+1/2)} = 2\int_{2\pi} \gamma^{+(\ell+1/2)}\, d\Omega, \tag{5.3b}$$

then subtract equation (5.2a) from the converged system, we obtain an exact equation for the corrections:

$$\int_{\partial\mathbf{D}} |\mathbf{n}\cdot\Omega|\gamma^{+(\ell+1/2)} w_i^+ \, dS + \int_{\mathbf{D}} (\Omega\cdot\nabla w_i^+)\frac{1}{\sigma_t}(\Omega\cdot\nabla\gamma^{+(\ell+1/2)})\, dV + \int_{\mathbf{D}} \sigma_t \gamma^{+(\ell+1/2)} w_i^+ \, dV = \int_{\mathbf{D}} \frac{\sigma_s}{4\pi}\left[\Gamma^{+(\ell+1/2)} + (\phi^{+(\ell+1/2)} - \phi^{+(\ell)})\right] w_i^+ \, dV. \quad (5.4)$$

We take the zeroth moment of equation (5.4) to obtain:

$$\int_{\partial\mathbf{D}} \left(\int_{4\pi} |\mathbf{n}\cdot\Omega|\gamma^{+(\ell+1/2)}\, d\Omega\right) w_i^+ \, dS + \int_{\mathbf{D}} \left[\int_{4\pi} (\Omega\cdot\nabla w_i^+)\frac{1}{\sigma_t}(\Omega\cdot\nabla\gamma^{+(\ell+1/2)})\, d\Omega\right] dV + \int_{\mathbf{D}} \sigma_a \Gamma^{+(\ell+1/2)} w_i^+ \, dV = \int_{\mathbf{D}} \sigma_s(\phi^{+(\ell+1/2)} - \phi^{+(\ell)}) w_i^+ \, dV. \quad (5.5)$$

Clearly, the first moment of equation (5.4) is zero, since all of the terms in that equation are even in angle. At this point, we enforce the assumption that $\gamma^{+(\ell+1/2)}$ is linearly anisotropic. That is:

$$\gamma^{+(\ell+1/2)} \simeq \frac{1}{2\pi}\int_{2\pi} \gamma^+ \, d\Omega + \frac{3}{4\pi}\Omega\cdot\int_{4\pi} \Omega\gamma^{+(\ell+1/2)}\, d\Omega = \frac{1}{4\pi}\Gamma^{+(\ell+1/2)}.$$

(Since $\Omega\gamma^{+(\ell+1/2)}$ is an odd function, its angular integral is zero.) We arrive at:

$$\int_{\partial\mathbf{D}} \frac{1}{2}\Gamma^{+(\ell+1/2)} w_i^+ \, dS + \int_{\mathbf{D}} \frac{1}{3\sigma_t}(\nabla w_i^+)\cdot(\nabla\Gamma^{+(\ell+1/2)})\, dV + \int_{\mathbf{D}} \sigma_a \Gamma^{+(\ell+1/2)} w_i^+ \, dV = \int_{\mathbf{D}} \sigma_s(\phi^{+(\ell+1/2)} - \phi^{+(\ell)}) w_i^+ \, dV, \quad (5.6)$$

where we have used the fact that

$$\int_{4\pi} |\mathbf{n}\cdot\Omega|\, d\Omega = 2\pi.$$

Hence, the DSA iteration scheme for the even-parity CFEM system is:

$$\int_{\partial\mathbf{D}} |\mathbf{n}\cdot\Omega|(\psi^{+(\ell+1/2)} - f^{+})w_i^{+}\,dS + \int_{\mathbf{D}} (\Omega\cdot\nabla w_i^{+})\frac{1}{\sigma_t}(\Omega\cdot\nabla\psi^{+(\ell+1/2)})\,dV + \int_{\mathbf{D}} \sigma_t\psi^{+(\ell+1/2)}w_i^{+}\,dV = \int_{\mathbf{D}} \frac{\sigma_s\phi^{+(\ell)} + q^{+}}{4\pi}w_i^{+}\,dV, \quad (5.7a)$$

$$\phi^{+(\ell+1/2)} = 2\int_{2\pi} \psi^{+(\ell+1/2)}(\Omega)\,d\Omega, \quad (5.7b)$$

$$\int_{\partial\mathbf{D}} \frac{1}{2}\Gamma^{+(\ell+1/2)}w_i^{+}\,dS + \int_{\mathbf{D}} \frac{1}{3\sigma_t}(\nabla w_i^{+})\cdot(\nabla\Gamma^{+(\ell+1/2)})\,dV + \int_{\mathbf{D}} \sigma_a\Gamma^{+(\ell+1/2)}w_i^{+}\,dV = \int_{\mathbf{D}} \sigma_s(\phi^{+(\ell+1/2)} - \phi^{+(\ell)})w_i^{+}\,dV, \quad (5.7c)$$

$$\phi^{+(\ell+1)} = \phi^{+(\ell+1/2)} + \Gamma^{+(\ell+1/2)}. \quad (5.7d)$$

We can analyze this iterative scheme with lumped linear continuous finite elements in slab geometry. The discrete equations in the interior with constant material properties and mesh size are:

$$-\mu^2\Big(\frac{\psi_{j+3/2}^{+(\ell+1/2)} - \psi_{j+1/2}^{+(\ell+1/2)}}{\Delta x^2} - \frac{\psi_{j+1/2}^{+(\ell+1/2)} - \psi_{j-1/2}^{+(\ell+1/2)}}{\Delta x^2}\Big) + \psi_{j+1/2}^{+(\ell+1/2)} = \frac{c}{2}\phi_{j+1/2}^{+(\ell)}, \quad (5.8a)$$

$$\phi_{j+1/2}^{+(\ell+1/2)} = 2\int_0^1 \psi_{j+1/2}^{+(\ell+1/2)}\,d\mu, \quad (5.8b)$$

$$-\frac{1}{3}\Big(\frac{\Gamma_{j+3/2}^{+(\ell+1/2)} - \Gamma_{j+1/2}^{+(\ell+1/2)}}{\Delta x^2} - \frac{\Gamma_{j+1/2}^{+(\ell+1/2)} - \Gamma_{j-1/2}^{+(\ell+1/2)}}{\Delta x^2}\Big) + (1-c)\Gamma_{j+1/2}^{+(\ell+1/2)} = c(\phi_{j+1/2}^{+(\ell+1/2)} - \phi_{j+1/2}^{+(\ell)}), \quad (5.8c)$$

and, finally,

$$\phi_{j+1/2}^{+(\ell+1)} = \phi_{j+1/2}^{+(\ell+1/2)} + \Gamma_{j+1/2}^{+(\ell+1/2)}. \tag{5.8d}$$

We propose the following ansatz:

$$\psi_{j+1/2}^{+(\ell)} = \omega^{\ell} a(\mu) e^{i\lambda x_{j+1/2}}, \tag{5.9a}$$

$$\phi_{j+1/2}^{+(\ell)} = \omega^{\ell} A e^{i\lambda x_{j+1/2}}, \tag{5.9b}$$

$$\Gamma_{j+1/2}^{+(\ell+1/2)} = \omega^{\ell} B e^{i\lambda x_{j+1/2}}. \tag{5.9c}$$

After inserting the ansatz into equations (5.8), we find that:

$$a(\mu) = \frac{cA}{2(1+\mu^2\Lambda^2)}, \tag{5.10a}$$

and

$$\omega(\lambda) = \frac{c}{\Lambda}\arctan(\Lambda) + \frac{\frac{c^2}{\Lambda}\arctan(\Lambda) - c}{(1-c) + \frac{1}{3}\Lambda^2} \quad \text{where } \Lambda = \frac{2}{\Delta x}\sin(\lambda \Delta x/2). \tag{5.10b}$$

The spectral radius is given by:

$$\rho_{dsa}^{+} = \sup_{\lambda} |\omega(\lambda)| \leq 0.2247c. \tag{5.10c}$$

This result is identical to the spatially analytic case discussed in Chapter II. We, therefore, expect the even-parity DSA iteration scheme to be very effective.

B. Odd-Parity DSA

Now we consider the odd-parity equations. We begin with the source iteration equations:

$$\int_{\partial \mathbf{D}} |\mathbf{n}\cdot\Omega|(\psi^{-(\ell+1/2)} - f^{-})w_i^{-}\,dS + \int_{\mathbf{D}} (\Omega\cdot\nabla w_i^{-})\frac{1}{\sigma_t}(\Omega\cdot\nabla\psi^{-(\ell+1/2)})\,dV + \int_{\mathbf{D}} \sigma_t\psi^{-(\ell+1/2)}w_i^{-}\,dV = \int_{\mathbf{D}} (\Omega\cdot\nabla w_i^{-})\frac{\sigma_s\phi^{-(\ell)}+q^{-}}{4\pi\sigma_t}\,dV, \quad (5.11a)$$

$$\mathbf{J}^{-(\ell+1/2)} = 2\int_{2\pi} \Omega\psi^{-(\ell+1/2)}\,d\Omega, \quad (5.11b)$$

$$\int_{\mathbf{D}} \nabla\cdot\mathbf{J}^{-(\ell+1/2)}v_k^{-}\,dV + \int_{\mathbf{D}} \sigma_t\phi^{-(\ell+1/2)}v_k^{-}\,dV = \int_{\mathbf{D}} (\sigma_s\phi^{-(\ell)}+q^{-})v_k^{-}\,dV, \quad (5.11c)$$

$$\phi^{-(\ell+1)} = \phi^{-(\ell+1/2)}. \quad (5.11d)$$

Note that the right hand side of equation (5.11c) involves the ℓ^{th} iterate of the scalar flux. This allows us to calculate the scalar flux even when $\sigma_a = 0$. Now, we form the exact equation for the corrections by subtracting equations (5.11a) and (5.11c) from their converged forms. We have:

$$\int_{\partial \mathbf{D}} |\mathbf{n}\cdot\Omega|\gamma^{-(\ell+1/2)}w_i^{-}\,dS + \int_{\mathbf{D}} (\Omega\cdot\nabla w_i^{-})\frac{1}{\sigma_t}(\Omega\cdot\nabla\gamma^{-(\ell+1/2)})\,dV + \int_{\mathbf{D}} \sigma_t\gamma^{-(\ell+1/2)}w_i^{-}\,dV = \int_{\mathbf{D}} (\Omega\cdot\nabla w_i^{-})\frac{\sigma_s}{4\pi\sigma_t}\left[\Gamma^{-(\ell+1/2)} + (\phi^{-(\ell+1/2)} - \phi^{-(\ell)})\right]dV, \quad (5.12a)$$

$$\int_{\mathbf{D}} \nabla \cdot \Gamma_1^{-(\ell+1/2)} v_k^- \, dV + \int_{\mathbf{D}} \sigma_t \Gamma^{-(\ell+1/2)} v_k^- \, dV$$
$$= \int_{\mathbf{D}} \sigma_s \left[\Gamma^{-(\ell+1/2)} + \left(\phi^{-(\ell+1/2)} - \phi^{-(\ell)} \right) \right] v_k^- \, dV. \quad (5.12b)$$

We have defined the following additive corrections:

$$\gamma^{-(\ell+1/2)} = \psi^- - \psi^{-(\ell+1/2)}, \quad (5.13a)$$

$$\Gamma^{-(\ell+1/2)} = \phi^- - \phi^{-(\ell+1/2)}, \quad (5.13b)$$

$$\Gamma_1^{-(\ell+1/2)} = \mathbf{J}^- - \mathbf{J}^{-(\ell+1/2)}. \quad (5.13c)$$

Equation (5.12a) can be greatly simplified by making the following definition:

$$\gamma_e^{-(\ell+1/2)} = \frac{1}{4\pi\sigma_t} \left[\sigma_s \Gamma^{-(\ell+1/2)} + \sigma_s \left(\phi^{-(\ell+1/2)} - \phi^{-(\ell)} \right) \right] - \frac{1}{\sigma_t} \left(\Omega \cdot \nabla \gamma^{-(\ell+1/2)} \right),$$

where

$$\Gamma^{-(\ell+1/2)} = 2 \int_{2\pi} \gamma_e^{-(\ell+1/2)} \, d\Omega.$$

Here, $\gamma_e^{-(\ell+1/2)}$ is a correction to the even-parity angular flux that, while not explicitly calculated in our formulation, underlies the odd-parity scalar flux. The odd-parity corrections equations become:

$$\int_{\partial\mathbf{D}} |\mathbf{n} \cdot \Omega| \gamma^{-(\ell+1/2)} w_i^- \, dS - \int_{\mathbf{D}} (\Omega \cdot \nabla w_i^-) \gamma_e^{-(\ell+1/2)} \, dV$$
$$+ \int_{\mathbf{D}} \sigma_t \gamma^{-(\ell+1/2)} w_i^- \, dV = 0, \quad (5.14a)$$

$$\int_{\mathbf{D}} \nabla \cdot \Gamma_1^{-(\ell+1/2)} v_k^- \, dV + \int_{\mathbf{D}} \sigma_t \Gamma^{-(\ell+1/2)} v_k^- \, dV$$
$$= \int_{\mathbf{D}} \left[\sigma_s \Gamma^{-(\ell+1/2)} + \sigma_s (\phi^{-(\ell+1/2)} - \phi^{-(\ell)}) \right] v_k^- \, dV. \quad (5.14b)$$

Now we again assume that the corrections are linearly anisotropic:

$$\gamma^{-(\ell+1/2)} = \frac{3}{4\pi} \Omega \cdot \Gamma_1^{-(\ell+1/2)},$$

and

$$\gamma_e^{-(\ell+1/2)} = \frac{1}{4\pi} \Gamma^{-(\ell+1/2)}.$$

In this case, we need only take the first moment of equation (5.14a) to obtain the DSA iteration scheme for the odd-parity CFEM system:

$$\int_{\partial \mathbf{D}} |\mathbf{n} \cdot \Omega| (\psi^{-(\ell+1/2)} - f^-) w_i^- \, dS + \int_{\mathbf{D}} (\Omega \cdot \nabla w_i^-) \frac{1}{\sigma_t} (\Omega \cdot \nabla \psi^{-(\ell+1/2)}) \, dV$$
$$+ \int_{\mathbf{D}} \sigma_t \psi^{-(\ell+1/2)} w_i^- \, dV = \int_{\mathbf{D}} (\Omega \cdot \nabla w_i^-) \frac{\sigma_s \phi^{-(\ell)} + q^-}{4\pi\sigma_t} \, dV, \quad (5.15a)$$

$$\mathbf{J}^{-(\ell+1/2)} = 2 \int_{2\pi} \Omega \psi^{-(\ell+1/2)} \, d\Omega, \quad (5.15b)$$

$$\int_{\mathbf{D}} \nabla \cdot \mathbf{J}^{-(\ell+1/2)} v_k^- \, dV + \int_{\mathbf{D}} \sigma_t \phi^{-(\ell+1/2)} v_k^- \, dV = \int_{\mathbf{D}} (\sigma_s \phi^{-(\ell)} + q^-) v_k^- \, dV, \quad (5.15c)$$

$$\int_{\partial \mathbf{D}} \frac{3}{2\pi} \Big(\int_{2\pi} |\mathbf{n} \cdot \Omega| \Omega \Omega \, d\Omega \Big) \cdot \Gamma_1^{-(\ell+1/2)} w_i^- \, dS + \int_{\mathbf{D}} \frac{1}{3} \Gamma^{-(\ell+1/2)} \nabla w_i^- \, dV$$
$$+ \int_{\mathbf{D}} \sigma_t \Gamma_1^{-(\ell+1/2)} w_i^- \, dV = 0, \quad (5.15d)$$

$$\int_{\mathbf{D}} \nabla \cdot \Gamma_1^{-(\ell+1/2)} v_k^- \, dV + \int_{\mathbf{D}} \sigma_a \Gamma^{-(\ell+1/2)} v_k^- \, dV = \int_{\mathbf{D}} \sigma_s (\phi^{-(\ell+1/2)} - \phi^{-(\ell)}) v_k^- \, dV, \quad (5.15e)$$

$$\phi^{-(\ell+1)} = \phi^{-(\ell+1/2)} + \Gamma^{-(\ell+1/2)}. \quad (5.15f)$$

In this case, we cannot collapse equations (5.15d) and (5.15e) into a single diffusion equation unless we make a number of assumptions regarding the weight and basis functions. For example, if we were to use lumped linear continuous elements, we could form a single cell-centered diffusion equation for the scalar flux corrections. We note that this equation becomes singular when $\sigma_a = 0$. In practice, we overcome this difficulty by introducing a small amount of false absorption that is set according to the geometric size of the problem under consideration. Specifically, we calculate the geometric buckling of the problem and a simple volume averaged diffusion coefficient. We then use the product of these two numbers (DB^2) in place of the absorption cross section.

Again, we can analyze this scheme in slab geometry with lumped linear continuous finite elements. In the problem interior, the equations for the model problem are:

$$-\mu^2 \left(\frac{\psi_{j+3/2}^{-(\ell+1/2)} - \psi_{j+1/2}^{-(\ell+1/2)}}{\Delta x^2} - \frac{\psi_{j+1/2}^{-(\ell+1/2)} - \psi_{j-1/2}^{-(\ell+1/2)}}{\Delta x^2} \right) + \psi_{j+1/2}^{-(\ell+1/2)} = -\frac{\mu c}{2\Delta x} (\phi_{j+1}^{-(\ell)} - \phi_j^{-(\ell)}), \quad (5.16a)$$

$$2 \int_0^1 \frac{\mu}{\Delta x} (\psi_{j+1/2}^{-(\ell+1/2)} - \psi_{j-1/2}^{-(\ell+1/2)}) \, d\mu + \phi_j^{-(\ell+1/2)} = c \phi_j^{-(\ell)} \quad (5.16b)$$

$$-\frac{1}{3}\Big(\frac{\Gamma_{j+1}^{-(\ell+1/2)}-\Gamma_{j}^{-(\ell+1/2)}}{\Delta x^2}-\frac{\Gamma_{j}^{-(\ell+1/2)}-\Gamma_{j-1}^{-(\ell+1/2)}}{\Delta x^2}\Big)+(1-c)\Gamma_{j}^{-(\ell+1/2)}$$
$$=c(\phi_{j}^{-(\ell+1/2)}-\phi_{j}^{-(\ell)}), \quad (5.16c)$$

and finally,

$$\phi_{j}^{-(\ell+1)}=\phi_{j}^{-(\ell+1/2)}+\Gamma_{j}^{-(\ell+1/2)}. \quad (5.16d)$$

We propose the following ansatz:

$$\psi_{j+1/2}^{-(\ell+1/2)}=\omega^{\ell}a(\mu)e^{\imath\lambda x_{j+1/2}} \quad (5.17a)$$

$$\phi_{j}^{-(\ell)}=\omega^{\ell}Ae^{\imath\lambda x_{j}} \quad (5.17b)$$

$$\Gamma_{j}^{-(\ell+1/2)}=\omega^{\ell}Be^{\imath\lambda x_{j}} \quad (5.17c)$$

After inserting the ansatz into equations (5.16), we find that:

$$a(\mu)=-\imath\mu\Lambda\frac{cA}{2(1+\mu^2\Lambda^2)}, \quad (5.18a)$$

and, just as in the even-parity case,

$$\omega(\lambda)=\frac{c}{\Lambda}\arctan(\Lambda)+\frac{\frac{c^2}{\Lambda}\arctan(\Lambda)-c}{(1-c)+\frac{1}{3}\Lambda^2}. \quad (5.18b)$$

The spectral radius is:

$$\rho_{dsa}^{-}=\sup_{\lambda}|\omega(\lambda)|\leq 0.2247c. \quad (5.18c)$$

Thus, odd-parity DSA should perform extremely well in slab geometry.

C. Odd-Parity Conjugate Gradient

We now briefly consider the application of the conjugate gradient method to the within-group problem. First, we rewrite the odd-parity CFEM source iteration system in matrix form:

$$L(\Omega)\psi^{(\ell+1)}(\Omega) = W_t\phi^{(\ell)} + F_t q, \tag{5.19a}$$

$$\mathbf{J}^{(\ell+1)} = 2\int_{2\pi} \Omega\psi^{(\ell+1)}(\Omega)\, d\Omega, \tag{5.19b}$$

$$\mathbf{D}\cdot\mathbf{J}^{(\ell+1)} + M\phi^{(\ell+1)} = W_d\phi^{(\ell)} + F_d q. \tag{5.19c}$$

L, W_t and F_t are the matrices result from evaluating the integrals in equation (5.11a) and M, W_d and F_d result from evaluating the integrals in equation (5.11c). $\mathbf{D}$ is a discrete divergence operator in matrix form. Here, ψ, ϕ and q represent vectors of discrete scalar values and $\mathbf{J}$ is a vector of discrete vector values. Now, we rearrange equation (5.19c) to obtain:

$$\phi^{(\ell+1)} = W_d\phi^{(\ell)} + F_d q - \mathbf{D}\cdot\mathbf{J}^{(\ell+1)}.$$

We use equation (5.19b) to arrive at:

$$\phi^{(\ell+1)} = W_d\phi^{(\ell)} + F_d q - \mathbf{D}\cdot 2\int_{2\pi} \Omega\psi^{(\ell+1)}\, d\Omega.$$

Equation (5.19a) can be solved for $\psi^{(\ell+1)}$ to obtain:

$$\phi^{(\ell+1)} = \left(W_d - \mathbf{D}\cdot 2\int_{2\pi} \Omega L^{-1}W_t\, d\Omega\right)\phi^{(\ell)} + \left(F_d q - \mathbf{D}\cdot 2\int_{2\pi} \Omega L^{-1}W_t q\, d\Omega\right).$$

If we identify

$$A = I - W_d + \mathbf{D} \cdot 2 \int_{2\pi} \Omega L^{-1} W_t \, d\Omega,$$

and

$$b = F_d q - \mathbf{D} \cdot 2 \int_{2\pi} \Omega L^{-1} W_t q \, d\Omega,$$

then we can write the source iteration system in the following form:

$$\phi^{(\ell+1)} = (I - A)\phi^{(\ell)} + b. \tag{5.20}$$

This is simply the stationary Richardson method applied to the odd-parity within-group problem. To evaluate the action of A on a vector, we simply evaluate equations (5.19) with the fixed source set to zero. Obviously, more efficient iterative methods such as CG can be applied to equation (5.20) so long as the inner product shown in equation (5.1) is used. We have implemented CG and DSA preconditioned CG iteration for the slab geometry odd-parity system, and present numerical results in Chapter VI. These algorithms are described in numerous numerical methods books [69, 54, 70].

D. SAAF DSA

The SAAF system differs from the even- and odd-parity systems in that its DSA scheme will consist of two correction systems that are coupled on the problem boundary. This is a direct consequence of the fact that SAAF involves explicit scattering sources from two different finite element spaces. If we discretize the SAAF in the same way as the parity systems, we expect the SAAF DSA systems to be identical to the even- and odd-parity DSA systems developed above *in the problem interior*. This is, in fact, the case.

We begin with the SAAF source iteration system:

$$\int_{\partial\mathbf{D}} (\mathbf{n}\cdot\Omega)\psi_b^{(\ell+1/2)} w_i\, dS + \int_{\mathbf{D}} (\Omega\cdot\nabla w_i)\frac{1}{\sigma_t}(\Omega\cdot\nabla\psi^{(\ell+1/2)})\, dV + \int_{\mathbf{D}} \sigma_t\psi^{(\ell+1/2)} w_i\, dV$$
$$= \int_{\mathbf{D}} \frac{\sigma_s\phi^{(\ell)}+q}{4\pi} w_i\, dV + \int_{\mathbf{D}} (\Omega\cdot\nabla w_i)\frac{\sigma_s\tilde{\phi}^{(\ell)}+\tilde{q}}{4\pi\sigma_t}\, dV, \quad (5.21a)$$

$$\int_{\mathbf{D}} \Omega\cdot\nabla\psi^{(\ell+1/2)} v_k\, dV + \int_{\mathbf{D}} \sigma_t\tilde{\psi}^{(\ell+1/2)} v_k\, dV = \int_{\mathbf{D}} \frac{\sigma_s\tilde{\phi}^{(\ell)}+\tilde{q}}{4\pi} v_k\, dV, \quad (5.21b)$$

$$\phi^{(\ell+1)} = \phi^{(\ell+1/2)} = \int_{4\pi} \psi^{(\ell+1/2)}\, d\Omega, \quad (5.21c)$$

$$\tilde{\phi}^{(\ell+1)} = \tilde{\phi}^{(\ell+1/2)} = \int_{4\pi} \tilde{\psi}^{(\ell+1/2)}\, d\Omega. \quad (5.21d)$$

Now, we define the corrections:

$$\gamma^{(\ell+1/2)} = \psi - \psi^{(\ell+1/2)}, \quad (5.22a)$$

$$\Gamma^{(\ell+1/2)} = \phi - \phi^{(\ell+1/2)} = \int_{4\pi} \gamma^{(\ell+1/2)}\, d\Omega, \quad (5.22b)$$

$$\Gamma_1^{(\ell+1/2)} = \int_{4\pi} \Omega\gamma^{(\ell+1/2)}\, d\Omega, \quad (5.22c)$$

$$\tilde{\gamma}^{(\ell+1/2)} = \tilde{\psi} - \tilde{\psi}^{(\ell+1/2)}, \quad (5.22d)$$

$$\tilde{\Gamma}^{(\ell+1/2)} = \tilde{\phi} - \tilde{\phi}^{(\ell+1/2)} = \int_{4\pi} \tilde{\gamma}^{(\ell+1/2)}\, d\Omega, \quad (5.22e)$$

$$\tilde{\Gamma}_1^{(\ell+1/2)} = \int_{4\pi} \Omega \tilde{\gamma}^{(\ell+1/2)}\, d\Omega. \tag{5.22f}$$

We subtract equations (5.21a) and (5.21b) from the converged equations to obtain the exact correction equations:

$$\int_{\partial \mathbf{D}} (\mathbf{n}\cdot\Omega)\gamma_b^{(\ell+1/2)} w_i\, dS + \int_{\mathbf{D}} (\Omega\cdot\nabla w_i)\frac{1}{\sigma_t}\Omega\cdot\nabla\gamma^{(\ell+1/2)}\, dV + \int_{\mathbf{D}} \sigma_t \gamma^{(\ell+1/2)} w_i\, dV = \int_{\mathbf{D}} \frac{\sigma_s}{4\pi}\left[\Gamma^{(\ell+1/2)} + (\phi^{(\ell+1/2)} - \phi^{(\ell)})\right] w_i\, dV + \int_{\mathbf{D}} (\Omega\cdot\nabla w_i)\frac{\sigma_s}{4\pi\sigma_t}\left[\tilde{\Gamma}^{(\ell+1/2)} + (\tilde{\phi}^{(\ell+1/2)} - \tilde{\phi}^{(\ell)})\right] dV, \tag{5.23a}$$

$$\int_{\mathbf{D}} \Omega\cdot\nabla\gamma^{(\ell+1/2)} v_k\, dV + \int_{\mathbf{D}} \sigma_t \tilde{\gamma}^{(\ell+1/2)} v_k\, dV = \int_{\mathbf{D}} \frac{\sigma_s}{4\pi}\left[\tilde{\Gamma}^{(\ell+1/2)} + (\tilde{\phi}^{(\ell+1/2)} - \tilde{\phi}^{(\ell)})\right] v_k\, dV, \tag{5.23b}$$

where

$$\gamma_b^{(\ell+1/2)} = \begin{cases} 0 & \text{for } \mathbf{n}\cdot\Omega < 0 \\ \gamma^{(\ell+1/2)} & \text{for } \mathbf{n}\cdot\Omega > 0. \end{cases} \tag{5.23c}$$

Assuming linearly anisotropic corrections, we take the zeroth moment of equation (5.23a) to obtain an equation for $\Gamma^{(\ell+1/2)}$:

$$\int_{\partial \mathbf{D}} (\frac{1}{4}\Gamma^{(\ell+1/2)} + \frac{1}{2}\mathbf{n}\cdot\Gamma_1^{(\ell+1/2)}) w_i\, dS + \int_{\mathbf{D}} \frac{1}{3\sigma_t}(\nabla w_i)\cdot(\nabla\Gamma^{(\ell+1/2)})\, dV + \int_{\mathbf{D}} \sigma_a \Gamma^{(\ell+1/2)} w_i\, dV = \int_{\mathbf{D}} \sigma_s(\phi^{(\ell+1/2)} - \phi^{(\ell)}) w_i\, dV. \tag{5.24}$$

With the exception of the boundary integral of $\Gamma_1^{(\ell+1/2)}$, this is an independent equation for the $\Gamma^{(\ell+1/2)}$ corrections. In practice, we find that we can, in fact, neglect $\Gamma_1^{(\ell+1/2)}$ without

significantly affecting the overall performance.

Now, we move on to the $\tilde{\Gamma}^{(\ell+1/2)}$ corrections. First, we insert

$$\tilde{\gamma}^{(\ell+1/2)} = \frac{1}{4\pi\sigma_t}\Big[\sigma_s\Gamma^{(\ell+1/2)} + \sigma_s(\phi^{(\ell+1/2)} - \phi^{(\ell)})\Big] - \frac{1}{\sigma_t}(\Omega\cdot\nabla\gamma^{(\ell+1/2)}),$$

which is exact, into equation (5.23a) then take the Ω moment to obtain:

$$\int_{\partial\mathbf{D}}\Big[\frac{1}{6}\mathbf{n}\Gamma^{(\ell+1/2)} + \frac{3\pi}{4}\int_{\mathbf{n}\cdot\Omega>0}(\mathbf{n}\cdot\Omega)\Omega\Omega\, d\Omega\cdot\Gamma_1^{(\ell+1/2)}\Big]w_i\, dS - \int_{\mathbf{D}}\frac{1}{3}\tilde{\Gamma}^{(\ell+1/2)}\nabla w_i\, dV + \int_{\mathbf{D}}\sigma_t\Gamma_1^{(\ell+1/2)}w_i\, dV = 0, \quad (5.25)$$

Finally, we take the zeroth moment of equation (5.23b) to obtain:

$$\int_{\mathbf{D}}\nabla\cdot\Gamma_1^{(\ell+1/2)}v_k\, dV + \int_{\mathbf{D}}\sigma_a\tilde{\Gamma}^{(\ell+1/2)}v_k\, dV = \int_{\mathbf{D}}\sigma_s(\tilde{\phi}^{(\ell+1/2)} - \tilde{\phi}^{(\ell)})v_k\, dV. \quad (5.26)$$

Thus, the SAAF DSA system is:

$$\int_{\partial\mathbf{D}}(\mathbf{n}\cdot\Omega)\psi_b^{(\ell+1/2)}w_i\, dS + \int_{\mathbf{D}}(\Omega\cdot\nabla w_i)\frac{1}{\sigma_t}\Omega\cdot\nabla\psi^{(\ell+1/2)}\, dV + \int_{\mathbf{D}}\sigma_t\psi^{(\ell+1/2)}w_i\, dV = \int_{\mathbf{D}}\frac{\sigma_s\phi^{(\ell)}+q}{4\pi}w_i\, dV + \int_{\mathbf{D}}(\Omega\cdot\nabla w_i)\frac{\sigma_s\tilde{\phi}^{(\ell)}+\tilde{q}}{4\pi\sigma_t}\, dV, \quad (5.27a)$$

$$\int_{\mathbf{D}}\Omega\cdot\nabla\psi^{(\ell+1/2)}v_k\, dV + \int_{\mathbf{D}}\sigma_t\tilde{\psi}^{(\ell+1/2)}v_k\, dV = \int_{\mathbf{D}}\frac{\sigma_s\tilde{\phi}^{(\ell)}+\tilde{q}}{4\pi}v_k\, dV, \quad (5.27b)$$

$$\phi^{(\ell+1/2)} = \int_{4\pi}\psi^{(\ell+1/2)}\, d\Omega, \quad (5.27c)$$

$$\tilde{\phi}^{(\ell+1/2)} = \int_{4\pi}\tilde{\psi}^{(\ell+1/2)}\, d\Omega, \quad (5.27d)$$

$$\int_{\partial \mathbf{D}} (\frac{1}{4}\Gamma^{(\ell+1/2)} + \frac{1}{2}\mathbf{n}\cdot\Gamma_1^{(\ell+1/2)}) w_i \, dS + \int_{\mathbf{D}} \frac{1}{3\sigma_t} (\nabla w_i)\cdot(\nabla\Gamma^{(\ell+1/2)}) \, dV + \int_{\mathbf{D}} \sigma_a \Gamma^{(\ell+1/2)} w_i \, dV = \int_{\mathbf{D}} \sigma_s (\phi^{(\ell+1/2)} - \phi^{(\ell)}) w_i \, dV, \quad (5.27e)$$

$$\int_{\partial \mathbf{D}} \left[\frac{1}{6}\mathbf{n}\Gamma^{(\ell+1/2)} + \frac{3\pi}{4}\int_{\mathbf{n}\cdot\Omega>0} (\mathbf{n}\cdot\Omega)\Omega\Omega \, d\Omega \cdot \Gamma_1^{(\ell+1/2)}\right] w_i \, dS - \int_{\mathbf{D}} \frac{1}{3}\tilde{\Gamma}^{(\ell+1/2)} \nabla w_i \, dV + \int_{\mathbf{D}} \sigma_t \Gamma_1^{(\ell+1/2)} w_i \, dV = 0, \quad (5.27f)$$

$$\int_{\mathbf{D}} \nabla \cdot \Gamma_1^{(\ell+1/2)} v_k \, dV + \int_{\mathbf{D}} \sigma_a \tilde{\Gamma}^{(\ell+1/2)} v_k \, dV = \int_{\mathbf{D}} \sigma_s (\tilde{\phi}^{(\ell+1/2)} - \tilde{\phi}^{(\ell)}) v_k \, dV, \quad (5.27g)$$

$$\phi^{(\ell+1)} = \phi^{(\ell+1/2)} + \Gamma^{(\ell+1/2)}, \quad (5.27h)$$

$$\tilde{\phi}^{(\ell+1)} = \tilde{\phi}^{(\ell+1/2)} + \tilde{\Gamma}^{(\ell+1/2)}. \quad (5.27i)$$

We conclude by considering how to solve equations (5.27). First, we again note that $\Gamma_1^{(\ell+1/2)}$ can be ignored in equation (5.27e). This allows us to solve that equation independently for $\Gamma^{(\ell+1/2)}$, which can then be used in the boundary integral of equation (5.27f). In general, equations (5.27f) and (5.27g) are difficult to collapse into a single diffusion equation.

Again, we perform a slab geometry Fourier analysis. In this case, since we have two scattering sources, we have two eigenvalue spectra to consider. The lumped, slab geometry

SAAF DSA system for the model problem is:

$$-\mu^2\Big(\frac{\psi_{j+3/2}^{(\ell+1/2)}-\psi_{j+1/2}^{(\ell+1/2)}}{\Delta x^2}-\frac{\psi_{j+1/2}^{(\ell+1/2)}-\psi_{j-1/2}^{(\ell+1/2)}}{\Delta x^2}\Big)+\psi_{j+1/2}^{(\ell+1/2)} = \frac{c}{2}\phi_{j+1/2}^{(\ell)}-\frac{\mu c}{2\Delta x}(\tilde{\phi}_{j+1}^{(\ell)}-\tilde{\phi}_{j}^{(\ell)}), \quad (5.28a)$$

$$\phi_{j+1/2}^{(\ell+1/2)} = \int_{-1}^{1}\psi_{j+1/2}^{(\ell+1/2)}\,d\mu, \quad (5.28b)$$

$$\int_{-1}^{1}\frac{\mu}{\Delta x}(\psi_{j+1/2}^{(\ell+1/2)}-\psi_{j-1/2}^{(\ell+1/2)})\,d\mu+\tilde{\phi}_{j}^{(\ell+1/2)} = \frac{c}{2}\tilde{\phi}_{j}^{(\ell)}, \quad (5.28c)$$

$$\tilde{\phi}_{j}^{(\ell+1/2)} = \int_{-1}^{1}\tilde{\psi}_{j}^{(\ell+1/2)}\,d\mu, \quad (5.28d)$$

$$-\frac{1}{3}\Big(\frac{\Gamma_{j+3/2}^{(\ell+1/2)}-\Gamma_{j+1/2}^{(\ell+1/2)}}{\Delta x^2}-\frac{\Gamma_{j+1/2}^{(\ell+1/2)}-\Gamma_{j-1/2}^{(\ell+1/2)}}{\Delta x^2}\Big)+(1-c)\Gamma_{j+1/2}^{(\ell+1/2)} = c(\phi_{j+1/2}^{(\ell+1/2)}-\phi_{j+1/2}^{(\ell)}), \quad (5.28e)$$

$$-\frac{1}{3}\Big(\frac{\tilde{\Gamma}_{j+1}^{(\ell+1/2)}-\tilde{\Gamma}_{j}^{(\ell+1/2)}}{\Delta x^2}-\frac{\tilde{\Gamma}_{j}^{(\ell+1/2)}-\tilde{\Gamma}_{j-1}^{(\ell+1/2)}}{\Delta x^2}\Big)+(1-c)\tilde{\Gamma}_{j}^{(\ell+1/2)} = c(\tilde{\phi}_{j}^{(\ell+1/2)}-\tilde{\phi}_{j}^{(\ell)}), \quad (5.28f)$$

and, finally,

$$\phi_{j+1/2}^{(\ell+1)} = \phi_{j+1/2}^{(\ell+1/2)}+\Gamma_{j+1/2}^{(\ell+1/2)}, \quad (5.28g)$$

$$\tilde{\phi}_{j}^{(\ell+1)} = \tilde{\phi}_{j}^{(\ell+1/2)}+\tilde{\Gamma}_{j}^{(\ell+1/2)}. \quad (5.28h)$$

We propose the following ansatz:

$$\psi_{j+1/2}^{(\ell+1/2)} = \omega^{\ell} a(\mu) e^{\imath\lambda x_{j+1/2}}, \tag{5.29a}$$

$$\phi_{j+1/2}^{(\ell)} = \omega^{\ell} A e^{\imath\lambda x_{j+1/2}}, \tag{5.29b}$$

$$\tilde{\psi}_{j}^{(\ell+1/2)} = \omega^{\ell} \tilde{a}(\mu) e^{\imath\lambda x_{j}}, \tag{5.29c}$$

$$\tilde{\phi}_{j}^{(\ell)} = \omega^{\ell} \tilde{A} e^{\imath\lambda x_{j}}, \tag{5.29d}$$

$$\Gamma_{j+1/2}^{(\ell+1/2)} = \omega^{\ell} B e^{\imath\lambda x_{j+1/2}}, \tag{5.29e}$$

$$\tilde{\Gamma}_{j}^{(\ell+1/2)} = \omega^{\ell} \tilde{B} e^{\imath\lambda x_{j}}. \tag{5.29f}$$

After inserting the ansatz into equations (5.28), we find that:

$$a(\mu) = \frac{c(A - \imath\mu\Lambda\tilde{A})}{2(1+\mu^2\Lambda^2)}, \tag{5.30a}$$

and

$$\tilde{a}(\mu) = \frac{c(\tilde{A} - \imath\mu\Lambda A)}{2(1+\mu^2\Lambda^2)}. \tag{5.30b}$$

The eigenvalues for both sets of unknowns are given by the now familiar relation:

$$\omega(\lambda) = \frac{c}{\Lambda}\arctan(\Lambda) + \frac{\frac{c^2}{\Lambda}\arctan(\Lambda) - c}{(1-c) + \frac{1}{3}\Lambda^2}. \tag{5.30c}$$

The spectral radius is again bounded by 0.2247:

$$\rho_{dsa}^{SAAF} = \sup_{\lambda} |\omega(\lambda)| \leq 0.2247c. \tag{5.30d}$$

We therefore expect the SAAF DSA scheme to be very effective.

E. CP DSA

Now we consider the mixed finite element discretization of the coupled even- and odd-parity system. We begin by writing the source iteration form of the equations:

$$\int_{\partial\mathbf{D}} |\mathbf{n}\cdot\Omega|(\mathbf{g}^{-(\ell+1/2)} - \Omega f^{-})\cdot\mathbf{w}_i^{-}\,dS - \int_{\mathbf{D}} \psi^{+(\ell+1/2)}\nabla\cdot\Omega(\Omega\cdot\mathbf{w}_i^{-})\,dV + \int_{\mathbf{D}} \sigma_t\mathbf{g}^{-(\ell+1/2)}\cdot\mathbf{w}_i^{-}\,dV = 0, \quad (5.31a)$$

$$\int_{\mathbf{D}} (\nabla\cdot\mathbf{g}^{-(\ell+1/2)})v_k^{+}\,dV + \int_{\mathbf{D}} \sigma_t\psi^{+(\ell+1/2)}v_k^{+}\,dV = \int_{\mathbf{D}} \frac{\sigma_s\phi^{+(\ell)} + q^{+}}{4\pi}v_k^{+}\,dV, \quad (5.31b)$$

$$\phi^{+(\ell+1)} = \phi^{+(\ell+1/2)} = 2\int_{2\pi} \psi^{+(\ell+1/2)}\,d\Omega. \quad (5.31c)$$

We define the corrections:

$$\gamma^{+(\ell+1/2)} = \psi^{+} - \psi^{+(\ell+1/2)}, \quad (5.32a)$$

$$\Gamma^{+(\ell+1/2)} = \phi^{+} - \phi^{+(\ell+1/2)} = 2\int_{2\pi} \gamma^{+(\ell+1/2)}\,d\Omega, \quad (5.32b)$$

$$\mathbf{h}^{-(\ell+1/2)} = \mathbf{g}^{-} - \mathbf{g}^{-(\ell+1/2)}, \quad (5.32c)$$

$$\mathbf{H}_1^{-(\ell+1/2)} = 2\int_{2\pi} \mathbf{h}^{-(\ell+1/2)}\,d\Omega. \quad (5.32d)$$

If we assume the angular corrections are linearly anisotropic, we have:

$$\gamma^{+(\ell+1/2)} = \frac{1}{4\pi}\Gamma^{+(\ell+1/2)}, \quad (5.33a)$$

and

$$\mathbf{h}^{-(\ell+1/2)} = \frac{3}{4\pi}\Omega\Omega\cdot\mathbf{H}_1^{-(\ell+1/2)}. \tag{5.33b}$$

Now, we write the exact correction equations:

$$\int_{\partial\mathbf{D}} |\mathbf{n}\cdot\Omega|\mathbf{h}^{-(\ell+1/2)}\cdot\mathbf{w}_i^-\,dS - \int_{\mathbf{D}} \gamma^{+(\ell+1/2)}\nabla\cdot\Omega(\Omega\cdot\mathbf{w}_i^-)\,dV + \int_{\mathbf{D}} \sigma_t\mathbf{h}^{-(\ell+1/2)}\cdot\mathbf{w}_i^-\,dV = 0, \tag{5.34a}$$

$$\int_{\mathbf{D}} \nabla\cdot\mathbf{h}^{-(\ell+1/2)}v_k^+\,dV + \int_{\mathbf{D}} \sigma_t\gamma^{+(\ell+1/2)}v_k^+\,dV = \int_{\mathbf{D}} \frac{\sigma_s}{4\pi}\left[\Gamma^{+(\ell+1/2)} + (\phi^{+(\ell+1/2)} - \phi^{+(\ell)})\right]v_k^+\,dV. \tag{5.34b}$$

Taking the zeroth moment of both equations, we arrive at the CP DSA iteration system:

$$\int_{\partial\mathbf{D}} |\mathbf{n}\cdot\Omega|(\mathbf{g}^{-(\ell+1/2)} - \Omega f^-)\cdot\mathbf{w}_i^-\,dS - \int_{\mathbf{D}} \psi^{+(\ell+1/2)}\nabla\cdot\Omega(\Omega\cdot\mathbf{w}_i^-)\,dV + \int_{\mathbf{D}} \sigma_t\mathbf{g}^{-(\ell+1/2)}\cdot\mathbf{w}_i^-\,dV = 0, \tag{5.35a}$$

$$\int_{\mathbf{D}} \nabla\cdot\mathbf{g}^{-(\ell+1/2)}v_k^+\,dV + \int_{\mathbf{D}} \sigma_t\psi^{+(\ell+1/2)}v_k^+\,dV = \int_{\mathbf{D}} \frac{\sigma_s\phi^{+(\ell)} + q^+}{4\pi}v_k^+\,dV, \tag{5.35b}$$

$$\phi^{+(\ell+1/2)} = 2\int_{2\pi} \psi^{+(\ell+1/2)}\,d\Omega, \tag{5.35c}$$

$$\int_{\partial\mathbf{D}} \left(\frac{3}{2\pi}\int_{2\pi} |\mathbf{n}\cdot\Omega|\Omega\Omega\, d\Omega\cdot\mathbf{H}_1^{-(\ell+1/2)}\right)\cdot\mathbf{w}_i^- \, dS - \int_{\mathbf{D}} \frac{1}{3}\Gamma^{+(\ell+1/2)}\nabla\cdot\mathbf{w}_i^- \, dV + \int_{\mathbf{D}} \sigma_t \mathbf{H}_1^{-(\ell+1/2)}\cdot\mathbf{w}_i^- \, dV = 0, \quad (5.35d)$$

$$\int_{\mathbf{D}} \nabla\cdot\mathbf{H}_1^{-(\ell+1/2)} v_k^+ \, dV + \int_{\mathbf{D}} \sigma_a \Gamma^{+(\ell+1/2)} v_k^+ \, dV = \int_{\mathbf{D}} \sigma_s(\phi^{+(\ell+1/2)} - \phi^{+(\ell)}) v_k^+ \, dV, \quad (5.35e)$$

$$\phi^{+(\ell+1)} = \phi^{+(\ell+1/2)} + \Gamma^{+(\ell+1/2)}. \quad (5.35f)$$

In slab geometry with mass matrix lumping and linear elements, this system is algebraically equivalent to the lumped CFEM odd-parity DSA system. Therefore, the results of the slab geometry Fourier analysis apply directly. That is, the spectral radius is bounded by 0.2247.

In general, this system is difficult to reduce to a single diffusion equation. However, its form is identical to the original coupled parity transport system, thus the method used to solve for the angular flux can also be applied to this diffusion system.

F. AFCD DSA

We now consider the MFEM angular flux/angular current density equations. The source iteration system is:

$$\int_{\partial\mathbf{D}} (\mathbf{n}\cdot\Omega)\mathbf{g}_b^{(\ell+1/2)}\cdot\mathbf{w}_i \, dS - \int_{\mathbf{D}} \psi^{(\ell+1/2)}\nabla\cdot\Omega(\Omega\cdot\mathbf{w}_i)\, dV + \int_{\mathbf{D}} \sigma_t \mathbf{g}^{(\ell+1/2)}\cdot\mathbf{w}_i \, dV = \int_{\mathbf{D}} \frac{\sigma_s\phi^{(\ell)} + q}{4\pi}(\Omega\cdot\mathbf{w}_i)\, dV, \quad (5.36a)$$

$$\int_{\mathbf{D}} \nabla \cdot \mathbf{g}^{(\ell+1/2)} v_k \, dV + \int_{\mathbf{D}} \sigma_t \psi^{(\ell+1/2)} v_k \, dV = \int_{\mathbf{D}} \frac{\sigma_s \phi^{(\ell)} + q}{4\pi} v_k \, dV, \tag{5.36b}$$

$$\phi^{(\ell+1)} = \phi^{(\ell+1/2)} = \int_{4\pi} \psi^{(\ell+1/2)} \, d\Omega. \tag{5.36c}$$

We define the following additive corrections:

$$\gamma^{(\ell+1/2)} = \psi - \psi^{(\ell+1/2)}, \tag{5.37a}$$

$$\Gamma^{(\ell+1/2)} = \phi - \phi^{(\ell+1/2)} = \int_{4\pi} \gamma^{(\ell+1/2)} \, d\Omega, \tag{5.37b}$$

$$\Gamma_1^{(\ell+1/2)} = \int_{4\pi} \Omega \gamma^{(\ell+1/2)} \, d\Omega, \tag{5.37c}$$

$$\mathbf{h}^{(\ell+1/2)} = \mathbf{g} - \mathbf{g}^{(\ell+1/2)}, \tag{5.37d}$$

$$\mathbf{H}_1^{(\ell+1/2)} = \int_{4\pi} \mathbf{h}^{(\ell+1/2)} \, d\Omega. \tag{5.37e}$$

If we assume the angular corrections are linearly anisotropic, we have:

$$\gamma^{(\ell+1/2)} = \frac{1}{4\pi} \Gamma^{(\ell+1/2)} + \frac{3}{4\pi} \Omega \cdot \Gamma_1^{(\ell+1/2)}, \tag{5.38a}$$

and

$$\mathbf{h}^{(\ell+1/2)} = \Omega \left(\frac{1}{4\pi} H + \frac{3}{4\pi} \Omega \cdot \mathbf{H}_1^{(\ell+1/2)} \right). \tag{5.38b}$$

The term $H^{(\ell+1/2)}$ in equation (5.38b) corresponds to a scalar correction to an angular flux. Recall that **g** is defined as the produce of an angular flux and the direction vector. The only terms $H^{(\ell+1/2)}$ will affect are the boundary integrals, in which case $\Gamma^{(\ell+1/2)}$ can be used to

approximate it.

The exact correction equations are, then:

$$\int_{\partial\mathbf{D}} (\mathbf{n}\cdot\Omega)\mathbf{h}_b^{(\ell+1/2)}\cdot\mathbf{w}_i\,dS - \int_{\mathbf{D}} \gamma^{(\ell+1/2)}\nabla\cdot\Omega(\Omega\cdot\mathbf{w}_i)\,dV + \int_{\mathbf{D}} \sigma_t\mathbf{h}^{(\ell+1/2)}\cdot\mathbf{w}_i\,dV = \int_{\mathbf{D}} (\Omega\cdot\mathbf{w}_i)\frac{\sigma_s}{4\pi}\left[\Gamma^{(\ell+1/2)} + \left(\phi^{(\ell+1/2)} - \phi^{(\ell)}\right)\right] dV, \quad (5.39a)$$

$$\int_{\mathbf{D}} \nabla\cdot\mathbf{h}^{(\ell+1/2)}v_k\,dV + \int_{\mathbf{D}} \sigma_t\gamma^{(\ell+1/2)}v_k\,dV = \int_{\mathbf{D}} \frac{\sigma_s}{4\pi}\left[\Gamma^{(\ell+1/2)} + \left(\phi^{(\ell+1/2)} - \phi^{(\ell)}\right)\right] v_k\,dV, \quad (5.39b)$$

where

$$\mathbf{h}_b^{(\ell+1/2)} = \begin{cases} 0 & \text{for } \mathbf{n}\cdot\Omega < 0 \\ \mathbf{h}^{(\ell+1/2)} & \text{for } \mathbf{n}\cdot\Omega > 0. \end{cases} \quad (5.39c)$$

We take the zeroth moment of equations (5.39a) and (5.39b) to arrive at the AFCD DSA system:

$$\int_{\partial\mathbf{D}} (\mathbf{n}\cdot\Omega)\mathbf{g}_b^{(\ell+1/2)}\cdot\mathbf{w}_i\,dS - \int_{\mathbf{D}} \psi^{(\ell+1/2)}\nabla\cdot\Omega(\Omega\cdot\mathbf{w}_i)\,dV + \int_{\mathbf{D}} \sigma_t\mathbf{g}^{(\ell+1/2)}\cdot\mathbf{w}_i\,dV = \int_{\mathbf{D}} \frac{\sigma_s\phi^{(\ell)} + q}{4\pi}(\Omega\cdot\mathbf{w}_i)\,dV, \quad (5.40a)$$

$$\int_{\mathbf{D}} \nabla\cdot\mathbf{g}^{(\ell+1/2)}v_k\,dV + \int_{\mathbf{D}} \sigma_t\psi^{(\ell+1/2)}v_k\,dV = \int_{\mathbf{D}} \frac{\sigma_s\phi^{(\ell)} + q}{4\pi}v_k\,dV, \quad (5.40b)$$

$$\phi^{(\ell+1/2)} = \int_{4\pi} \psi^{(\ell+1/2)}\,d\Omega, \quad (5.40c)$$

$$\int_{\partial\mathbf{D}} \Big[\frac{1}{6}\mathbf{n}H^{(\ell+1/2)} + \frac{3\pi}{4}\int_{\mathbf{n}\cdot\Omega>0} (\mathbf{n}\cdot\Omega)\Omega\Omega\, d\Omega\cdot\mathbf{H}_1^{(\ell+1/2)}\Big]\cdot\mathbf{w}_i\, dS - \int_{\mathbf{D}} \frac{1}{3}\Gamma^{(\ell+1/2)}(\nabla\cdot\mathbf{w}_i)\, dV + \int_{\mathbf{D}} \sigma_t \mathbf{H}_1^{(\ell+1/2)}\cdot\mathbf{w}_i\, dV = 0, \quad (5.40d)$$

$$\int_{\mathbf{D}} \nabla\cdot\mathbf{H}_1^{(\ell+1/2)} v_k\, dV + \int_{\mathbf{D}} \sigma_a\Gamma^{(\ell+1/2)} v_k\, dV = \int_{\mathbf{D}} \sigma_s(\phi^{(\ell+1/2)} - \phi^{(\ell)}) v_k\, dV, \quad (5.40e)$$

$$\phi^{(\ell+1)} = \phi^{(\ell+1/2)} + \Gamma^{(\ell+1/2)}. \quad (5.40f)$$

We again mention that, in practice, in equations (5.40d) and (5.40e), we replace $H^{(\ell+1/2)}$ with $\Gamma^{(\ell+1/2)}$. We have found that this approximation does not adversely affect the convergence properties of this scheme in slab geometry. Equations (5.40d) and (5.40e) can be easily combined into a single diffusion equation if mass matrix lumping is applied.

In slab geometry with lumped linear elements, we have for the model problem:

$$-\mu^2\Big(\frac{g_{j+3/2}^{(\ell+1/2)} - g_{j+1/2}^{(\ell+1/2)}}{\Delta x^2} - \frac{g_{j+1/2}^{(\ell+1/2)} - g_{j-1/2}^{(\ell+1/2)}}{\Delta x^2}\Big) + g_{j+1/2}^{(\ell+1/2)} = \frac{\mu c}{4}(\phi_{j+1}^{(\ell)} + \phi_j^{(\ell)}) - \frac{\mu^2 c}{2\Delta x}(\phi_{j+1}^{(\ell)} - \phi_j^{(\ell)}), \quad (5.41a)$$

$$\frac{1}{\Delta x}(g_{j+1/2}^{(\ell+1/2)} - g_{j-1/2}^{(\ell+1/2)}) + \psi_j^{(\ell+1/2)} = \frac{c}{2}\phi_j^{(\ell)}, \quad (5.41b)$$

$$-\frac{1}{3}\Big(\frac{\Gamma_{j+1}^{(\ell+1/2)} - \Gamma_j^{(\ell+1/2)}}{\Delta x^2} - \frac{\Gamma_j^{(\ell+1/2)} - \Gamma_{j-1}^{(\ell+1/2)}}{\Delta x^2}\Big) + (1-c)\Gamma_j^{(\ell+1/2)} = c(\phi_j^{(\ell+1/2)} - \phi_j^{(\ell)}), \quad (5.41c)$$

and, finally,

$$\phi_j^{(\ell+1)} = \phi_j^{(\ell+1/2)} + \Gamma_j^{(\ell+1/2)}. \quad (5.41d)$$

We propose the following ansatz:

$$g_{j+1/2}^{(\ell+1/2)} = \omega^{\ell} b(\mu) e^{\imath\lambda x_{j+1/2}}, \tag{5.42a}$$

$$\psi_{j}^{(\ell+1/2)} = \omega^{\ell} a(\mu) e^{\imath\lambda x_{j}}, \tag{5.42b}$$

$$\phi_{j}^{(\ell)} = \omega^{\ell} A e^{\imath\lambda x_{j}}, \tag{5.42c}$$

$$\Gamma_{j}^{(\ell+1/2)} = \omega^{\ell} B e^{\imath\lambda x_{j}}. \tag{5.42d}$$

After inserting the ansatz into equations (5.41), we find that:

$$a(\mu) = \frac{cA[1 - \imath\mu\Lambda\cos(\lambda\Delta x/2)]}{2(1+\mu^2\Lambda^2)}, \tag{5.43a}$$

and,

$$\omega(\lambda) = \frac{c}{\Lambda}\arctan(\Lambda) + \frac{\frac{c^2}{\Lambda}\arctan(\Lambda) - c}{(1-c) + \frac{1}{3}\Lambda^2}. \tag{5.43b}$$

The spectral radius is:

$$\rho_{dsa}^{AFCD} = \sup_{\lambda} |\omega(\lambda)| \leq 0.2247c. \tag{5.43c}$$

G. Summary

The diffusion synthetic acceleration discretizations developed in this chapter are identical to the corresponding diffusion limit discretizations, except for certain boundary terms. Unlike many DSA schemes for first order transport discretizations, the diffusion discretizations developed here are all relatively simple to solve when compared to solving the underlying transport problem. Our simple Fourier analyses indicate that these DSA schemes will rapidly attenuate all of the error modes, at least in slab geometry.

We show in Chapter VI that this is indeed the case. The slab geometry implementations of our DSA schemes exhibit exactly the performance that we have described in this chapter. The XY geometry implementations display behavior typical of consistent multidimensional DSA. That is, the observed spectral radii are bounded by 0.5 in all cases.

CHAPTER VI

NUMERICAL RESULTS

In the previous chapters, we developed and analyzed several discretizations of the transport equation in the thick diffusive limit. Further, we proposed and implemented DSA schemes for each of the methods. In this chapter, we present numerical results that allow us to assess our analyses and predictions.

We begin by presenting slab geometry results for all of the discretizations we have developed. First, we consider problems with thick diffusive regions. We then study the convergence behavior as the spatial mesh is refined for a model problem with an analytic solution. Finally, we discuss the performance of the DSA schemes we implemented. Unless otherwise noted, all slab geometry calculations use S_{16} Gauss-Legendre quadrature and mass matrix lumping.

The functional form of the slab geometry scalar fluxes is linear continuous for the even-parity and the SAAF cell edge solutions. For the odd-parity, SAAF cell centers and AFCD, the scalar fluxes are piecewise constant. The hybrid parity scalar flux is linear discontinuous.

We then consider several XY geometry problems. We restrict our results to the even- and odd-parity equations discretized with mass lumped linear continuous finite elements. We present results for a suite of thick diffusive problems. We then study the global convergence behavior of the parity systems as the spatial mesh is refined and evaluate performance of our DSA preconditioners. Finally, we examine several relatively difficult problems that highlight potential problem areas in standard finite element discretizations of parity forms of the transport equation. Unless otherwise noted, all of the XY geometry numerical results use the discrete ordinates angular approximation with S_{16} level symmetric quadrature.

Again, the form of the even-parity flux is linear continuous and the odd-parity flux is

piecewise constant on triangles. Thus, the hybrid-parity scalar flux is linear discontinuous.

A. Accuracy for Thick Diffusive Problems

1. Slab Geometry

A general slab geometry spatial grid is shown in Fig. 4. All of our results use uniform mesh spacing in each material region.

a. The ε Problem

The first slab geometry problem we consider is the well-known ε problem [71]. In this problem, the cross sections and fixed source are scaled in the same way as they are in our diffusion limit analyses. That is, we set $\sigma_t \rightarrow \sigma_t/\varepsilon$, $\sigma_a \rightarrow \varepsilon\sigma_a$, and $q \rightarrow \varepsilon q$, with $\sigma_t = \sigma_a = q = 1$. As the scaling parameter, ε, tends to zero, the correct transport solution approaches the diffusion solution. For each method, we plot the diffusion solution along with our transport results for $\varepsilon = 0.1$ and 0.001 for a 1cm thick slab with vacuum boundaries.

As our analyses predicted, each method we consider performs well in this problem. As ε approaches zero, the transport solutions approach the diffusion solution. First, we plot the even- and odd-parity results in Fig. 9 and 10. The SAAF results, for both the cell edge and cell centered unknowns are shown in Fig. 11 and 12. We note that for values of ε smaller than 0.001, none of the solutions change noticeably. The AFCD results are interesting. Recall that we showed that the AFCD boundary condition will differ from the odd-parity boundary condition in that it will extrapolate to a half cell beyond the physical boundary. This can be observed in Fig. 13, where the AFCD solution is clearly too high. If we refine the mesh near the boundary, the AFCD solution falls to the correct diffusion solution.

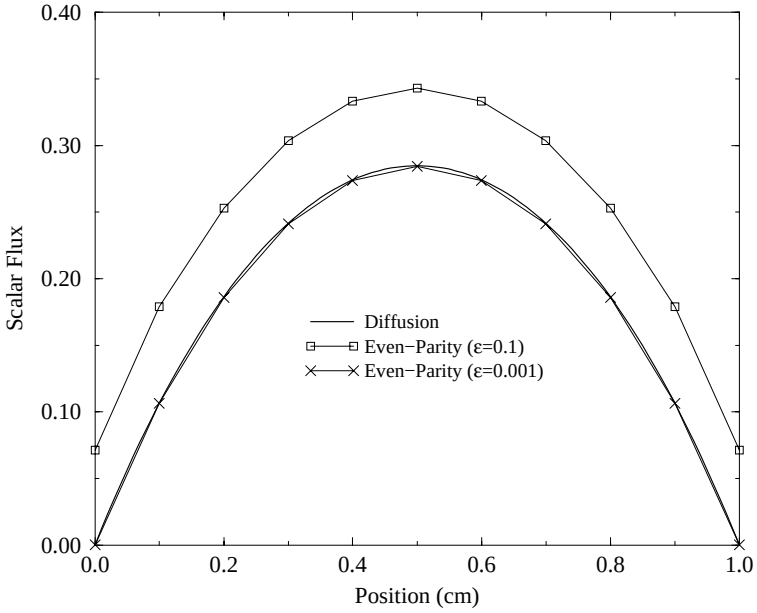

Fig. 9. EP ε problem.

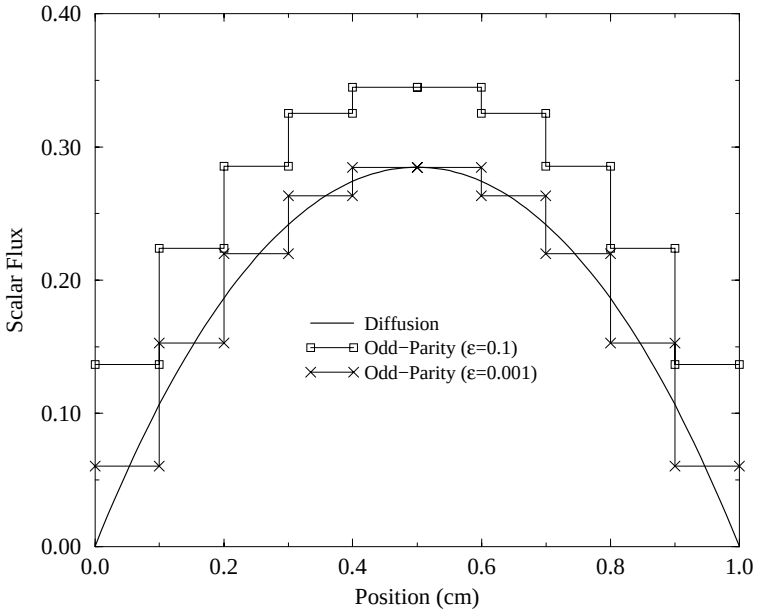

Fig. 10. OP ε problem.

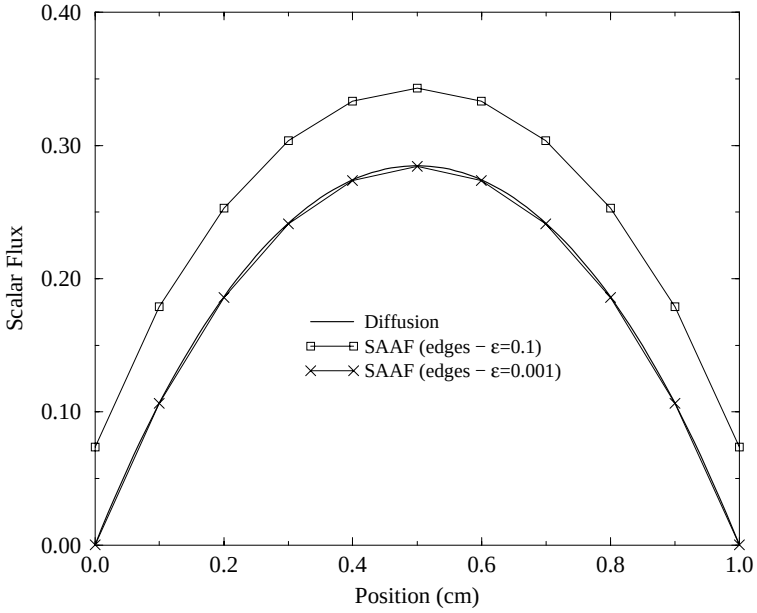

Fig. 11. SAAF(edges) ε problem.

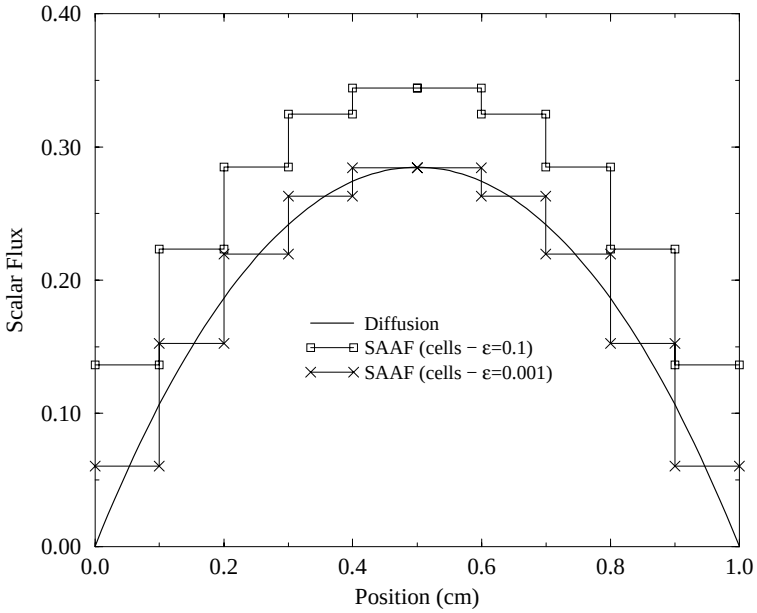

Fig. 12. SAAF(cells) ε problem.

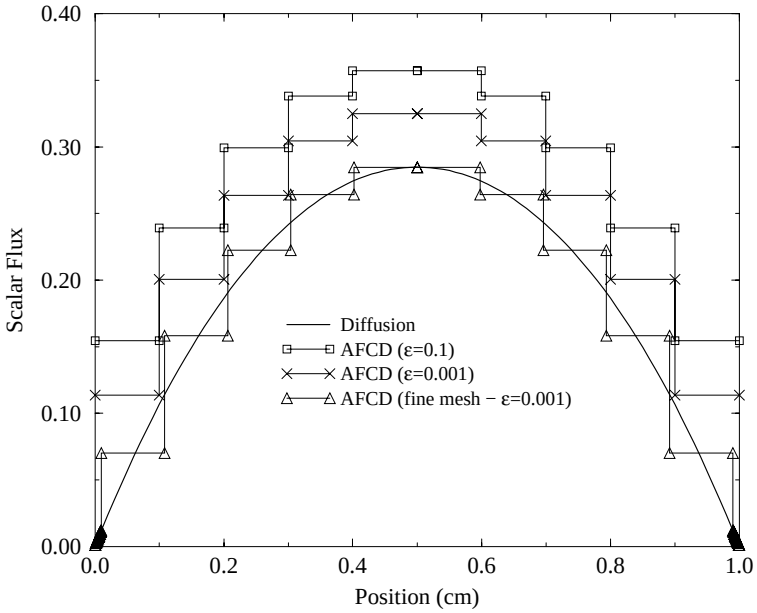

Fig. 13. AFCD ε problem.

b. External Boundaries

Now, we consider a 1cm thick, source free, $c = 1$ slab with $\sigma_t = 1000$. We drive the problem with incident angular fluxes on the left side of the problem and use a very fine mesh (10000 cells)diamond difference (DD) calculation as the reference solution.

The results for a nearly normal incident boundary angular flux are shown in Fig. 14. In our analysis, we predicted that the EP and SAAF(edges) should satisfy a Marshak (2μ) boundary condition, while the OP, SAAF(cells) and AFCD satisfy a $3\mu^2$ boundary condition for thick diffusive problems. Thus, we expect the EP and SAAF(edges) to be lower than the correct solution on the boundary since $2\mu < \mu + \frac{3}{2}\mu^2$ for μ near unity. The other methods should be higher, since $3\mu^2 > \mu + \frac{3}{2}\mu^2$ for μ near unity.

Nearly grazing boundary condition results are plotted in Fig. 15. Here, with μ small, we expect the EP and SAAF(edges) solution to be higher than the correct solution, while the other methods will be lower. Again, this is observed in the results. For both problems, the

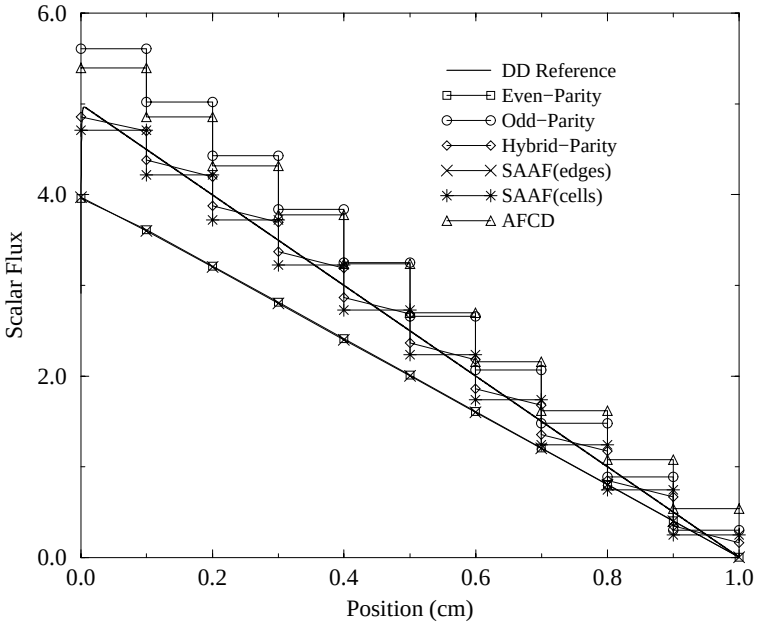

Fig. 14. Normal incident problem.

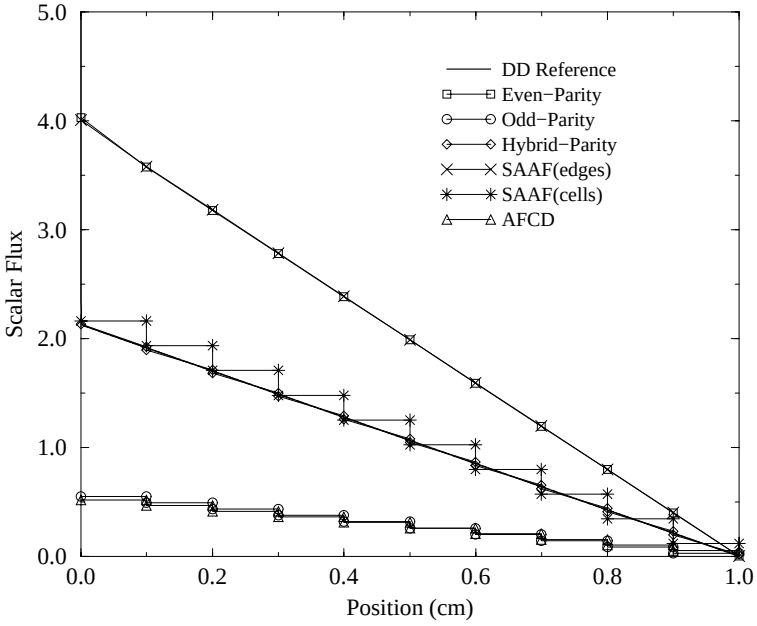

Fig. 15. Grazing incident problem.

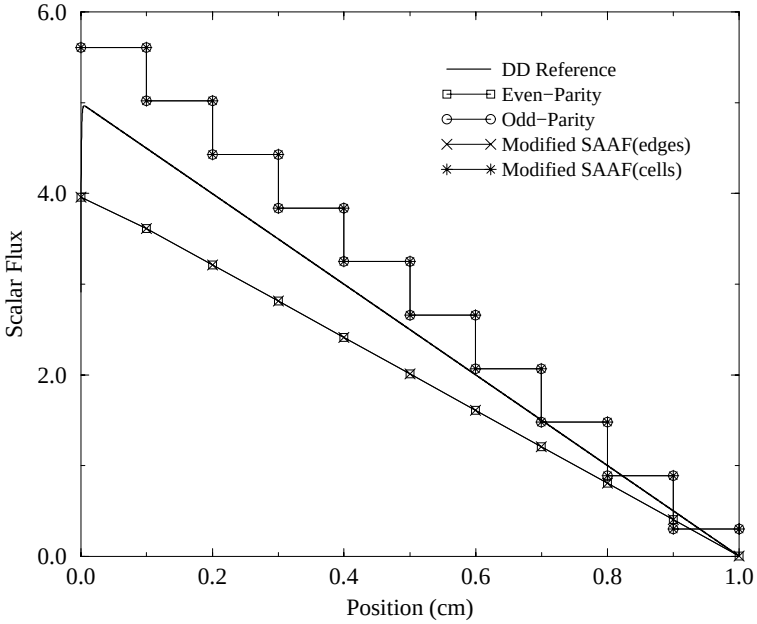

Fig. 16. Modified SAAF normal incident problem.

hybrid-parity results are very accurate, as we predicted. In the case of an isotropic incoming angular flux, all methods produce results that agree well with the reference solution. We do not display this simple result.

In the development of the SAAF system, we were able to show that the only difference between it and the average of the even- and odd-parity system was in the boundary conditions. If we replace the standard incoming boundary condition, $\psi_b = f_l$, with $\psi_b = 2f_l - \psi_{1/2}$ then we expect the SAAF results to be identical to the parity results. This is, in fact, the case, as we show in Fig. 16

c. Internal Interfaces

Now, we consider a model internal interface problem. This problem consists of a two region slab. The first region ($0 < x < 1.0$) contains a source free pure absorber one mean free path thick. The second region ($1.0 < x < 2.0$) contains a source free pure scatterer one

thousand mean free paths thick. The problem is driven by an incident angular flux at $x = 0$.

In Chapter II, we described the angular flux in the transport region with equations (2.41) and (2.42). If the transport region consists of a pure absorber, we can explicitly calculate the solution in that region. First, we attenuate the external boundary condition from the left boundary to the interface. Then we use the albedo condition, equation (2.42), to determine the angular flux emerging from the diffusive region and attenuate that from the interface to the left boundary. We note that we use the discrete ordinates method to treat the angle variable, though that is by no means necessary. We simply want the spatially analytic results to correspond as closely as possible to the numerical results.

In Chapter III, we determined that the even- and odd-parity systems each satisfied albedo conditions at the interface. These interface albedo conditions, equations (3.72b) and (3.80b), significantly differ from the exact condition. Their average results in a 2μ weighted isotropic return which we think may be an acceptable approximation to the exact condition.

Fig. 17 shows the exact analytic scalar flux in the transport region along with the analytic even- and odd-parity results calculated with equations (3.72b) and (3.80b). We have also plotted even- and odd-parity numerical results for this problem. The numerical results in the transport region agree quite well with the analytic predictions, and the hybrid-parity solution is very accurate for this problem. As we showed in Fig. 8, the hybrid-parity albedo differs from the exact mainly at small values of μ, which influence the overall solution the least.

Now, we consider the model interface problem driven by a left boundary angular flux in the most normal direction. We use 10 cells in the transport region and 10 cells in the diffusive region. The reference solution displays an abrupt jump in magnitude (a boundary layer) at the interface as shown in Fig. 18. Assuming that the transport region is zoned finely enough to resolve the angular flux for $\mu > 0$, we expect the even-parity solution to

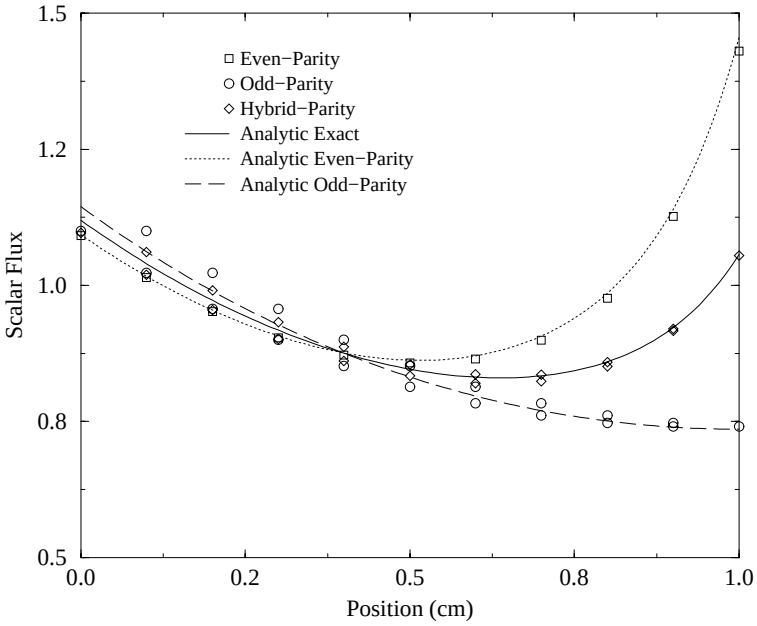

Fig. 17. Analytic internal interface solution for $x < 1$.

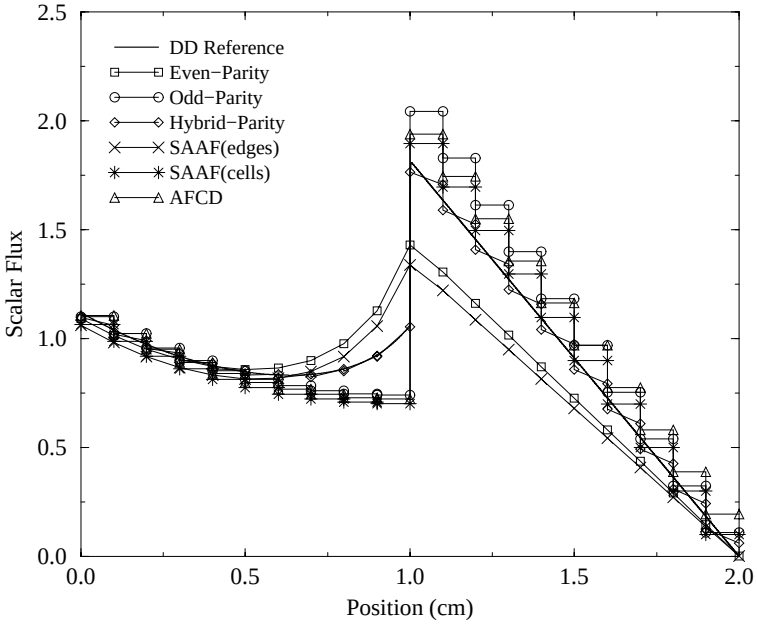

Fig. 18. Normal incident interface problem.

satisfy a 2μ weighted boundary condition on the interface, and the odd-parity to satisfy a $3\mu^2$ condition. Thus, the even-parity solution should be lower than the exact for $\mu \simeq 1$, and the odd-parity high. That is exactly what we observe. Their average, as predicted, is very accurate in both the transport and diffusive region. Recall that we can formally relate the SAAF solutions to the parity solutions at the interface. That is, we expect the SAAF cell edge scalar fluxes to be nearly identical to the even-parity values, and the SAAF cell center fluxes to match the odd-parity values. This is very nearly the case and we postulate that the observed differences are a result of the way we treat the external boundary condition. While we were not able to formally predict the behavior of the AFCD discretization at internal interfaces, we suggested that it would be similar in character to the odd-parity solution, as it indeed appears to be. It once again extrapolates the $3\mu^2$ boundary condition a half cell to the left of the physical interface.

In Fig. 19 we consider the model problem driven by a nearly grazing incoming angular flux. In this case, we use 100 zones in the transport region and 10 in the diffusive. The larger number of zones in the transport region is required to account for the exponential attenuation of the solution over a longer path length (the distance that a beam must travel to reach the interface is $1/\mu$, thus for small μ more cells are required to resolve the solution). This problem has a strong boundary layer in which the reference solution changes by an order of magnitude. Despite this, the hybrid-parity solution is extremely accurate.

Finally, we plot the SAAF results obtained with the $\psi_b = 2f_l - \psi_{1/2}$ boundary condition in Fig. 20. Here, we expect the SAAF edge scalar fluxes to be identical to the even-parity fluxes, and the SAAF cell fluxes to correspond to the odd-parity fluxes. This is precisely what we observe. Finally, we note that though the standard SAAF boundary condition results in cell centered scalar fluxes that are correct on the external boundaries of thick diffusive problems, the cell centered flux is not accurate at internal interfaces. Using the modified boundary condition, the average of the cell edge and cell centered SAAF

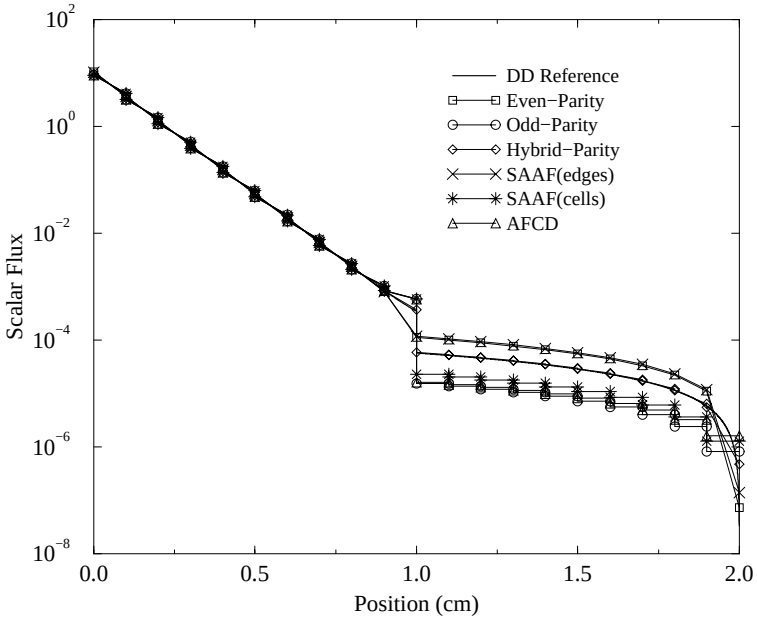

Fig. 19. Grazing incident interface problem (log scale).

scalar fluxes is extremely accurate at both external boundaries and internal interfaces.

d. Truncation Error Problems

Miller [3] has shown that the slab geometry even-parity equation discretized with linear continuous finite elements is second order accurate. While we have not performed truncation error analyses, we expect all of the methods to display second order convergence.

The first problem we consider is a four region slab with vacuum boundary conditions originally described by Alcouffe [72]. We display the problem layout in Fig. 21. The region thicknesses are measured in mean free paths and the relative number of cells per region is shown in parenthesis. The exact solution to this problem varies by nearly eight orders of magnitude. A fine mesh (9600 cells) diamond difference calculation is used as the reference solution and is displayed in Fig. 22. The solution is converged to a maximum relative pointwise error of 10^{-7}. In Fig. 23 we plot the absolute value of the difference

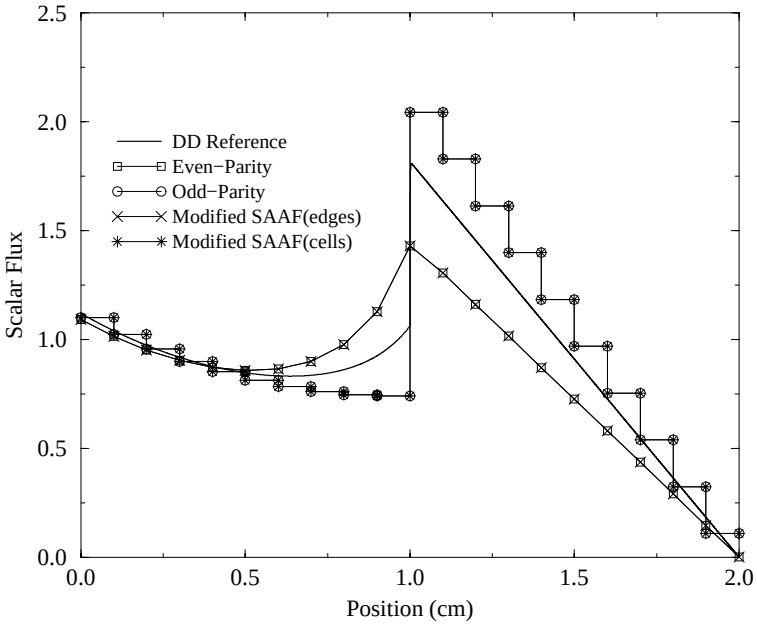

Fig. 20. Normal incident modified SAAF interface problem.

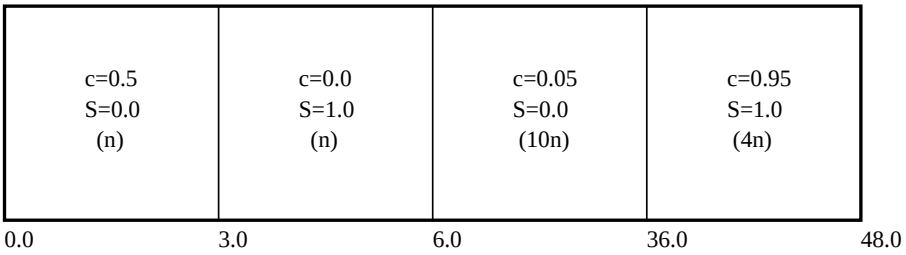

Fig. 21. Alcouffe's four region problem.

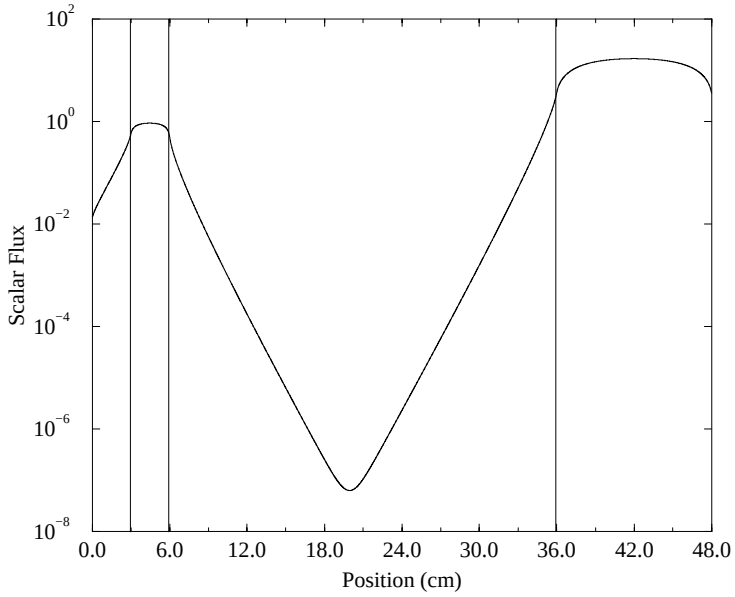

Fig. 22. Fine mesh DD solution to Alcouffe's four region problem.

between the reference and calculated total absorption rate as a function of the number of uniform spatial cells. There are several things to note. First, all the methods display second order convergence. Second, the diamond difference edge angular fluxes were negative and oscillatory for coarse meshes, though the cell average fluxes were acceptable. The hybrid-parity solution was far more accurate than the individual parity solutions and was comparable to the DD solution on fine meshes. Finally, recall that for vacuum boundaries the SAAF edge fluxes correspond the even-parity scalar fluxes and the SAAF cell centered fluxes correspond to the odd-parity scalar fluxes.

Next, we compute the exiting partial current from a 50 mean free path slab with an isotropic boundary condition on one face. We do this as a function of scattering ratio and cell thickness and present the ratio of the calculated results to a fine mesh (50,000 cells) DD reference solution in Tables I through III. Note that the linear discontinuous (LD) results are from reference [73]. For thin cells, LD is third order accurate and exhibits the

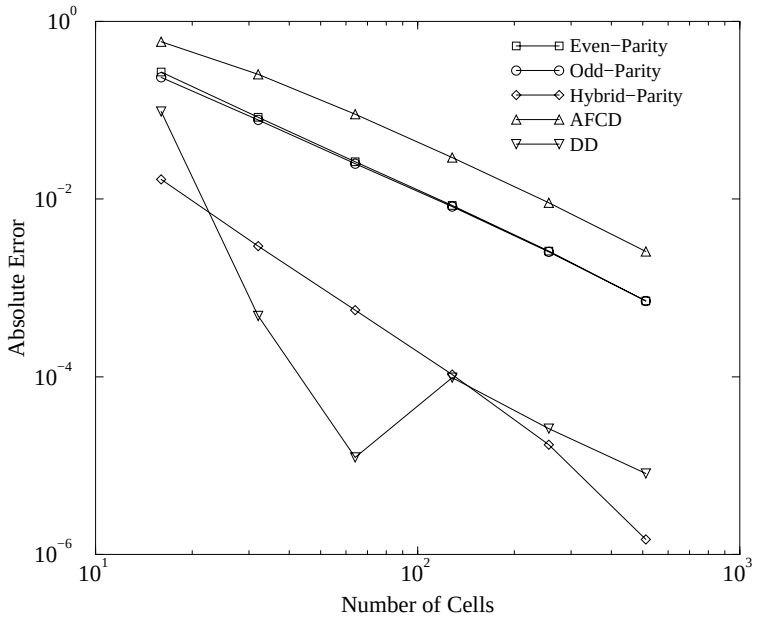

Fig. 23. Absorption rate error for Alcouffe's problem.

Table I. Exiting partial current as a function of c for $\sigma_t \Delta x = 1.0$.

c	EP	OP	SAAF	AFCD	DD	LD
0.0	8.2E+00	8.2E+00	8.2E+00	7.7E+00	5.4E+05	5.1E-01
0.1	7.9E+00	7.9E+00	7.9E+00	7.6E+00	1.4E+05	5.1E-01
0.3	7.1E+00	6.9E+00	7.0E+00	6.9E+00	4.3E+03	5.4E-01
0.5	5.5E+00	5.2E+00	5.3E+00	5.3E+00	2.0E+01	6.1E-01
0.7	3.1E+00	2.9E+00	3.0E+00	3.1E+00	7.2E-02	7.4E-01
0.9	1.4E+00	1.3E+00	1.3E+00	1.5E+00	5.3E-01	9.4E-01
0.99	1.0E+00	1.0E+00	1.0E+00	1.2E+00	9.8E-01	1.0E+00
0.999	1.0E+00	1.0E+00	1.0E+00	1.3E+00	1.0E+00	1.0E+00

Table II. Exiting partial current as a function of c for $\sigma_t \Delta x = 2.5$.

c	EP	OP	SAAF	AFCD	DD	LD
0.0	6.8E+03	6.8E+03	6.8E+03	5.5E+03	7.6E+19	1.6E+01
0.1	6.2E+03	6.0E+03	6.1E+03	5.3E+03	3.8E+19	1.0E+01
0.3	4.2E+03	3.8E+03	4.0E+03	4.0E+03	5.1E+18	2.6E+00
0.5	1.6E+03	1.4E+03	1.5E+03	1.6E+03	1.2E+17	1.3E-01
0.7	1.9E+02	1.5E+02	1.7E+02	1.9E+02	5.4E+13	1.0E-02
0.9	5.5E+00	4.4E+00	4.9E+00	6.1E+00	3.2E+06	4.2E-01
0.99	1.1E+00	1.0E+00	1.1E+00	1.8E+00	8.8E-01	9.8E-01
0.999	1.0E+00	1.0E+00	1.0E+00	2.0E+00	1.0E+00	1.0E+00

Table III. Exiting partial current as a function of c for $\sigma_t \Delta x = 5.0$.

c	EP	OP	SAAF	AFCD	DD	LD
0.0	7.7E+07	7.7E+07	7.7E+07	5.2E+07	7.5E+21	9.E+12
0.1	6.5E+07	6.2E+07	6.3E+07	5.2E+07	4.1E+21	6.E+12
0.3	3.4E+07	2.9E+07	3.1E+07	3.4E+07	6.5E+20	1.E+12
0.5	6.8E+06	5.1E+06	6.0E+06	7.2E+06	1.8E+19	3.E+10
0.7	1.6E+05	1.0E+05	1.3E+05	1.6E+05	9.8E+15	2.E+07
0.9	1.2E+02	6.9E+01	9.3E+01	1.2E+02	7.0E+08	1.2E+00
0.99	1.4E+00	1.2E+00	1.3E+00	2.9E+00	3.0E+00	8.7E-01
0.999	1.0E+00	1.0E+00	1.0E+00	3.3E+00	9.8E-01	1.0E+00

best overall performance. For c near zero, LD is superior to the parity solutions, but for diffusive problems the parity solutions are comparable to LD. With thick cells, all of the methods perform poorly for small values of c. However, for c near one they are quite accurate with the exception of the AFCD results. This is because the AFCD vector unknown only converges with first order accuracy. Diamond differencing performs poorly in these problems because, even on the finest mesh, the cell thickness is greater than $2\mu_{min}/\sigma_t$ so that oscillations can result.

Finally, consider a slab of thickness L with vacuum boundaries, fixed cross sections, isotropic scattering, and isotropic sources. In slab geometry S_2 problems are equivalent to P_1 problems with Mark boundary conditions. Thus, if we run a S_2 calculation for such a problem, we can completely isolate the error associated with the spatial discretization. The scalar flux in such a problem is given by:

$$\phi(x) = \frac{q}{\sigma_a}\left[1 - \frac{e^{\sqrt{3\sigma_a\sigma_t}x} + e^{-\sqrt{3\sigma_a\sigma_t}x}}{(1+\sqrt{\sigma_a/\sigma_t})e^{\sqrt{3\sigma_a\sigma_t}L/2} + (1-\sqrt{\sigma_a/\sigma_t})e^{-\sqrt{3\sigma_a\sigma_t}L/2}}\right].$$

In Fig. 24 we plot the absolute value of the difference between the calculated total absorption rate and the exact value for a 1cm thick slab with $\sigma_t = 2, \sigma_a = 1$ and $q = 1$. All methods exhibit second order convergence as we expected. We note that both the hybrid-parity and SAAF edge results are superior to the DD result.

Finally, in Fig. 25, we study the effect that mass matrix lumping has on accuracy. We expect that there will be some degradation in accuracy, though the order of convergence should remain the same. This is observed in the plot. It is interesting to note that the hybrid-parity accuracy is insensitive to mass matrix lumping despite the fact that both the even- and odd-parity errors change when lumping is used. We observe this behavior in several other more complex tests of the global error.

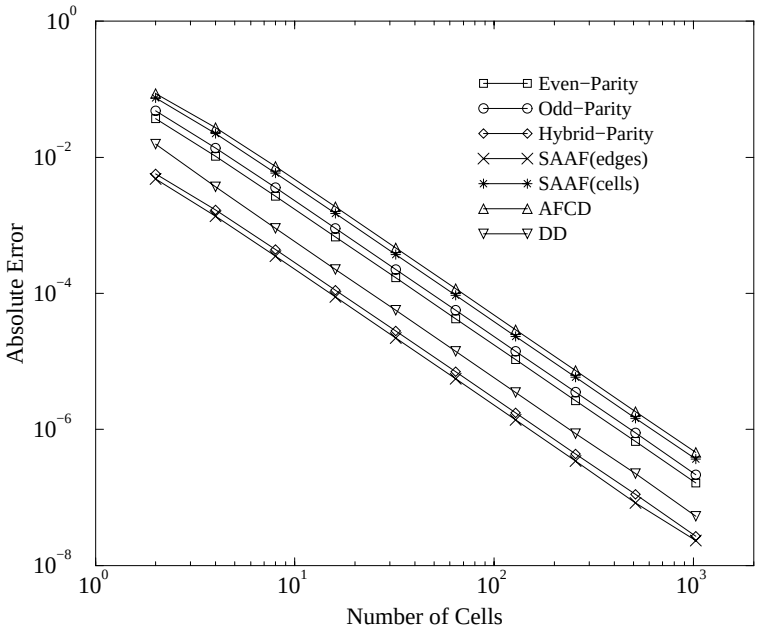

Fig. 24. Absorption rate error for the analytic problem.

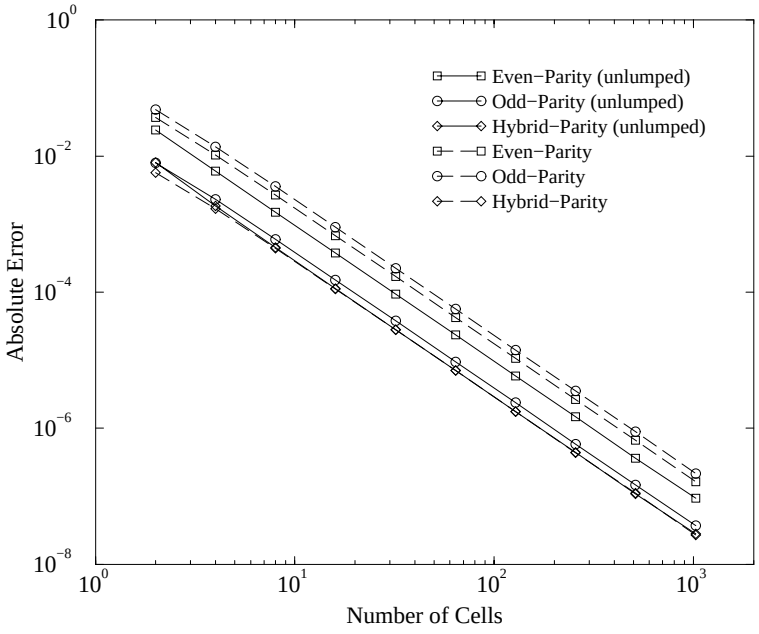

Fig. 25. Effect of lumping on the absorption rate error.

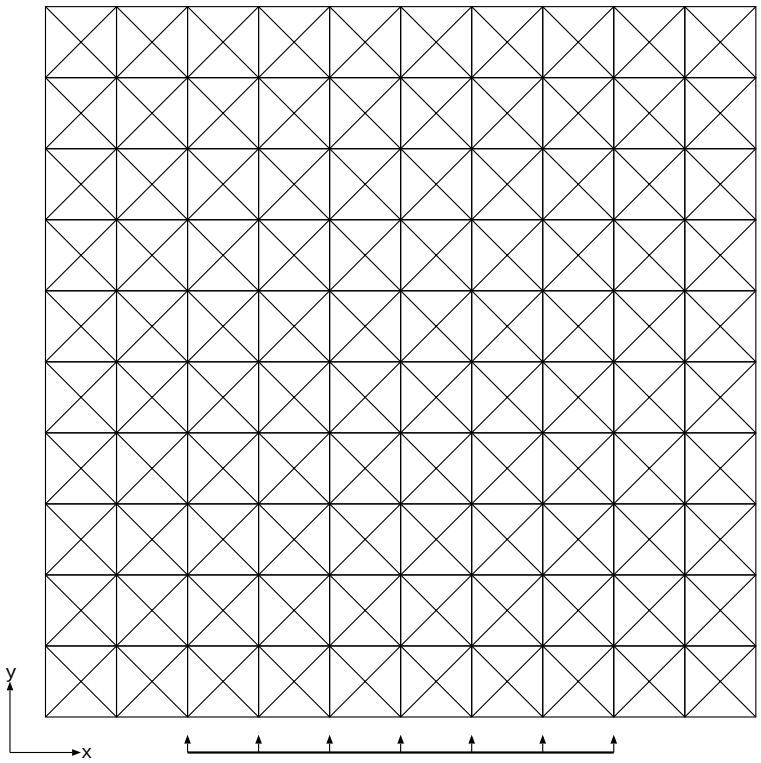

Fig. 26. Regular XY geometry mesh.

2. XY Geometry

In this section, we will use three different spatial grids. The first is the regular triangular grid shown in Fig. 26. The origin is in the lower left corner, and various incident angular fluxes are applied to the middle six boundary edges on the bottom face.

We will also generate results for several test problems on two irregular grids. The first belongs to a family of meshes known as Z-meshes [74] and is depicted in Fig. 27. The second grid is simply a randomly distorted version of the regular grid. We refer to it as the random grid and display it in Fig. 28. Note that the double border around Fig. 27 and 28 is an artifact of the mesh generation program and that the underlying triangular mesh is obtained by inserting edges from the vertices to the geometric center of each quadrilateral.

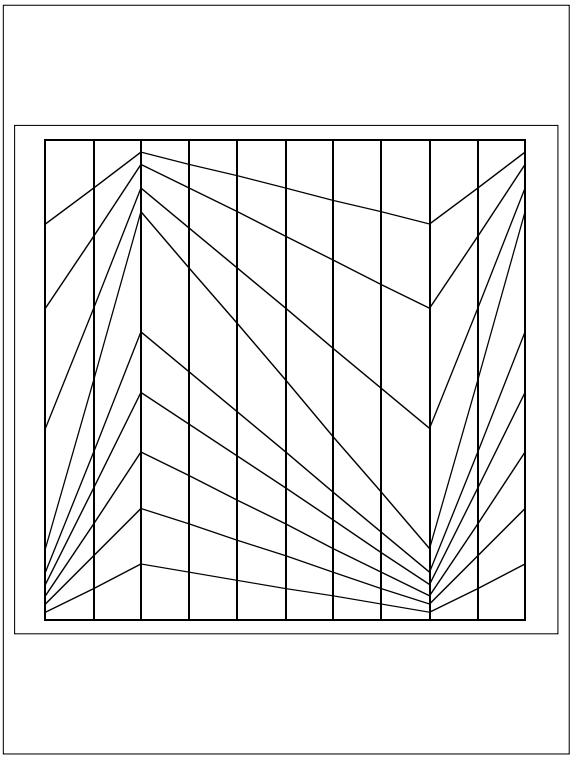

Fig. 27. XY geometry Z-mesh.

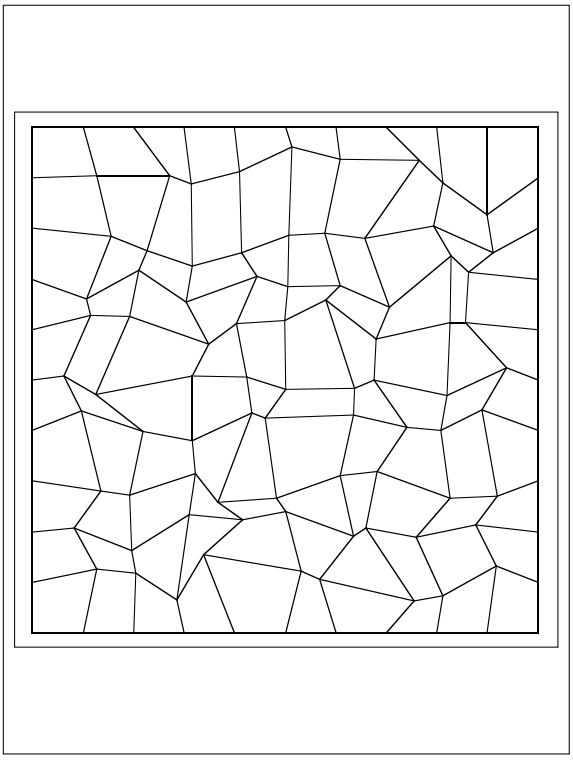

Fig. 28. XY geometry random mesh.

In this section, we will use the bilinear discontinuous finite element discretization (BLD) on a square grid as a reference for comparison. Its behavior is well understood for thick diffusive problems. On a problem boundary, the magnitude of the BLD flux is given by a Marshak weighting of the incoming angular flux, just as in the even-parity case. However, over the first cell, the flux falls to $\mu + \frac{3}{2}\mu^2$ interior magnitude. The BLD method is also known to exhibit second order convergence on regular grids.

a. The ε Problem

We first consider the ε problem on a regular, 400 element mesh with S_4 quadrature. Our analysis indicates that the even- and odd-parity transport solutions should approach a diffusion solution as ε tends to zero. Fig. 29 and 30 show the value of the even- and odd-parity scalar fluxes along the diagonal extending from the lower left corner to the upper right corner. The solutions are symmetric and smooth in both cases, and behave just as we expected. As in the slab geometry case, for values of ε less than 0.001, the even- and odd-parity solutions do not change. We note that many methods yield solutions that tend to zero as ε approaches zero [71].

b. External Boundaries

We now turn to purely scattering problems driven by boundary conditions. Here, we use the mesh shown in Fig. 26. We consider a 1cm by 1cm square with $\sigma_t = \sigma_s = 1000$, no source and S_{16} quadrature. In our first problem, we drive the problem with an isotropic incoming angular flux. Here, we expect both the even- and odd-parity solutions to be accurate. In Fig. 31 we plot a square mesh bilinear discontinuous (BLD) solution along with even- and odd-parity solutions along the centerline of the problem. The solutions behave as expected; all are approximately the same and reasonably accurate.

Now, we drive the same problem described above with an angular flux in the most

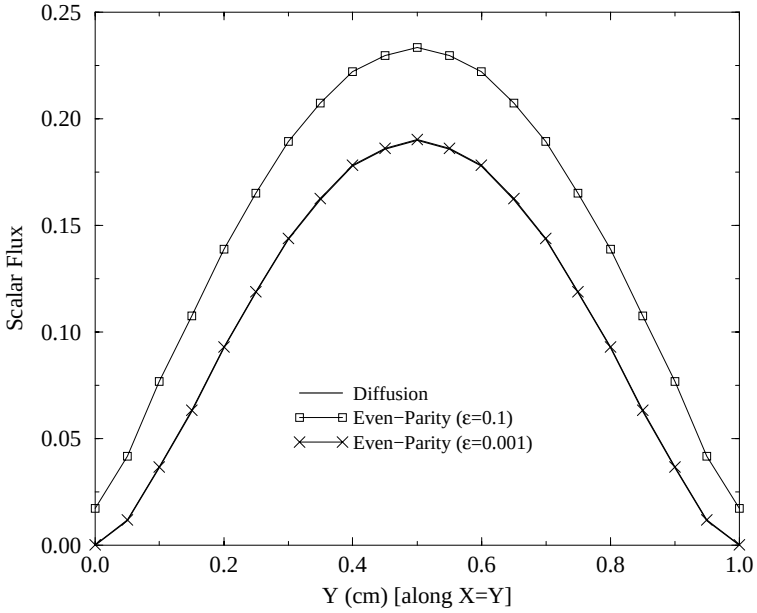

Fig. 29. XY EP ε problem.

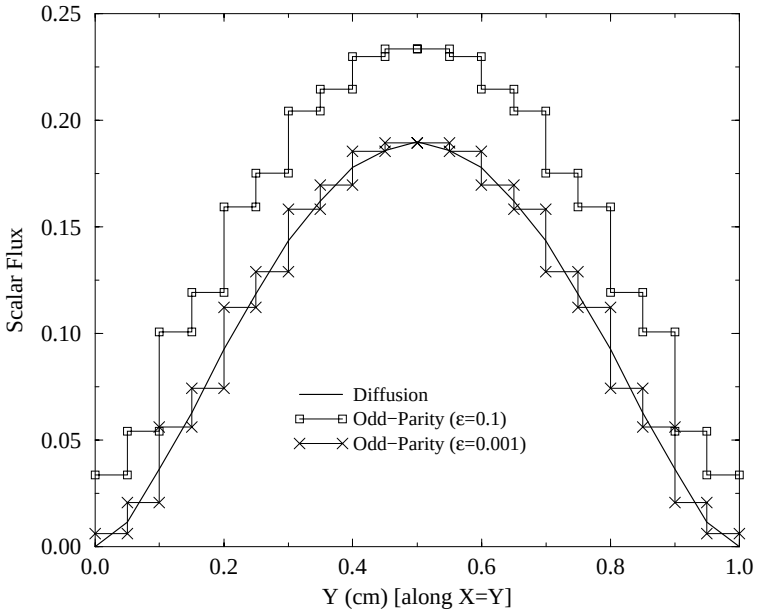

Fig. 30. XY OP ε problem.

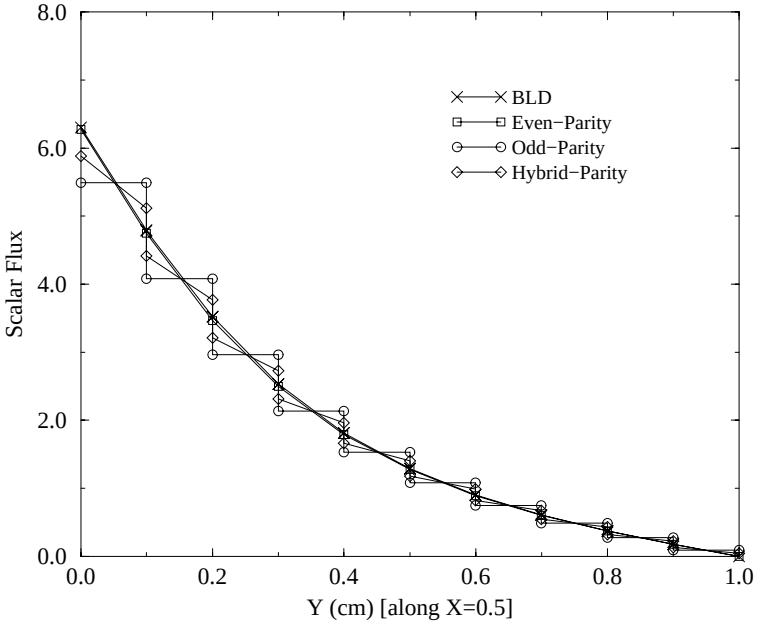

Fig. 31. XY isotropic incident problem.

nearly normal incident angles. That is, the two angles with the smallest $|\mu|$ and the largest η, where $\mu = \Omega \cdot \mathbf{e_x}$ and $\eta = \Omega \cdot \mathbf{e_y}$. We have scaled the magnitude of the incoming angular flux so that the interior solution should be the same as in an isotropic incoming case with a $\mu + \frac{3}{2}\mu^2$ weighting. We plot BLD, even- and odd-parity results along the centerline in Fig. 32. Our analysis predicts that the even-parity solution will be lower than the exact and that the odd- parity solution will be higher. This can be seen in the graph. Note that the BLD and even-parity solutions are identical on the problem boundary, and that the hybrid-parity solution follows the BLD solution in the interior.

We now consider a boundary condition in the most nearly grazing incident angles (the two angles with the largest $|\mu|$ and the smallest η). We have again scaled the magnitude of the incoming angular flux to produce the same interior magnitude as in the isotropic incoming case. We plot BLD, even- and odd-parity results along the centerline in Fig. 33. In this case, our analysis predicts that the even-parity solution will be higher than the exact

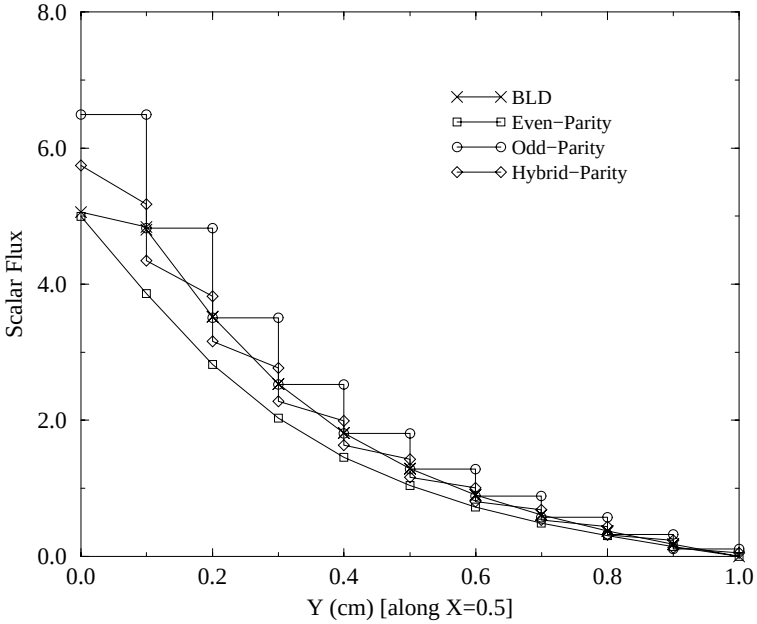

Fig. 32. XY normal incident problem.

and that the odd-parity solution will be lower. Again, the results agree quite well with our predictions, and the hybrid-parity solution again follows the BLD solution closely in the problem interior. Note that the BLD solution falls from the even-parity value on the boundary to the hybrid-parity value in the next cell. Clearly, given that our goal when deriving the diffusion limit boundary condition was to extrapolate the correct interior solution to the boundary, the hybrid-parity method is more accurate than the BLD on the boundary.

In our analysis of the odd-parity system, we noted that we obtain the $3\mu^2$ weighting only when the incoming angular flux is azimuthally symmetric. In order to evaluate the effect of an asymmetric incoming angular flux, we now consider a problem identical to the previous grazing angle problem except that instead of having an incoming angular flux with equal magnitudes in the two most grazing angles, we put twice the original magnitude into one (the angle pointing form left to right) direction.

Physically, in a thick diffusive problem, the azimuthal asymmetries in the boundary

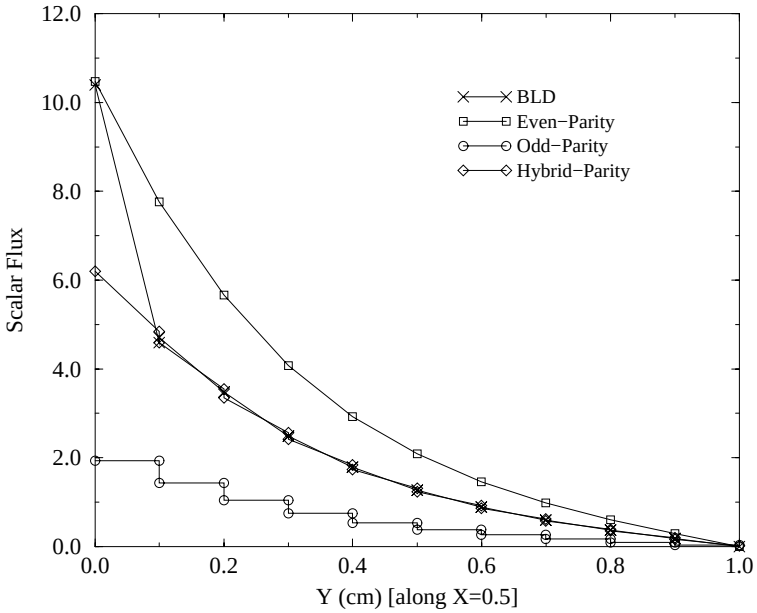

Fig. 33. XY grazing incident problem.

condition do not affect the interior solution (though they do strongly affect the boundary layer). In the case of the odd-parity system, however, an azimuthally asymmetric angular flux does affect the interior solution. In Figs. 34 through 37 we plot the value of the odd-parity angular flux along constant values of the Y coordinate for both a symmetric incoming angular flux and for an asymmetric angular flux. We see that the odd-parity solution is very adversely affected by asymmetry in the boundary condition. Near the boundary itself we obtain negative fluxes. In the interior, a non-physical oscillatory solution propagates throughout the entire problem.

c. Internal Interfaces

Though our internal interface analysis was restricted to slab geometry, we do expect the results to apply to multidimensional problems. Therefore we consider a problem where the region from ($0 < Y < 0.5$) contains a pure absorber with $\sigma_t = \sigma_a = 1$ and the region

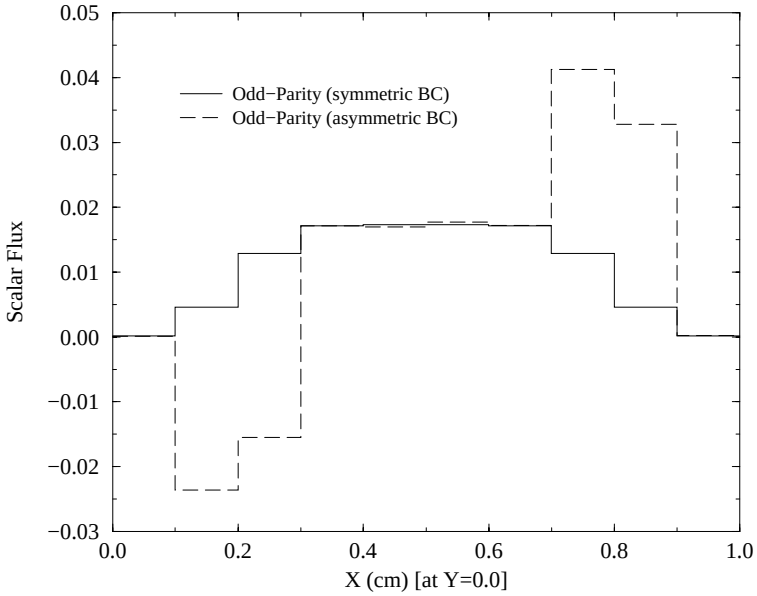

Fig. 34. OP asymmetric BC problem for Y=0.0.

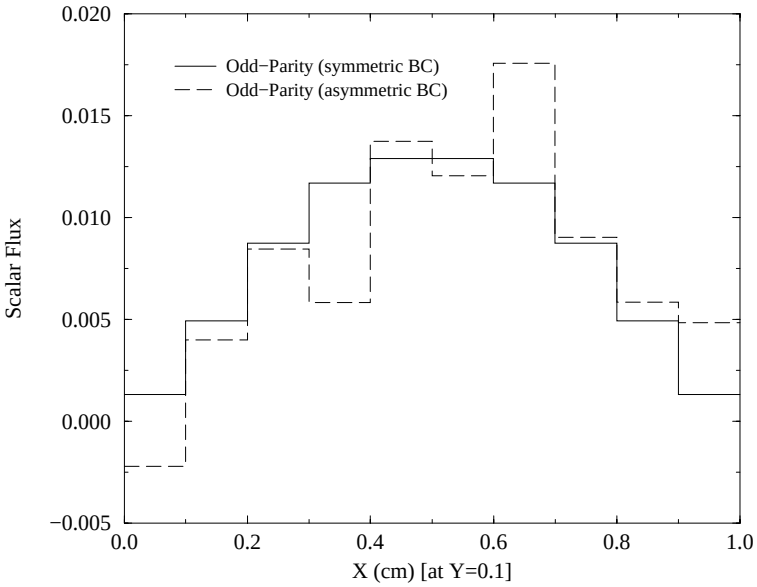

Fig. 35. OP asymmetric BC problem for Y=0.1.

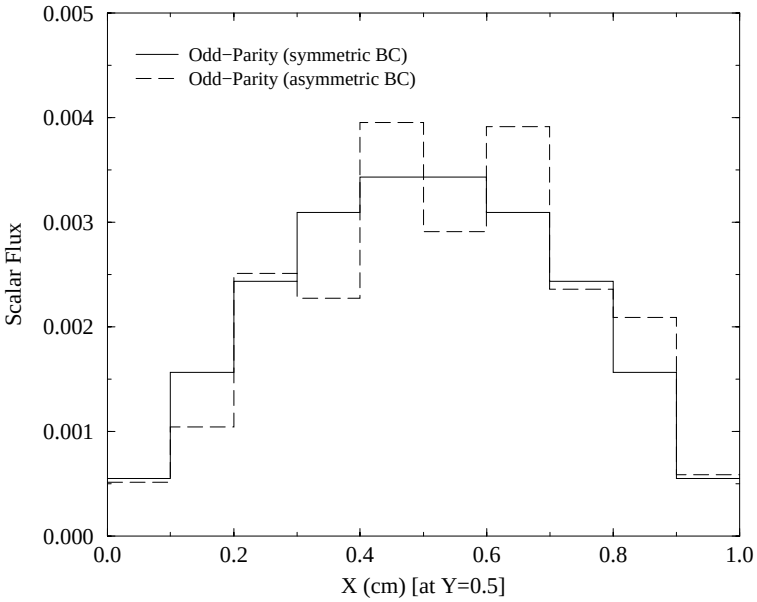

Fig. 36. OP asymmetric BC problem for Y=0.5.

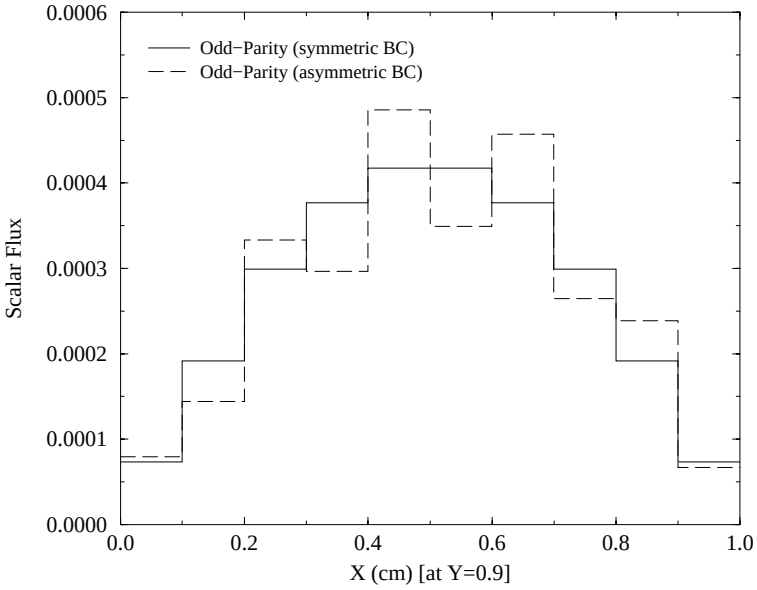

Fig. 37. OP asymmetric BC problem for Y=0.9.

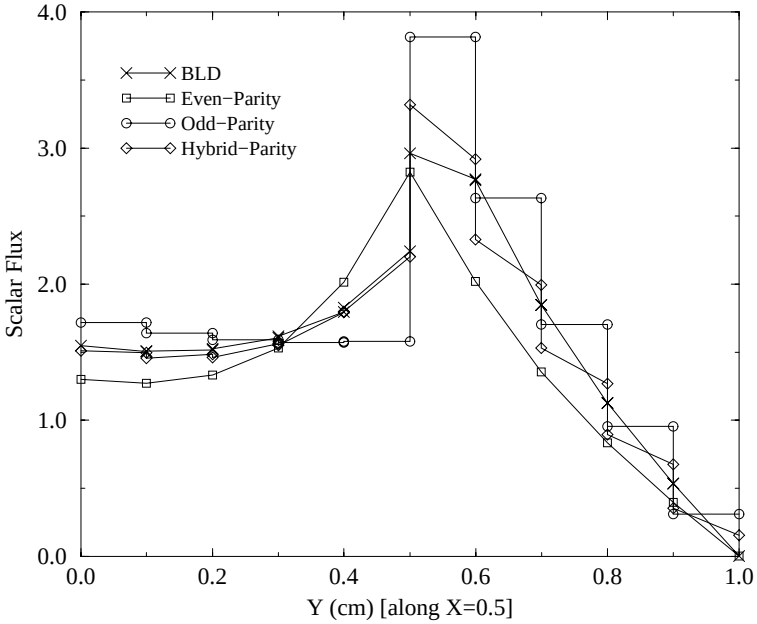

Fig. 38. XY internal interface problem.

from $(0.5 < Y < 1.0)$ contains a pure scatterer with $\sigma_t = \sigma_s = 1000$. In Fig. 38 we display BLD, even- and odd- parity results along the centerline of the problem. In this case, we drive the problem with a nearly normal boundary condition. Though the BLD method cannot be considered a reference solution, we do expect it to perform well for problems of this type. We see that, with the exception of the value on the interface, the hybrid-parity method again mimics the BLD solution. In fact, the hybrid-parity method comes much closer to the actual extrapolated interior diffusion solution on the interface than the BLD, which satisfies a Marshak condition on the boundary.

d. Truncation Error Problems

First, we consider a 1cm by 1cm square with a uniform isotropic source, vacuum boundary conditions and S_2 quadrature. We set $\sigma_t = 1.0$ and $\sigma_s = 0.5$ then calculate the total absorption rate error as a function of the number of elements, where we use a fine mesh

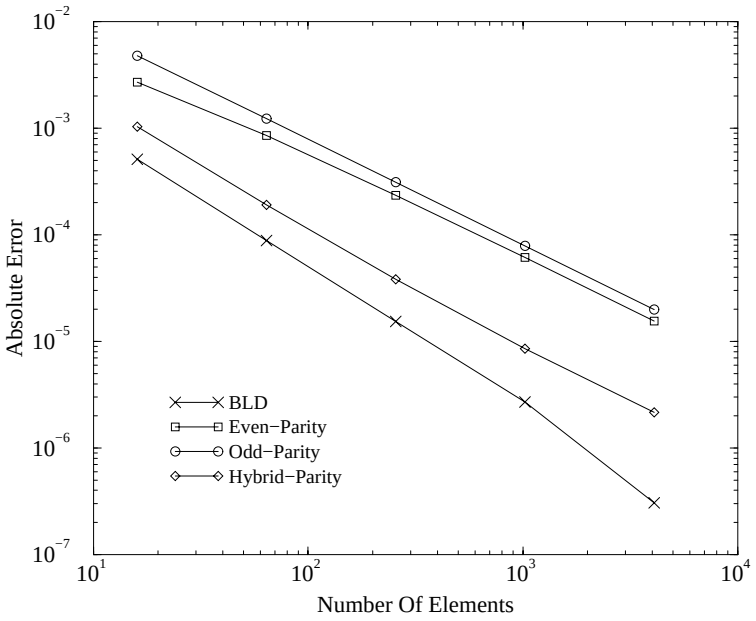

Fig. 39. XY absorption rate error versus number of elements.

(16,384 cells) BLD calculation converged to a maximum relative pointwise error of 10^{-6} to determine the reference value. The results are displayed in Fig. 39. All the methods display second order convergence. Note that the hybrid-parity solution is significantly more accurate than either the even-parity solution or the odd-parity solution alone.

Finally, we consider the four region problem shown in Fig. 40. This problem consists of a $c = 1$ source region surrounded by an absorbing region, then by water. We calculate the absorption rate in the top right region, which is a pure absorber, as a function of decreasing the uniform mesh spacing along each axis. The results are shown in Fig. 41. We note that all of the methods display second order convergence. However, it is obvious that the hybrid-parity and BLD solutions are much more accurate than the individual parity solutions. Here, we see that the odd-parity solution approaches the correct solution from below, while the even-parity solution approaches from above. This is a characteristic of the parity systems.

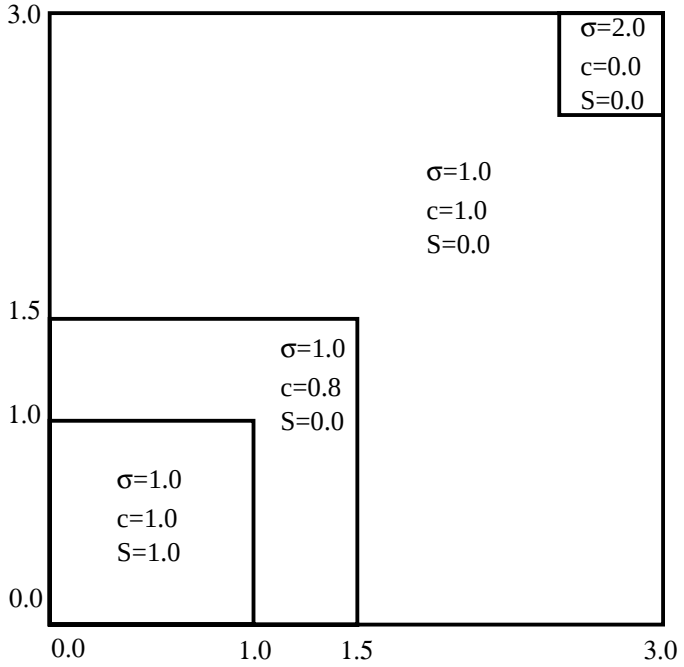

Fig. 40. XY four region problem configuration.

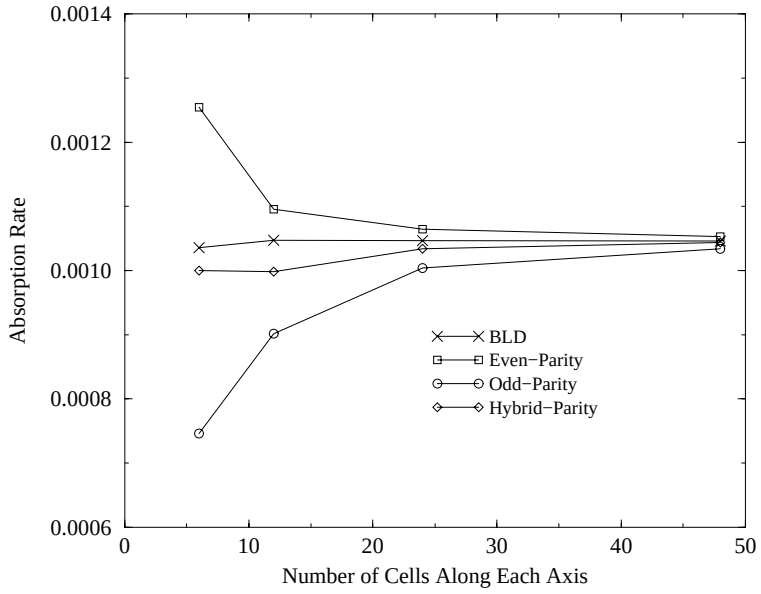

Fig. 41. Absorption rate in top right corner.

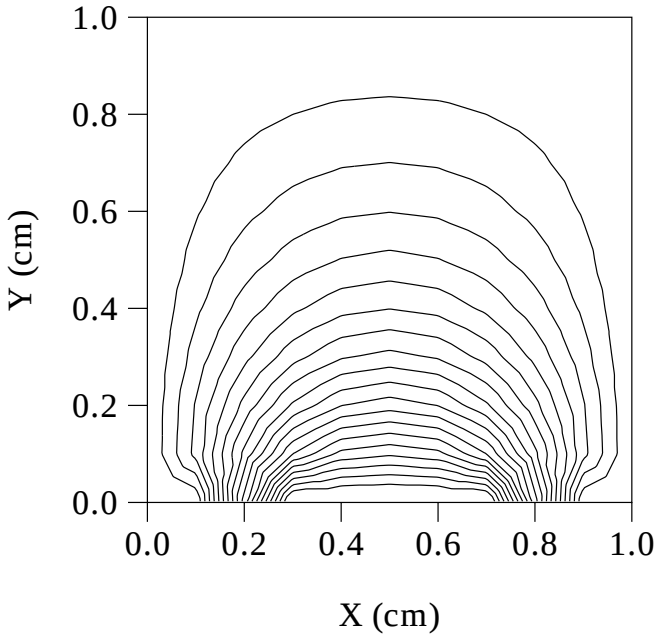

Fig. 42. Regular Mesh Even-Parity XY isotropic BC problem.

e. Irregular Mesh Problems

We now consider a series of more challenging problems. We hope to identify potential problems in our discretizations by considering several non-uniform grids. The problem we consider is the isotropic incoming boundary condition problem whose solution is shown in Fig. 31. We use the regular mesh solutions as a reference point. Note that we are unable to present BLD results for these problems since we do not have access to a non-orthogonal grid BLD solver.

In Fig. 42 we plot contours of the regular grid even-parity solution for this problem. The peak value of 6.2 occurs in the center of the bottom face and the contours begin at 6.0 and are 0.3 apart. The solution is symmetric about X=0.5, smooth and positive throughout the problem.

Using the same contours as in the regular mesh case, we display the Z-mesh and ran-

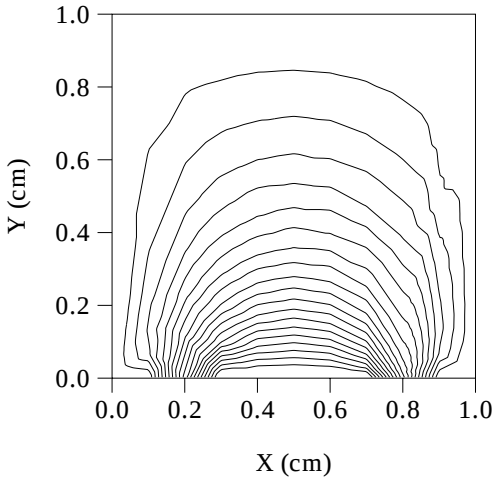

Fig. 43. Z-Mesh EP problem.

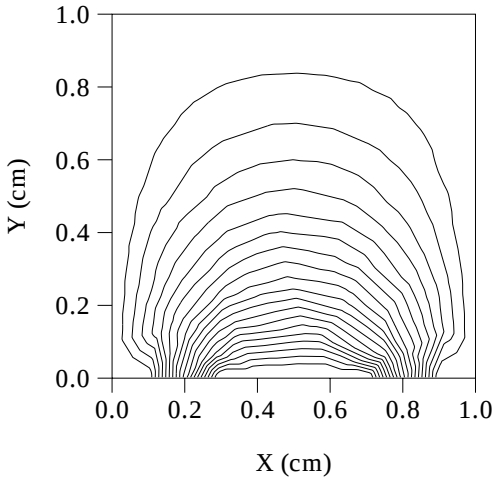

Fig. 44. Random-Mesh EP problem.

dom mesh results for this problem in Figs. 43 and 44, respectively. The Z-mesh problem clearly exhibits some skewing along the distorted grid lines, though the magnitude of the solution remains approximately correct. The random mesh results are quite good, though there is a small amount of asymmetry introduced. Both the Z-mesh and random mesh solution remain positive throughout the problem. In Fig. 45 we plot the regular grid odd-parity solution for this problem. The peak value of 6.0 occurs in the center of the bottom face. The solution is symmetric about X=0.5 positive throughout the problem. We present the Z-mesh and random mesh results for this problem in Figs. 46 and 47, respectively. These results require some explanation. First, we note that it is impossible to converge these problems for $c = 1$, thus, we were forced to introduce a small amount of absorption. Specifically, we set $c = 0.99999$, which we determined would result in an amount of absorption approximately two orders of magnitude smaller than the leakage from the problem. That is, we do not expect this amount of absorption to measurably affect the characteristics of problem.

Despite this, we see that the solutions are neither symmetric nor positive. Though it is difficult to see in the plots, the negative fluxes occur only in the lower left and lower right

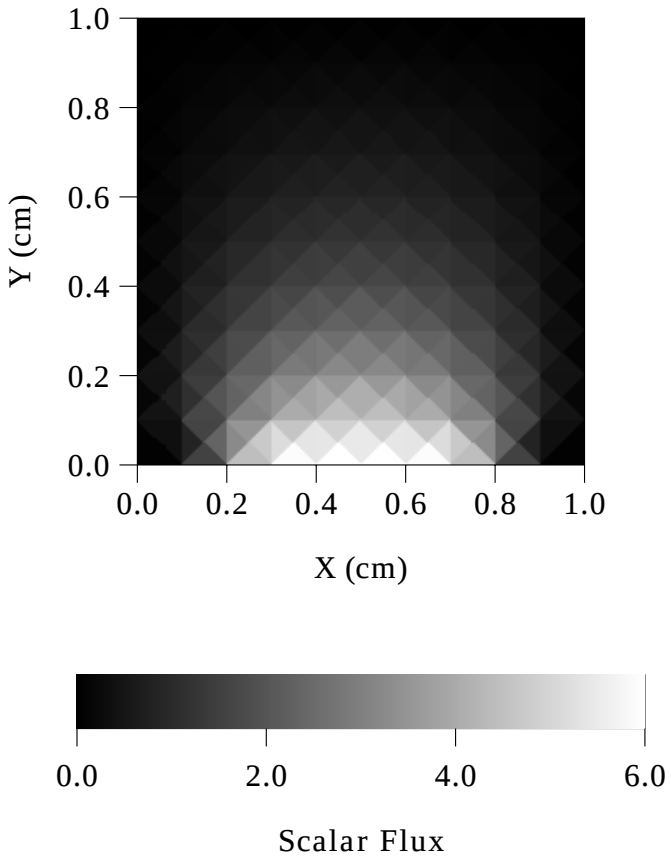

Fig. 45. Regular Mesh Odd-Parity XY isotropic BC problem.

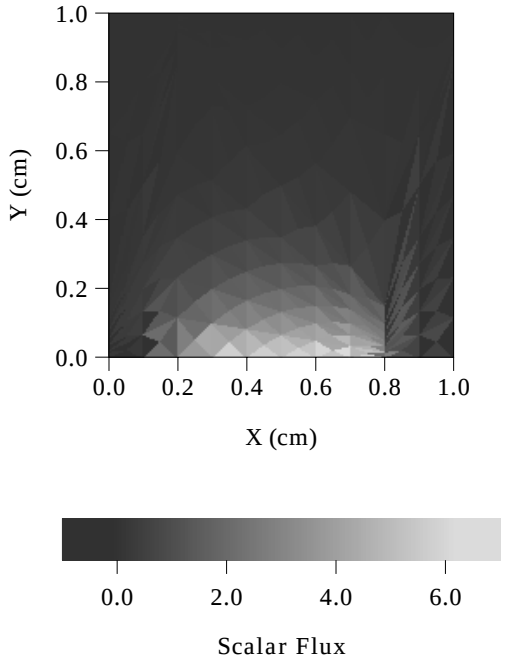

Fig. 46. Z-Mesh OP problem.

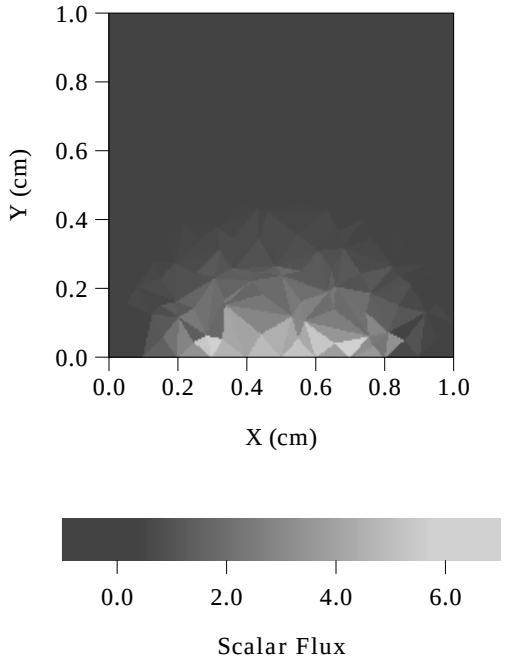

Fig. 47. Random-Mesh OP problem.

corners of the two problems. The Z-mesh solution is more negative fluxes and oscillatory than the random-mesh solution. While these results at first appear disappointing, we stress that they are not unexpected. As we discussed in Chapter III, the odd-parity equation discretized with linear continuous finite elements violates the discrete inf-sup condition. As a result, the matrix equation that the leading order odd-parity solution satisfies in the thick diffusive limit is *singular* when $c = 1$. As we mentioned Chapter III, the odd-parity LCFEM source matrix has a non-zero null-space, leading to the inability of the method to yield a unique scalar flux.

In fact, it is rather surprising that we are able to obtain odd-parity results for any XY geometry problem. In order to understand what is happening, we now consider a very simple $c = 1$ XY geometry problem. Consider the mesh shown in Fig. 48. We constructed the discrete odd-parity LCFEM matrix system for this problem and found that the null-

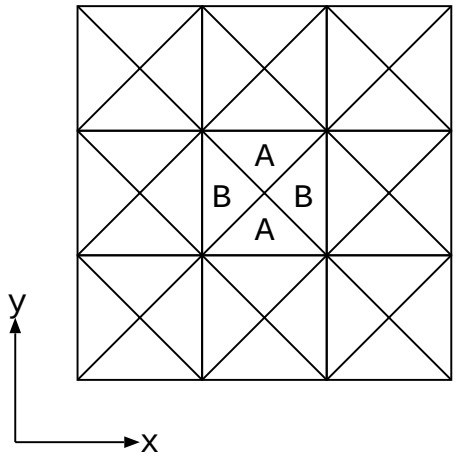

Fig. 48. 3 by 3 grid.

space of the source operator consisted of symmetric but highly oscillatory vectors. In order to excite these error modes, we contrived the following problem. Using the grid shown in Fig. 48, we inserted a fixed source of 1 in the elements labeled A, and a fixed source of 0 in those labeled B. We ran the problem using source iteration and plot the scalar fluxes in elements A and B in Fig. 49. Just as we expected, the scalar flux in these elements grows with each iteration because the fixed source was selected to be in a space that is completely invisible to the odd-parity CFEM operator. As was stated in Chapter III, this discretization should be used only with great caution.

B. DSA Performance

In this section we study the performance of our DSA routines for a variety of slab and XY problems. First, we consider a 1cm thick, c=1 slab with 10 cells, a fixed source of 0.0001 and S_{16} quadrature. We vary the value of σ_t to change the optical thickness of the problem and use a maximum pointwise relative error of 10^{-6} as the convergence criterion.

The number of iterations for each method are shown in Table IV. The final two rows show the number of odd-parity conjugate gradient (OPCG) and odd-parity DSA precondi-

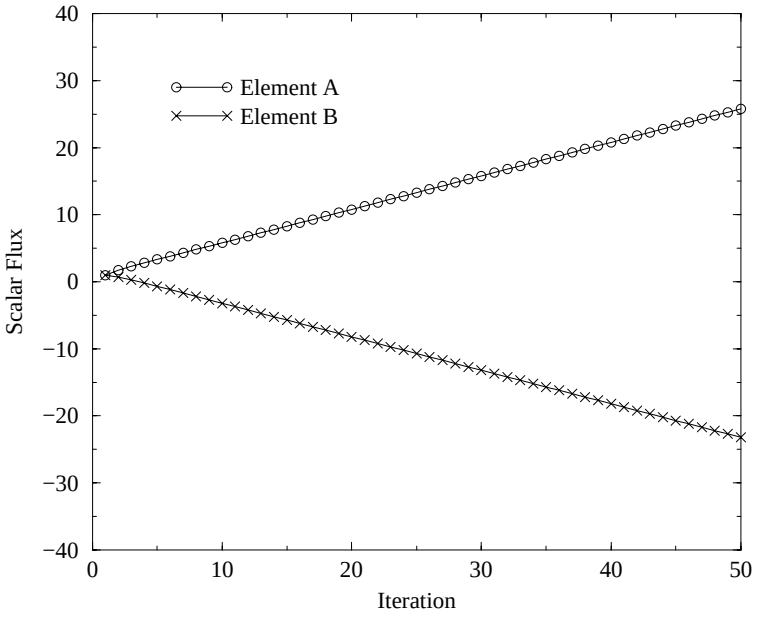

Fig. 49. Null space error mode excitation problem.

tioned conjugate gradient (OPPCG) iterations required to converge the problem.

Our Fourier analyses indicate that all our DSA methods should have spectral radii bounded by 0.2247 (which corresponds to less than 10 iterations for the problem under consideration assuming an O(1) initial error). All of the results, with the exception of the SAAF, agree well with our predictions.

Recall that in the derivation of the SAAF DSA system we were forced to make an approximation to the boundary terms of the DSA system in order to decouple the cell edge and cell center unknowns. In thin problems, where the boundary terms have the greatest impact, this approximation adversely affects the performance of the SAAF DSA, though not to a problematic degree.

The conjugate gradient results are impressive for this small problem. Using DSA to precondition the conjugate gradient method results in only a minor decrease in iteration count. However, we expect the number of conjugate gradient iterations to increase as the

Table IV. Slab DSA results for a 10 cell problem.

Method	$\sigma_t = 10^0$	$\sigma_t = 10^1$	$\sigma_t = 10^2$	$\sigma_t = 10^3$
EP	9	9	5	3
OP	9	8	4	3
SAAF	15	17	11	6
AFCD	8	9	7	4
OPCG	5	6	6	6
OPPCG	5	5	3	3

Table V. Slab DSA results for a 100 cell problem.

Method	$\sigma_t = 10^0$	$\sigma_t = 10^1$	$\sigma_t = 10^2$	$\sigma_t = 10^3$
EP	9	9	5	4
OP	9	8	4	3
SAAF	21	17	11	6
AFCD	9	9	7	4
OPCG	12	36	51	51
OPPCG	6	6	4	3

size of the problem increases. To test this we consider the same problem discretized with 100 cells show the results in Table V.

As expected, the conjugate gradient method now requires far more iterations than the DSA method. Though the DSA preconditioned conjugate gradient method exhibits excellent performance in terms of iteration count, it requires more memory and floating point operations than the standard DSA method.

Finally, in Table VI we present iteration counts for a simple XY geometry problem. The problem consists of a regular, 400 element XY geometry mesh with $c = 1$, a uniform

Table VI. XY DSA results for a 400 element problem.

Method	$\sigma_t = 10^0$	$\sigma_t = 10^1$	$\sigma_t = 10^2$	$\sigma_t = 10^3$	$\sigma_t = 10^4$
EP	9	9	5	5	5
OP	22	15	7	5	5

fixed source and S_{16} quadrature. Again, we vary to total cross section to alter the optical thickness of the problem.

We predicted that the spectral radii of the parity DSA schemes would be bounded by 0.5, which corresponds to approximately 20 iterations in this problem, again assuming O(1) initial errors. Our results agree well with this prediction, though we note that the odd-parity method is somewhat less efficient than the even-parity for optically thin problems.

In summary, the numerical results we have presented here agree well with the analysis, and we have confidence that we understand the behavior of these methods in thick diffusive problems. Further, we have successfully implemented DSA for all of the methods in slab geometry and for the even- and odd-parity CFEM methods in XY geometry. Finally, we have demonstrated that the use of LCFEM discretizations of the odd-parity (and the SAAF system by virtue of its similarity to the odd-parity system) are suspect except in very idealized ($c < 1$, regular grid) problems.

CHAPTER VII

CONCLUSIONS AND RECOMMENDATIONS

A. Conclusions

In this dissertation have derived very general Cartesian coordinate finite element discretizations for several second order forms of the transport equation. We have identified the relationship between finite element discretizations of the even- and odd-parity equations and corresponding discretizations of the SAAF equation. We have demonstrated that if they are discretized with the same finite element method, the average of the discrete even- and odd-parity equations is the same as the discrete SAAF equation in the problem interior. Further, if we replace the standard SAAF boundary condition $\psi_b = f$ with $\psi_b = 2f - \psi$ for incoming directions, the SAAF discretization becomes identical to the average of the discretized even- and odd-parity equations everywhere. Throughout this work, we have assumed very little about the weight and basis functions underlying the discretizations, in the hope that our results can be very generally applied.

We have analyzed the finite element discretizations for thick diffusive problems and found that for each transport discretization, the leading order solution in a thick diffusive problem satisfies a corresponding finite element discretization of the diffusion equation. However, the discrete boundary conditions may not be accurate. Nevertheless, this is a powerful result. If we select a finite element method that is *appropriate* for a diffusion problem on a particular grid, then the application of that method to a second order form of the transport equation will ensure that the leading order transport solution in a thick diffusive problem satisfies that *appropriate* finite element discretization of the diffusion equation. Our analysis also revealed that the average of the even- and odd-parity solutions should be very accurate for thick diffusive problems, provided the odd-parity diffusion

discretization is not singular.

Notably, one of the most straightforward discretizations of the odd-parity system, the linear continuous finite element method on triangles and tetrahedra, is not an appropriate discretization. In this case, the diffusion unknown is a cell centered quantity and that choice of weight and basis functions corresponds to a dual mixed variational finite element discretization that violates the discrete inf-sup condition. The SAAF system is also subject to this problem. As we have shown, the SAAF system is identical to the average of the even- and odd-parity systems except for boundary conditions.

Application of appropriate mixed finite element methods resolves the violation of the discrete inf-sup condition, though at the expense of more unknowns on a given mesh and introduction of symmetric indefinite matrices in place of the SPD matrices we enjoy for CFEM discretizations.

We also characterized the behavior of the finite element discretizations at interfaces between diffusive and non-diffusive regions in slab geometry. We showed that the behavior in the diffusive region was identical to the behavior on outer boundaries. By carefully analyzing the even- and odd-parity methods in the transport region we were able to show that the hybrid-parity solution satisfies a Marshak weighted, isotropic return albedo condition at the interface. Though this condition is not identical to the exact albedo, it appears to be a very good approximation.

Finally, we developed and implemented consistent DSA for each method. Our Fourier analysis suggests that these schemes will be very successful. We note that the SAAF DSA scheme requires scalar flux corrections in both finite element spaces in question. Our efforts to accelerate only one (the cell centered scalar flux, for example) were not successful.

We summarize our development and analysis results in Table VII. Unless otherwise noted, these results are for linear continuous finite elements on a triangular mesh. Recall that we denote the lowest order Raviart-Thomas finite elements as RT_0.

Table VII. Summary of analysis results.

Method	Ext./Int. BC	Unknowns	Satisfies Inf-Sup?
Even-Parity	2μ / 2μ	$\frac{1}{4}NK$	Yes
Odd-Parity	$3\mu^2$ / $3\mu^2$	$\frac{1}{4}NK$	No
Hybrid-Parity	$\mu+\frac{3}{2}\mu^2$ / $\mu+\frac{3}{2}\mu^2$	$\frac{1}{2}NK$	No
SAAF Cells	$\mu+\frac{3}{2}\mu^2$ / $3\mu^2$	NK	No
SAAF Vertices	2μ / 2μ	$\frac{1}{2}NK$	No
RT_0 CP	$3\mu^2$ / $3\mu^2$	$\frac{5}{4}NK$	Yes
RT_0 Hybrid-Parity	$\mu+\frac{3}{2}\mu^2$ / $\mu+\frac{3}{2}\mu^2$	$\frac{3}{2}NK$	Yes
RT_0 AFCD	$3\mu^2$ / $3\mu^2$	$\frac{5}{2}NK$	Yes
LD	$\mu+\frac{3}{2}\mu^2$ / $\mu+\frac{3}{2}\mu^2$	$3NK$	N/A

We also performed numerous test cases that support our predictions and verify our understanding of these methods. Our diffusion limit analyses yielded sharp predictions that were all supported in our test cases. The parity LCFEM discretizations exhibited 2^{nd} order convergence in XY geometry, and all methods appear to be 2^{nd} order in slab geometry. Only the SAAF DSA scheme exhibited less effectiveness than our Fourier analysis predicted. This was simply because we made an approximation for the boundary cells in this case. We demonstrated that the even-parity method works well on irregular grids, though the CFEM odd-parity method does not perform well for thick diffusive problems on these grids. The reason appears to be that the underlying discretization violates the discrete inf-sup condition. We were able to excite non-converging solutions in a simple problem by analyzing the odd-parity CFEM matrix problem, supporting our explanation of the problem.

We now face the question of which method is the best for thick diffusive problems. First, both the hybrid-parity and the average of the vertex and cell center solutions in the

modified SAAF LCFEM scheme satisfy the correct boundary and internal interface conditions. However, these methods are subject to potentially spurious solutions since the LCFEM discretization does not satisfy the discrete inf-sup condition. Their use for general problems is likely to be unpredictable and possibly very inaccurate.

It would appear that the RT_0 discretization of the coupled-parity system averaged with the LCFEM even- parity system would be the best overall performer. The total number of unknowns is half that of the linear discontinuous (LD) method applied to the first order transport equation. However, with the RT_0 discretization we are faced with inverting symmetric indefinite matrices. Whether this is more or less efficient than the LD method remains to be seen, and is likely dependent upon the specific computer architecture in question. Further, the implementation of reflective boundary conditions and the treatment of voids are troublesome. It is difficult to say *a priori* which method is best, though mixed finite element methods for coupled-parity system along with standard linear continuous finite elements for the even-parity appears to offer several advantages. First, rather than writing complex sweeping routines for unstructured grids as in the LD case, we simply form matrices with known structure. Efficient matrix inversion routines are available for both SPD and indefinite problems. Further, the behavior of the hybrid-parity based on RT_0 odd-parity should be more accurate on boundaries and interfaces of thick diffusive problems. Recall the LD/BLD satisfy a Marshak condition on the boundary, then the solution drops to the correct interior magnitude in the first cell. The hybrid-parity method results are much closer to the exact result in the first cell. We stress that it is not possible to apply a corresponding discretization to the SAAF system as it is currently written. Recall that the discretized SAAF system is simply the average of the discrete even- and odd-parity equations in the interior. Since the even- and odd-parity unknowns are not spatially co-located when we apply RT_0 to the CP system and LCFEM to the even-parity equation, it appears that no corresponding SAAF discretization exists.

It would appear that we have achieved the goals we set forth in the introduction. We have rigorously characterized the behavior of our discretizations for thick diffusive problems without making restrictive assumptions about the details of the finite element weight and basis functions or about the spatial mesh. Further, we have derived and implemented efficient and stable DSA routines for the methods we developed. We have also completely identified the relationship between the hybrid-parity method and the SAAF method. We have suggested using powerful mixed finite element methods to avoid the discrete inf-sup violation, though we implemented this only in slab geometry. All of our predictions were well supported with numerical results.

B. Recommendations for Future Work

There are several outstanding questions that warrant future work. First, the RT_0 method should be implemented in XY and XYZ geometry. Our analysis indicates that it should perform very well, without concern about spurious solutions that plague our LCFEM odd-parity discretization. We also note that the support operator method [75, 76] may offer another powerful method for addressing these problems, and that too should be investigated.

Though we had originally hoped that the mixed finite element discretization of the AFCD system would satisfy the correct boundary weighting for thick diffusive problems, we found that it did not. We propose to investigate the effect of reformulating the boundary condition (perhaps in the same way we modified the SAAF boundary condition to match the parity results) in an effort to achieve better behavior.

We also are interested in the possibility of applying a more standard method, such as LD, to the odd-parity system. Finally, we note that by formulating the RT_0 as a discontinuous method, we may be able to sweep for a solution rather than inverting a matrix. This

could be an advantage, depending on the type of problem to be run and on the specifics of the computer architecture.

REFERENCES

[1] M. L. Adams, "Even-parity finite-element transport methods in the diffusion limit," *Prog. Nucl. Energy*, vol. 25, no. 2–3, pp. 159–197, 1991.

[2] M. L. Adams, "Even- and odd-parity finite-element transport solutions in the thick diffusion limit," in *Proceedings of the International Topical Meeting on Advances in Mathematics, Computations and Reactor Physics*, Pittsburgh, Pennsylvania, 1991, The American Nuclear Society, pp. 21.1 (2–1 to 2–12).

[3] W. F. Miller, Jr., "An analysis of the finite differenced, even-parity, discrete ordinates equation in slab geometry," *Nucl. Sci. Eng.*, vol. 108, pp. 247–266, 1991.

[4] J. E. Morel and J. M. McGhee, "A self-adjoint angular flux equation," *Nucl. Sci. Eng.*, vol. 132, pp. 312–325, 1999.

[5] Franco Brezzi and Michel Fortin, *Mixed and Hybrid Finite Element Methods*, Springer-Verlag, New York, New York, 1991.

[6] V. S. Vladimirov, "Mathematical problems in the one-velocity theory of particle transport," Tech. Rep. AECL-1661, Atomic Energy of Canada, Limited, 1963.

[7] G. C. Pomraning and M. Clark, Jr., "The variational method applied to the monoenergetic Boltzmann equation. Part II," *Nucl. Sci. Eng.*, vol. 16, pp. 155–164, 1963.

[8] J. A. Davis, "Variational vacuum boundary conditions for a P_n approximation," *Nucl. Sci. Eng.*, vol. 25, pp. 189–197, 1966.

[9] S. Kaplan and J. A. Davis, "Canonical and involutory transformations of the variational problems of transport theory," *Nucl. Sci. Eng.*, vol. 28, pp. 166–176, 1967.

[10] S. Kaplan, J. A. Davis, and M. Natelson, "Angle-space synthesis - an approach to transport approximations," *Nucl. Sci. Eng.*, vol. 28, pp. 364–375, 1967.

[11] P. Feautrier, "Sur la resolution numerique de l'equation de transfert," *C.R. Acad. Sc. Paris*, vol. 258, pp. 3189–3191, 1964.

[12] W. F. Miller, Jr., E. E. Lewis, and E. C. Rossow, "The application of phase-space finite elements to the two-dimensional neutron transport equation in x-y geometry," *Nucl. Sci. Eng.*, vol. 52, pp. 12–22, 1973.

[13] R. A. Lillie and J. C. Robinson, "A linear triangle finite element formulation for multi-group neutron transport analysis with anisotropic scattering," Tech. Rep. ORNL/TM-5281, Oak Ridge National Laboratory, 1976.

[14] E. E. Lewis, "Finite element approximation to the even-parity transport equation," *Advances in Nuclear Science and Technology*, vol. 13, pp. 155–325, 1981.

[15] R. T. Ackroyd, "Some recent developments in finite element methods for neutron transport," *Advances in Nuclear Science and Technology*, vol. 19, pp. 381–483, 1987.

[16] R. T. Ackroyd, "Foundations of finite element applications to neutron transport," *Prog. Nucl. Energy*, vol. 29, no. 1, pp. 43–56, 1995.

[17] Dimitri Mihalas, *Stellar Atmospheres*, W. H. Freeman, San Francisco, California, 1978.

[18] D. Mihalas, "The computation of radiation transport using Feautrier variables I. Static media," *J. Comput. Phys.*, vol. 57, pp. 1–25, 1985.

[19] D. Mihalas and P. B. Kunasz, "The computation of radiation transport using Feautrier variables II. Spectrum line formation in moving media," *J. Comput. Phys.*, vol. 64, pp. 1–26, 1986.

[20] E. E. Lewis, "Interface angular coupling reducitons in variational nodal methods for neutron transport," *Nucl. Sci. Eng.*, vol. 102, pp. 140–152, 1989.

[21] E. E. Lewis, G. Palmiotti, and C.B. Carrico, "Variational nodal transport methods with anisotropic scattering," *Nucl. Sci. Eng.*, vol. 115, pp. 233–243, 1993.

[22] E. E. Lewis, "Progress in multidimensional neutron transport computation," *Nucl. Sci. Eng.*, vol. 64, pp. 279–293, 1977.

[23] J. E. Morel and J. M. McGhee, "A diffusion-synthetic acceleration technique for the even-parity S_n equations with anisotropic scattering," *Nucl. Sci. Eng.*, vol. 120, pp. 147–164, 1995.

[24] W. F. Miller, Jr. and T. Noh, "Finite difference versus finite elements in slab geometry, even-parity transport theory," *Transp. Theory Stat. Phys.*, vol. 22, no. 2–3, pp. 247–270, 1993.

[25] E. W. Larsen and J. B. Keller, "Asymptotic solution of neutron transport problems for small mean free paths," *J. Math. Phys.*, vol. 15, no. 1, pp. 75–81, 1974.

[26] E. W. Larsen, "On numerical solutions of transport problems in the diffusion limit," *Nucl. Sci. Eng.*, vol. 83, pp. 90–99, 1983.

[27] E. W. Larsen, J. E. Morel, and W. F. Miller, Jr., "Asymptotic solutions of numerical transport problems in optically thick, diffusive regimes," *J. Comput. Phys.*, vol. 69, pp. 283–324, 1987.

[28] E. W. Larsen, J. E. Morel, and J. M. McGhee, "Asymptotic solutions of numerical transport problems in optically thick, diffusive regimes II," *J. Comput. Phys.*, vol. 83, pp. 212–236, 1989.

[29] E. W. Larsen, "The asymptotic diffusion limit of discretized transport problems," *Nucl. Sci. Eng.*, vol. 112, pp. 336–346, 1992.

[30] F. Malvagi and G. C. Pomraning, "Initial and boundary conditions for diffusive linear transport problems," *J. Math. Phys.*, vol. 32, no. 3, pp. 805–820, 1991.

[31] R. T. Ackroyd and M. M. Nanneh, "Hybrid principle with application to synthesis," *Prog. Nucl. Energy*, vol. 25, no. 2–3, pp. 199–208, 1991.

[32] H. J. Kopp, "Synthetic method solution of the transport equation," *Nucl. Sci. Eng.*, vol. 17, pp. 65–74, 1963.

[33] E. M. Gelbard and L. A. Hageman, "The synthetic method as applied to the S_n equations," *Nucl. Sci. Eng.*, vol. 37, pp. 288–298, 1969.

[34] W. H. Reed, "The effectiveness of acceleration techniques for iterative methods in transport theory," *Nucl. Sci. Eng.*, vol. 45, pp. 245–254, 1971.

[35] R. E. Alcouffe, "Diffusion synthetic acceleration methods for the diamond-differenced discrete-ordinates equations," *Nucl. Sci. Eng.*, vol. 64, pp. 344–355, 1977.

[36] E. W. Larsen, "Diffusion-synthetic acceleration methods for discrete ordinates problems," *Transp. Theory Stat. Phys.*, vol. 13, no. 1–2, pp. 107–126, 1984.

[37] J. E. Morel and J. M. McGhee, "A fission source acceleration technique for time-dependent even-parity S_n calculations," *Nucl. Sci. Eng.*, vol. 116, pp. 73–85, 1994.

[38] R. T. Ackroyd, "Least-squares derivation of extremum and weighted-residual methods for equations of reactor physics - I. The first-order Boltzmann equation and a first-order initial-value equation," *Ann. Nucl. Energy*, vol. 10, pp. 65–99, 1983.

[39] R. T. Ackroyd, J. G. Issa, and N. S. Riyait, "Treatment of voids in finite element transport methods," *Prog. Nucl. Energy*, vol. 18, no. 1–2, pp. 85–89, 1986.

[40] P. A. Raviart and J. M. Thomas, "A mixed finite element method for 2-nd order elliptic problems," in *Lecture Notes in Mathematics 606*, A. Dold and B. Eckmann, Eds., pp. 292–315. Springer-Verlag, New York, New York, 1977.

[41] George I. Bell and Samuel Glasstone, *Nuclear Reactor Theory*, Robert E. Krieger, Malabar, Florida, 1970.

[42] James J. Duderstadt and Louis J. Hamilton, *Nuclear Reactor Analysis*, Wiley, New York, New York, 1976.

[43] Kenneth M. Case and Paul M. Zweifel, *Linear Transport Theory*, Addison-Wesley, Reading, Massachusetts, 1967.

[44] James J. Duderstadt and William R. Martin, *Transport Theory*, Wiley, New York, New York, 1979.

[45] E. E. Lewis and W. F. Miller, Jr., *Computational Methods of Neutron Transport*, Wiley, New York, 1984.

[46] B. G. Carlson and K. D. Lathrop, "Transport theory - the method of discrete ordinates," in *Computing Methods in Reactor Physics*, H. Greenspan, C. N. Kelber, and D. Okrent, Eds., chapter 3, pp. 167–266. Gordon and Breach, New York, New York, 1968.

[47] R. T. Ackroyd, "Generalized least squares as a generator of variational principles and weighted residual methods for FEM transport methods," *Prog. Nucl. Energy*, vol. 18, no. 1–2, pp. 45–62, 1986.

[48] R. T. Ackroyd, "Finite element methods for neutron transport based on maximum and minimum principles for discontinous trial funcitons," *Ann. Nucl. Energy*, vol. 19, no. 10–12, pp. 565–592, 1992.

[49] E. E. Lewis and I. Dilber, "Finite element, nodal and response matrix methods: A variational synthesis for neutron transport," *Prog. Nucl. Energy*, vol. 18, no. 1–2, pp. 63–74, 1986.

[50] T. Noh and W. F. Miller, Jr., "The even-parity and simplified even-parity transport equations in two-dimensional x-y geometry," *Nucl. Sci. Eng.*, vol. 123, pp. 38–56, 1996.

[51] E. W. Larsen, "Solutions of the steady, one-speed neutron transport equation for small mean free paths," *J. Math. Phys.*, vol. 15, no. 3, pp. 299–305, 1974.

[52] G. J. Habetler and B. J. Matkowsky, "Uniform asymptotic expansion in transport theory with small mean free paths, and the diffusion approximation," *J. Math. Phys.*, vol. 16, no. 4, pp. 846–854, 1975.

[53] S. Chandrasekhar, *Radiative Transfer*, Dover, New York, New York, 1960.

[54] Wolfgang Hackbusch, *Iterative Solution of Large Sparse Systems of Equations*, Springer-Verlag, New York, New York, 1994.

[55] E. W. Larsen and D. R. McCoy, "Unconditionally stable diffusion-synthetic acceleration methods for the slab geometry discrete ordinates equations. Part II: Numerical results," *Nucl. Sci. Eng.*, vol. 82, pp. 64–70, 1982.

[56] E. W. Larsen, "Unconditionally stable diffusion-synthetic acceleration methods for the slab geometry discrete ordinates equations. Part I: Theory," *Nucl. Sci. Eng.*, vol. 82, pp. 47–63, 1982.

[57] M. L. Adams and T. A. Wareing, "Diffusion-synthetic acceleration given anisotropic scattering, general quadrature, and multidimensions," *Trans. Am. Nucl. Soc.*, vol. 68, pp. 203–204, 1993.

[58] O. C. Zienkiewicz and R. L. Taylor, *The Finite Element Method*, McGraw-Hill Book Company, New York, New York, 1994.

[59] R. E. Ewing, R. D. Lazarov, J. E. Pasciak, and A. T. Vassilev, "Mathematical modelling, numerical techniques, and computer simulation of flows and transport in porous media," Tech. Rep. ISC-95-03-MATH, Texas A&M University Institute for Scientific Computation, 1995.

[60] T. Arbogast, G. N. Dawson, P. T. Keenan, M. F. Wheeler, and I. Yotov, "Enhanced cell-centered finite differences for elliptic equations on general geometry," *SIAM J. Sci. Comput.*, vol. 19, pp. 404–425, 1998.

[61] J. Shen, "Mixed finite element methods on distored rectangular grids," Tech. Rep. ISC-94-13-MATH, Texas A&M University Institute for Scientific Computation, 1994.

[62] J. H. Bramble, J. E. Pasciak, and A. T. Vassilev, "Analysis of the inexact Uzawa algorithm for saddle point problems," *SIAM J. Numer. Anal.*, vol. 34, pp. 1072–1092, 1997.

[63] G. L. Ramone, M. L. Adams, and P. F. Nowak, "A transport synthetic acceleration method for transport iterations," *Nucl. Sci. Eng.*, vol. 125, pp. 257–283, 1997.

[64] S. Nakamura, *Computational Science Methods in Engineering and Science*, chapter 8, pp. 285–332, Robert E. Krieger, Malabar, Florida, 1986.

[65] V. Y. Gol'din, "A quasi-diffusion method of solving the kinetic equation," *U.S.S.R. Computational Mathematics and Mathematical Physics*, vol. 4, no. 6, pp. 136–149, 1964.

[66] D. Y. Anistratov and V. Y. Gol'din, "Nonlinear methods for solving particle transport problems," *Transp. Theory Stat. Phys.*, vol. 22, no. 2–3, pp. 125–163, 1993.

[67] M. M. Miften and E. W. Larsen, "The quasi-diffusion method for solving transport problems in planar and spherical geometries," *Transp. Theory Stat. Phys.*, vol. 22, no. 2–3, pp. 165–186, 1993.

[68] M. L. Adams and W. R. Martin, "Boundary projection acceleration: A new approach to synthetic acceleration of transport calculations," *Nucl. Sci. Eng.*, vol. 100, pp. 177–189, 1988.

[69] Gene E. Golub and Charles F. Van Loan, *Matrix Computations*, Johns Hopkins, Baltimore, Maryland, 1996.

[70] Yousef Saad, *Iterative Methods for Sparse Linear Systems*, PWS Publishing Company, Boston, Massachusetts, 1996.

[71] M. L. Adams, "Discontinuous finite-element transport solutions in the thick diffusion limit in Cartesian geometry," in *Proceedings of the International Topical Meeting on Advances in Mathematics, Computations and Reactor Physics*, Pittsburgh, Pennsylvania, 1991, The American Nuclear Society, pp. 21.1 (3–1 to 3–12).

[72] R. E. Alcouffe, E. W. Larsen, W. F. Miller, Jr., and B. R. Wienke, "Computational efficiency of numerical methods for the multigroup, discrete ordinates neutron transport equations: The slab geometry case," *Nucl. Sci. Eng.*, vol. 71, pp. 111–127, 1979.

[73] M. L. Adams and T. L. Eaton, "New corner balance/linear discontinous method for transport in slab geometry," *Trans. Am. Nucl. Soc.*, vol. 70, pp. 158–159, 1994.

[74] D. S. Kershaw, "Differencing of the diffusion equation in Lagrangian hydrodynamics codes," *J. Comput. Phys.*, vol. 39, pp. 375–395, 1981.

[75] M. Shashkov and S. Steinberg, "Solving diffusion equations with rough coefficients in rough grids," *J. Comput. Phys.*, vol. 129, pp. 383–405, 1996.

[76] J. E. Morel, R. M. Roberts, and M. J. Shashkov, "A local support-operator diffusion discretization scheme for quadrilateral r-z meshes," *J. Comput. Phys.*, vol. 144, pp. 17–51, 1998.

VITA

Christopher John Gesh was born September 14, 1966 in Haverhill, Massachusetts. He earned a B.S. with Highest Scholarship in Nuclear Engineering at Oregon State University in 1988. He earned a M.S.E. in Nuclear Engineering at the University of Michigan in 1990, where he held an appointment as a Department of Energy Nuclear Science and Engineering Fellow. He worked in the Reactor Systems Analysis Group at Pacific Northwest Laboratory from 1990 until 1993. In the fall of 1993, he returned to school at Texas A&M University as a Department of Energy Computational Sciences Fellow. He is currently a technical staff member in the X-Division Transport Methods Group at Los Alamos National Laboratory. His mailing address is 320 Rim Road, Los Alamos, New Mexico 87544.

The typist for this thesis was Christopher Gesh.